

TURUN YLIOPISTON JULKAISUJA
ANNALES UNIVERSITATIS TURKUENSIS

SARJA - SER. A I OSA - TOM. 431

ASTRONOMICA - CHEMICA - PHYSICA - MATHEMATICA

DPS-LIKE PEROXIDE RESISTANCE PROTEIN:

Structural and Functional Studies
on a Versatile Nanocontainer

by

Teemu Haikarainen

TURUN YLIOPISTO
UNIVERSITY OF TURKU
Turku 2011

From

Turku Centre for Biotechnology, University of Turku and Åbo Akademi University
Department of Biochemistry and Food Chemistry, Faculty of Mathematics and Natural
Sciences, University of Turku

Supervised by

Docent Anastassios C. Papageorgiou, Ph. D.

Turku Centre for Biotechnology, University of Turku and Åbo Akademi University
Turku, Finland

Reviewed by

Professor Ritva Serimaa, Ph. D.

Division of Materials Physics, Department of Physics, University of Helsinki
Helsinki, Finland

Associate Professor Derek Logan, Ph. D.

Centre for Molecular Protein Science, Department of Biochemistry and Structural Biology,
Lund University
Lund, Sweden

Opponent

Professor Giuseppe Zanotti, Ph. D.

Department of Biological Chemistry, University of Padua
Padova, Italy

ISBN 978-951-29-4812-3 (PRINT)

ISBN 978-951-29-4813-0 (PDF)

ISSN 0082-7002

Painosalama Oy – Turku, Finland 2011

TABLE OF CONTENTS

1 LIST OF ORIGINAL PUBLICATIONS	6
2 LIST OF ORIGINAL PUBLICATIONS NOT INCLUDED IN THE THESIS	7
3 ABBREVIATIONS	8
4 ABSTRACT	10
5 REVIEW OF THE LITERATURE	11
5.1 Transition metals and oxygen in bacteria	11
5.1.1 Role of transition metals in bacteria	12
5.1.2 Transition metals and oxidative stress	13
5.1.3 Transition metal homeostasis in bacteria	15
5.1.3.1 Metal uptake and efflux	15
5.1.3.2 Regulation of genes involved in metal homeostasis	16
5.1.4 Antioxidant enzymes in bacteria	18
5.1.4.1 Hydrogen peroxide scavengers	18
5.1.4.2 Superoxide scavengers	20
5.1.4.3 Other mechanisms	21
5.2 Overview of the ferritin-like superfamily	21
5.2.1 Classical ferritins	22
5.2.2 Bacterioferritins	23
5.2.3 Other members of the superfamily	24
5.3 Dps proteins	25
5.3.1 Structural characteristics	25
5.3.1.1 Monomer architecture	25
5.3.1.2 Packing of the dodecamer	26
5.3.1.3 Ferroxidase center	27
5.3.2 Detoxification of iron	29
5.3.2.1 Entry to the protein shell	29
5.3.2.2 Ferroxidase reaction	30
5.3.2.3 Nucleation of iron and the structure of the iron core	31
5.3.3 DNA shielding	32
5.3.3.1 DNA-binding signatures	33
5.3.3.2 Biocrystallization	33
5.3.4 Regulation in response to stress signals	34

5.3.5 Other biological functions.....	35
5.3.6 Applications in nanotechnology	38
6 AIMS OF THE STUDY	40
7 SUMMARY OF MATERIALS AND METHODS.....	41
7.1 Protein expression and purification	41
7.2 <i>In vitro</i> iron loading and end-point iron staining.....	41
7.3 X-ray crystallography	41
7.3.1 Crystallizations	41
7.3.1.1 <i>S. suis</i> Dpr	41
7.3.1.2 <i>S. pyogenes</i> Dpr.....	42
7.3.2 Data collection and processing	43
7.3.3 Structure determination, refinement, and validation.....	45
7.3.3.1 <i>S. suis</i> Dpr	45
7.3.3.2 <i>S. pyogenes</i> Dpr.....	45
7.4 X-ray absorption spectroscopy	45
7.4.1 Data collection	45
7.4.2 Data analysis	46
7.5 Isothermal titration calorimetry	46
7.6 Mössbauer spectroscopy.....	46
7.7 Magnetic measurements	46
7.8 Inductively coupled plasma mass spectrometry	47
8 RESULTS AND DISCUSSION	48
8.1 Crystal structures of <i>S. pyogenes</i> Dpr (STUDIES I AND II).....	48
8.1.1 Description of the structures	49
8.1.2 Novel N-terminal helix	50
8.1.3 Variant ferroxidase centers	50
8.1.3.1 Binding of iron and changes in the ferroxidase center.....	50
8.1.3.2 The di-zinc ferroxidase center.....	51
8.1.3.3 Comparison of di-metal ferroxidase centers of Dps proteins	52
8.1.3.4 The effect of point-mutations to iron and zinc binding	53
8.1.4 Surface zinc-binding site and potential implications	53
8.2 Metal cation binding to <i>S. suis</i> Dpr (STUDY III)	54
8.2.1 Metal binding to the ferroxidase center	54

8.2.2 Thermodynamic properties of the metal binding.....	56
8.3 Structural and magnetic properties of <i>S. suis</i> Dpr iron core (STUDY IV).....	57
8.3.1 Structures of the iron cores	58
8.3.2 Magnetic properties of the iron nanoparticles	59
8.3.2.1 Magnetic measurements of the iron cores.....	60
8.3.2.2 Mössbauer analysis of the iron cores	60
8.3.3 Potential nanotechnological applications of Dpr	61
9 CONCLUSIONS AND FUTURE PERSPECTIVES	63
10 ACKNOWLEDGEMENTS.....	65
11 REFERENCES.....	67
ORIGINAL PUBLICATIONS	79

1 LIST OF ORIGINAL PUBLICATIONS

This thesis is based on the following articles that are referred to by their Roman numerals.

- I **Haikarainen T**, Tsou CC, Wu JJ, Papageorgiou AC (2010) Crystal structures of *Streptococcus pyogenes* Dpr reveal a dodecameric iron-binding protein with a ferroxidase site. *J Biol Inorg Chem* **15**: 183-194

- II **Haikarainen T**, Tsou CC, Wu JJ, Papageorgiou AC (2010) Structural characterization and biological implications of di-zinc binding in the ferroxidase center of *Streptococcus pyogenes* Dpr. *Biochem Biophys Res Commun* **398**: 361-365

- III **Haikarainen T**, Thanassoulas A, Stavros P, Nounesis G, Haataja S, Papageorgiou AC (2011) Structural and thermodynamic characterization of metal ion binding in *Streptococcus suis* Dpr. *J Mol Biol* **405**: 448-460

- IV **Haikarainen T**, Paturi P, Linden J, Haataja S, Meyer-Klaucke W, Finne J, Papageorgiou AC (2011) Magnetic properties and structural characterization of iron oxide nanoparticles formed by *Streptococcus suis* Dpr and four mutants. *J Biol Inorg Chem* **16**: 799-807

The articles have been reprinted with the permission of the copyright holders.

2 LIST OF ORIGINAL PUBLICATIONS NOT INCLUDED IN THE THESIS

- I Havukainen H, Haataja S, Kauko A, Pulliainen AT, Salminen A, **Haikarainen T**, Finne J, Papageorgiou AC (2008) Structural basis of the zinc- and terbium-mediated inhibition of ferroxidase activity in Dps ferritin-like proteins. *Protein Sci* **17**: 1513-1521

- II **Haikarainen T**, Papageorgiou AC (2010) Dps-like proteins: structural and functional insights into a versatile protein family. *Cell Mol Life Sci* **67**: 341-351

- III Wakadkar S, Zhang LQ, Li DC, **Haikarainen T**, Dhavala P, Papageorgiou AC (2010) Expression, purification and crystallization of *Chaetomium thermophilum* Cu,Zn superoxide dismutase. *Acta Crystallogr Sect F Struct Biol Cryst Commun* **66**: 1089-1092

3 ABBREVIATIONS

ABC	ATP-binding cassette
AC	alternating current
Ahp	alkyl hydroperoxide reductase
ATP	adenosine-5'-triphosphate
<i>BbDps</i>	<i>Bacillus brevis</i> Dps
<i>BbNapA</i>	<i>Borrelia burgdorferi</i> neutrophil-activating protein A
Bfr	bacterioferritin
Clp	ATP-dependent caseinolytic protease
DC	direct current
Dpr	Dps-like peroxide resistance protein
Dps	DNA-binding protein from starved cells
<i>EcDps</i>	<i>Escherichia coli</i>
EXAFS	extended X-ray absorption fine structure
FC	field-cooled
FOC	ferroxidase center
Ftn	classical ferritin
Fur	ferric-uptake regulator
GBS	Guillain-Barré syndrome
<i>HpNap</i>	<i>Helicobacter pylori</i> neutrophil-activating protein
<i>HsDpsA</i>	<i>Halobacterium salinarum</i> DpsA
ICP-MS	inductively coupled plasma mass spectrometry
IL	interleukin
IM	inner membrane
ITC	isothermal titration calorimetry
K_d	dissociation constant
<i>LiDps</i>	<i>Listeria innocua</i> Dps

MME	monomethyl ether
MrgA	metal-regulated gene A
OM	outer membrane
PDB	Protein Data Bank
PEG	polyethylene glycol
PerR	redox sensing Fur-like transcriptional regulator
ROS	reactive oxygen species
SBP	solute binding protein
SOD	superoxide dismutase
<i>SpDpr</i>	recombinant <i>Streptococcus pyogenes</i> Dpr
<i>SsDpr</i>	recombinant <i>Streptococcus suis</i> Dpr
SQUID	superconducting quantum interference device
XANES	X-ray absorption near edge structure
XAS	X-ray absorption spectroscopy
ZFC	zero-field-cooled
ZntR	zinc-responsive regulator
Zur	zinc uptake regulator

4 ABSTRACT

Oxidative stress is a constant threat to almost all organisms. It damages a number of biomolecules and leads to the disruption of many crucial cellular functions. It is caused by reactive oxygen species (ROS), such as hydrogen peroxide (H_2O_2), superoxide (O_2^\cdot), and hydroxyl radical (OH^\cdot). The most harmful of these compounds is OH^\cdot , which is only formed in cells in the presence of redox-cycling transition metals, such as iron and copper.

Bacteria have developed a number of mechanisms to cope with ROS. One of the most widespread means employed by bacteria is the DNA-binding proteins from starved cells (Dps). Dps proteins protect the cells by binding and oxidizing Fe^{2+} , thus greatly reducing the production of OH^\cdot . The oxidized iron is stored inside the protein as an iron core. In addition, Dps proteins bind directly to DNA forming a protective coating that shields DNA from harmful agents. Moreover, Dps proteins have been found to elicit other protective functions in cells and to participate in bacterial virulence. Dps proteins are of special importance to *Streptococci* owing to the lack of catalase in this genus of bacteria.

This study was focused on structural and functional characterization of streptococcal Dps-like peroxide resistance (Dpr) proteins. Initially, crystal structures of *Streptococcus pyogenes* Dpr were determined. The data confirmed the presence of a di-metal ferroxidase center (FOC) in Dpr proteins and revealed the presence of a novel N-terminal helix as well as a surface metal-binding site. The crystal structures of *Streptococcus suis* Dpr complexed with transition metals demonstrated the metal specificity of the FOC. Solution binding studies also indicated the presence of a di-metal FOC. These results suggested a possible role for Dpr in the detoxification of various metals. Iron was found to mineralize inside the protein as ferrihydrite based on X-ray absorption spectroscopy data. The iron core was found to exhibit clear superparamagnetic behaviour using magnetic and Mössbauer measurements.

The results from this study are expected to further increase our understanding on the binding, oxidation, and mineralization of iron and other metals in Dpr proteins. In particular, the structural and magnetic properties of the iron core can form a basis for potential new applications in nanotechnology. From the streptococcal viewpoint, the results would help in understanding better the complicated picture of bacterial pathogenesis. Dpr proteins may also provide a novel target for drug design due to their tight involvement in bacterial virulence.

5 REVIEW OF THE LITERATURE

5.1 Transition metals and oxygen in bacteria

Transition metal cations are necessary for all living cells. They have a common basic electronic configuration in their *s* valence shell with a few exceptions (for example, copper) but differ in the occupation of their incomplete *d* orbitals. The variable oxidation states of transition metals allow them to form complex compounds in cells and to act as co-factors at the active sites of numerous enzymes.

Transition metals are usually complexed to nitrogen, oxygen, or sulphur atoms in molecules. Approximately one-third of all proteins require transition metals for efficient function. However, the usage of various metals varies from organism to organism and has probably evolved as a response to metal availability in the environment [1,2]. In the absence of transition metals, many of the necessary reactions for life and probably life itself would have been impossible.

Despite their necessity, transition metals can also cause stress. The stress can result from the deficiency of necessary metals or from the excess of metals leading to disruption of cellular function and toxic effects, respectively. In addition, the reaction of oxygen, and especially reduced oxygen species, with transition metals can result in the production of extremely harmful radicals [3]. Thus, cells have to be able to sense metal levels to properly respond to environmental changes in metal concentrations.

Transition metals can be divided into two groups based on the cell requirements: necessary and toxic metals (Table 1). Fe, Zn, Cu, Co, Ni, Mn, V, Mo, and W are essential to life and bacteria need to acquire them from the environment. However, they can become toxic if they are present in excess. Conversely, metals for which no biological function has been discovered so far are treated as toxic metals. These are Al, Au, Ag, Bi, Cd, Cr, Hg, Pb, Sn, and Tl, although not all of them are transition metals. The rest of the transition metals not mentioned above are generally treated as non-toxic metals because they are either very rare or not soluble at physiological conditions and, therefore, are present at too low concentrations to become toxic [4-6].

Table 1. Transition metals or *d*-block elements. The atoms of these elements have 1-10 *d* electrons. Essential transition metals are coloured in green and toxic metals are coloured in red. The elements on the white background are not essential and are too rare or insoluble to be considered toxic.

Group	3	4	5	6	7	8	9	10	11	12 [#]
Period 4	21 Sc	22 Ti	23 V	24 Cr	25 Mn	26 Fe	27 Co	28 Ni	29 Cu	30 Zn
Period 5	Y 39	40 Zr	41 Nb	42 Mo	43 Tc	44 Ru	45 Rh	46 Pd	47 Ag	48 Cd
Period 6	57- 71*	72 Hf	73 Ta	74 W	75 Re	76 Os	77 Ir	78 Pt	79 Au	80 Hg
Period 7	89- 103*	104 Rf	105 Db	106 Sg	107 Bh	108 Hs	109 Mt	109 Ds	111 Rg	112 Cn

* The classification of some lanthanides and actinides as transition metals (or *d*-block elements) varies.

[#] Group 12 elements, such as zinc, do not have an incomplete *d* sub-shell, and they do not give rise to cations with an incomplete *d* sub-shell. They are, therefore, not always classified as transition metals.

5.1.1 Role of transition metals in bacteria

In biology, the most important transition metals are iron, zinc, manganese, copper, cobalt, and nickel. They are crucial constituents of a variety of proteins in bacteria [7]. Owing to their unique properties, these metal cations can be used to perform diverse functions in the cell. Transition metal cations act as structural components of proteins, as catalytic cofactors in oxidation-reduction reactions, and in electron transfer chemistry, to name a few of their biological roles.

Iron is the only macroelement of the transition metals and, with a few exceptions, an essential element for all organisms [8,9]. Owing to its low solubility in physiological pH and aerobic conditions, iron is also the growth-limiting factor for many bacteria. Iron has three biologically relevant oxidation states: Fe²⁺, Fe³⁺, and Fe⁴⁺. Despite the fact that Fe²⁺ and Fe³⁺ are far more common than Fe⁴⁺, the latter is an extremely important intermediate in a variety of metalloproteins, such as peroxidases and cytochromes P450 [10,11]. The redox potential of Fe²⁺/Fe³⁺ makes iron a versatile cofactor in catalytic centers of enzymes and a suitable electron carrier in proteins. In addition, iron can change its electronic spin state and redox potential depending on the needs of the enzyme. In the high spin state all five 3*d* orbitals of Fe²⁺ have the same energy and four of its electrons are unpaired. When Fe²⁺ is surrounded by six ligands, the unpaired electrons can pair with lower energy orbitals. This results in low-spin state of Fe²⁺ with no unpaired electrons [12]. In this state, iron is more difficult to oxidize and low-spin Fe²⁺ is present, for example, in oxyhaemoglobin. In contrast, deoxyhaemoglobin has iron in high-spin state [13]. In bacteria, low-spin and high-spin iron is found, for instance, in nitric oxide reductases [14].

Zinc is the second most important transition metal for living organisms after iron. However, there is a distinct difference between zinc and iron: while iron is able to change its redox state, zinc exists solely as Zn²⁺ [4]. Most intracellular Zn²⁺ is complexed to different

proteins and hence the pool of bioavailable Zn^{2+} in bacteria is very small. Zn^{2+} is involved in crucial tasks in many proteins and plays either structural, regulatory, or catalytic role in proteins [15]. Zn^{2+} has been reported in many key enzymes, such as in DNA and RNA polymerases [16,17]. Zn^{2+} is also found in ribosome, where it functions as a structural component of many ribosomal proteins [18-20].

Manganese exists in many oxidation states. Notably, every oxidation state of manganese from Mn^{2+} to Mn^{7+} occurs in cells. Mn^{2+} homeostasis, in particular, plays an important role in virulence of many human microbial pathogens [21]. Perhaps the most important role of manganese in biology appears in the water splitting in oxygenic photosynthesis [22]. In addition, manganese plays key roles in various enzymatic reactions, such as in signal transduction through the Mn^{2+} -dependent phosphatase [23] and in DNA-synthesis under iron-deprived conditions through the Mn^{2+} -dependent ribonucleotide reductase [24].

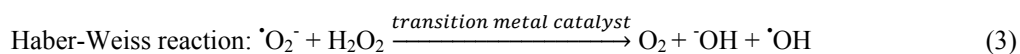
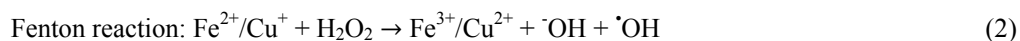
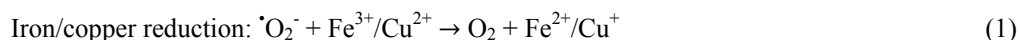
In striking contrast to iron, zinc, and manganese, the requirements for copper, cobalt, and nickel in the cytosol are quite low in most bacteria. Copper is also extremely dangerous owing to the redox potential of Cu^{2+}/Cu^+ ($E_0 = 0.15$ V), which is close to that of the cytosol. The ease of the Cu^{2+}/Cu^+ redox cycling allows copper to participate in the generation of radicals [12]. With the exception of the photosynthetic cyanobacteria, which contain copper-requiring organelles termed thylakoids responsible for photosynthesis, no known bacterial species express a cytosolic enzyme that absolutely requires copper [25]. The copper-containing enzymes are either in the periplasm (in Gram-negative bacteria) or embedded in the plasma membrane. These enzymes include tyrosinases [26] and copper-containing monoamine oxidase [27].

Both nickel and cobalt are mostly found as divalent cations, whereas their trivalent form is stable only in complex compounds. They both perform a few specific tasks in the cell in association with certain metalloenzymes. Cobalt is part of the corrin ring of coenzyme B_{12} which is present in certain enzymes [28]. Non-corrinoid cobalt enzymes include nitrile hydratase, which catalyzes the hydration of nitriles to form amides [29], and transcarboxylase, which transfers a carboxyl group from methylmalonyl-CoA to pyruvate to form propionyl-CoA and oxaloacetate [30]. Nickel is present in a few enzymes, such as NiFe-hydrogenase which catalyzes the reversible oxidation of H_2 [31], and urease which catalyzes the hydrolysis of urea into ammonia and carbon dioxide [32].

5.1.2 Transition metals and oxidative stress

After the evolution of oxygen-producing cyanobacteria 2.2-2.7 billion years ago, the anaerobic organisms at that time had to respond to new oxidative conditions. In order to survive, they either had to retreat to anaerobic habitats or develop antioxidant defences. One of the major consequences of the oxidative atmosphere was the conversion of the highly soluble and easily utilizable Fe^{2+} to a rather insoluble Fe^{3+} . In other words, iron was transformed from a “friendly” metal to a potentially toxic one as it could react with reduced oxygen species with deleterious effects.

Today, every aerobic organism encounters reduced oxygen species that can react with transition metals. Reactive oxygen species (ROS) are partially reduced forms of molecular oxygen formed as by-products of aerobic metabolism (Fig. 1). The one- and two-electron reduction products of oxygen, superoxide ($\cdot\text{O}_2^-$) and hydrogen peroxide (H_2O_2), respectively, are the most common by-products of aerobic metabolism and are formed by various routes. The respiratory chain, in particular, has been identified as a major source of $\cdot\text{O}_2^-$ [33,34]. $\cdot\text{O}_2^-$ is also formed by the function of redox-cycling compounds excreted by microbes and plants that diffuse into the bacteria. There, $\cdot\text{O}_2^-$ also generates H_2O_2 through a dismutation reaction [35]. The external media is a constant source of H_2O_2 , because H_2O_2 can pass through membranes, unlike the charged $\cdot\text{O}_2^-$ [36]. Many lactic acid bacteria also utilize pyruvate and lactate oxidases to excrete H_2O_2 in order to gain advantage over other microbes or use it as a virulence factor against host cells [37-40]. In addition, phagocytes produce $\cdot\text{O}_2^-$ through NADPH oxidases to fight microbial infection [41]. Although $\cdot\text{O}_2^-$ and H_2O_2 are by themselves only mildly reactive, they can still damage some biomolecules. In particular, they are able to damage proteins containing $[\text{4Fe-4S}]^{2+}$ clusters. $[\text{4Fe-4S}]^{2+}$ -containing dehydratases, such as isopropylmalate isomerase, 6-phosphogluconate dehydratase, and dihydroxy-acid dehydratase have been identified as targets for H_2O_2 and $\cdot\text{O}_2^-$ inactivation [42-44]. However, H_2O_2 and $\cdot\text{O}_2^-$ become truly dangerous only in the presence of a transition metal catalyst, often iron, or to some extent copper, resulting in the formation of the more toxic compound hydroxyl radical ($\cdot\text{OH}$). The transition metal catalyst can react with $\cdot\text{O}_2^-$ and H_2O_2 in a series of reactions that eventually lead to the production of $\cdot\text{OH}$:



The transition metal catalyst in the net reaction (Haber-Weiss reaction) is required for $\cdot\text{OH}$ production, since the second order rate constant of the reaction in an aqueous solution is practically zero [45]. The hydroxyl radical formed as the net result is highly reactive and can damage a variety of biomolecules, including proteins, nucleic acids, and lipids [46]. DNA damage is especially severe as $\cdot\text{OH}$ causes strand breaks, depurination/depyrimidation, and oxidation of bases. Lipids are damaged by peroxidation that decreases membrane fluidity. Protein damage occurs *via* oxidation of amino acids leading, for example, to fragmentation [47]. The diffusion of $\cdot\text{OH}$ is limited because after its formation it is likely to react with an oxidizable substrate before travelling a long distance. However, $\cdot\text{OH}$ can start a radical reaction, which can result in injury far away from the site of $\cdot\text{OH}$ formation [45].

Since $\cdot\text{OH}$ formation requires a transition metal catalyst under physiological conditions, it is imperative that a proper balance with metal uptake and efflux is maintained. Accordingly, bacteria have developed multiple systems to maintain the appropriate concentrations of metal ions in the cell. These systems will be discussed in the next section.

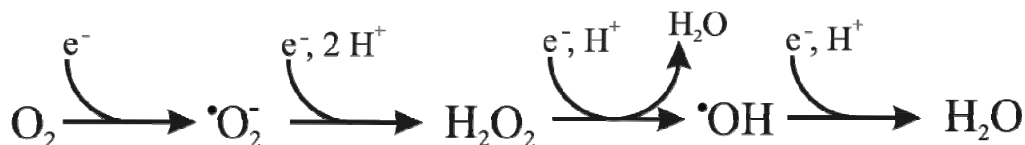


Figure 1. Reduction series of oxygen.

5.1.3 Transition metal homeostasis in bacteria

5.1.3.1 Metal uptake and efflux

The homeostasis of essential transition metals is mediated by the control of metal uptake, efflux, and storage (Fig. 2). Since metal cations cannot diffuse across the membrane bilayer, metal uptake and efflux are mainly accomplished by metal transporters, which are integral membrane proteins in both the outer and inner membranes (OM and IM, respectively). In Gram-negative bacteria, metals must pass through both OM and IM before gaining access to cytosol, whereas Gram-positive bacteria lack periplasm. Non-selective, passive metal transport through the OM occurs by diffusion through trimeric β -barrel proteins called porins [48,49]. However, this passive diffusion is unable to deliver enough metals to cytosol to fulfil the cellular needs. Therefore, several high-affinity transport systems exist in OM and IM that facilitate metal transport to cytosol. The IM transport proteins use the energy created by ATP hydrolysis for the transport (e.g., ATP-binding cassette (ABC) transporters and P-type ATPases) or couple the transport with the energetically favourable transfer of protons or ions across the bilayer (e.g., cation diffusion facilitator, natural resistance-associated macrophage protein) [50-54]. Some metal transporters are capable of transporting a variety of metals into and out of the cell but some tend to be more selective for certain metals over others. For example, ABC transporters have been identified in most bacteria and transport nearly all biologically required transition metal ions. The specificity of this transport is mediated by the solute binding protein (SBP) component of the transporter. SBP is freely diffusible in the periplasm of Gram-negative bacteria, whereas in Gram-positive bacteria it is covalently anchored to the plasma membrane [50].

Metal transport has evolved according to the needs of the organism. Pathogenic bacteria encounter elevated concentrations of zinc in the host; thus, various methods of exporting Zn^{2+} from the cytosol have evolved [55]. In addition, *Lactobacillus plantarum*, which requires large intracellular concentration of Mn^{2+} , utilizes Mn^{2+} - and Cd^{2+} -specific P-type ATPase (MntA) to transport Mn^{2+} inside the cell [56].

As iron is the most important but rather insoluble transition metal, bacteria have developed a wide array of uptake systems to obtain iron either from the environment or from the host. Bacteria produce high-affinity extracellular ferric chelators, namely siderophores, which are small molecular weight compounds that chelate iron, and the complexes are then transported back into the cell. The iron-siderophore complexes are taken up by specific receptors in the OM. The uptake is driven by the IM potential and mediated by the energy-transducing TonB-ExbB-ExbD system. SBPs shuttle the iron-siderophores to ABC transporters, which deliver

the complexes into the cytosol [57,58]. Gram-positive bacteria, which lack the periplasm, do not have OM receptors or TonB-ExbB-ExbD systems but instead they have the ABC transporters and SBPs directly tethered to the cytosolic membrane. Under anaerobic conditions, Fe^{3+} can also be reduced to Fe^{2+} by reductases and taken up by ferrous iron transporters. In addition, pathogenic bacteria can take iron from the host iron-binding proteins transferrin and lactoferrin or from the heme of haemoglobin. Unlike other transition metals, iron is not transported out from the cells when toxic levels have been reached. Instead, iron is mineralized in iron storage proteins, mainly ferritins, in a bioavailable form [57].

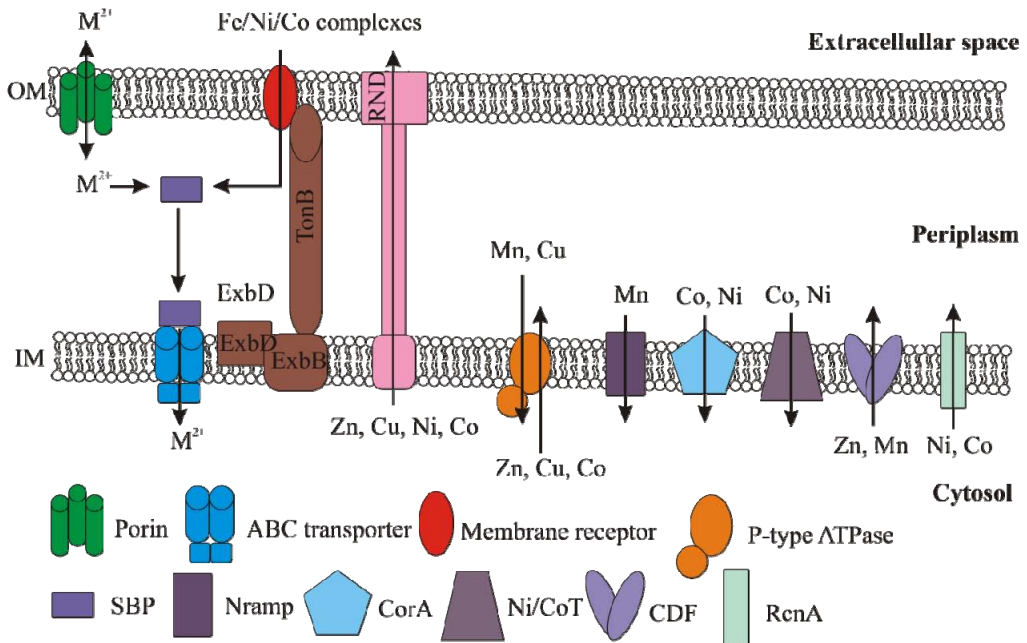


Figure 2. Overview of the iron, zinc, manganese, copper, nickel, and cobalt uptake and efflux in Gram-negative bacteria. This depiction is not exhaustive and not all the mechanisms are present in every bacterium. Porins mediate the diffusion of transition metals (M^{2+}) through the OM [48,49]. Nickel and cobalt complexes are brought to cells by TonB-ExbB-ExbD-activated processes analogous to those used for iron complexes [59]. ABC transporters mediate the transfer of SBP-transported metals to the cytosol [60]. P-type ATPases, natural resistance-associated macrophage proteins (Nrpam), magnesium transport protein (CorA), and nickel/cobalt transporters (Ni/CoT) mediate the cytosolic transport of transition metals [53,61,62]. The metal efflux is achieved by resistance-nodulation-cell division (RND) transporters, cation diffusion facilitators (CDF), resistance to cobalt and nickel (RcnA) transporters, and P-type ATPases [51,52,63,64].

5.1.3.2 Regulation of genes involved in metal homeostasis

Proteins involved in metal homeostasis are tightly regulated by metalloregulatory proteins in order to quickly respond to the changes of metals levels in the environment and to maintain a strict control over the concentration of metal cations in the cell. Based on their function, the regulators can be divided into those that control the gene expression of metal efflux and

storage proteins, and those that control the gene expression of metal uptake proteins. In general, regulators that control metal uptake bind metal ions as co-repressors (i.e., metal binding causes the repression of the genes involved in metal uptake) and regulators that control the metal efflux and storage function *via* activation or transcriptional derepression [65]. Till date, ten structural families of metalloregulatory proteins have been identified (Table 2).

Metal sensors define the boundaries of metal excess and metal deficiency in the cell. These values are defined by the affinities of the sensors for metals. Accordingly, two zinc sensors, zinc uptake regulator (Zur) and zinc-responsive regulator (ZntR), from *Escherichia coli* have very high affinities (10^{-15} M) for zinc. At higher zinc concentrations, Zur represses the transcription of zinc-importing ABC-type transporter and ZntR activates zinc-exporting P₁-type ATPase expression [66-68]. Similarly, high affinities (10^{-21} M, less than one atom per cell) have also been measured for *E. coli* copper efflux regulator (CueR) that regulates the expression of copper-exporting P₁-type ATPase and multi-copper oxidase (CueO) [69]. These high affinities indicate that practically all zinc and copper within cells are complexed and the levels of free zinc and copper in the cytosol are vanishingly low.

In respect to oxidative stress, the regulators of genes involved in iron homeostasis are the most important. Bacterial iron metabolism is regulated in response to iron availability and the regulation is mediated in many bacteria by ferric-uptake regulator protein (Fur). Fur acts as a positive repressor and controls iron-dependent expression of over 90 genes [70]. It represses the transcription of genes by Fe²⁺ binding, and derepresses the transcription in the absence of Fe²⁺. The affinity of Fur for Fe²⁺ (10 μM) matches the concentration of ferrous iron in the cytosol and is, therefore, well suited for sensing the changes in Fe²⁺ levels in the cytosol [71,72]. It is interesting that oxidative stress regulators OxyR and SoxRS also activate the expression of Fur, emphasizing the link between iron homeostasis and redox stress management [73]. Other Fur orthologs have been characterized as well, and they include sensors for various transition metal ions, like the Zn²⁺-sensor Zur [68], the Mn²⁺/Fe²⁺-sensor Mur [74] and the Ni²⁺-sensor Nur [75]. Although Fur is the major iron sensor, other iron sensors have been characterized, such as the DtxR (diphtheria toxin repressor) family, which also includes Mn²⁺-sensors. Like Fur, DtxR is a Fe²⁺-dependent repressor, although it bears no sequence similarity to Fur [57]. In some Gram-positive bacteria, DtxR performs functionally analogous roles to Fur [76].

Table 2. Structural families of metalloregulatory proteins.

Regulators that control the gene expression of metal efflux and storage proteins		
Protein family	Metal sensing	Oxidative stress sensing*
ArsR [77,78]	Co, Ni, Cu, Zn, As, Cd, Sb, Hg, Pb, Bi	Yes
CopY [79]	Cu	No
CsoR [80]	Co, Ni, Cu	Yes
MerR [81,82]	Co, Cu, Zn, Ag, Cd, Au, Hg, Pb	Yes
TetR [55]	Zn	No
Regulators that control the gene expression of metal uptake proteins		
Protein family	Metal sensing	Oxidative stress sensing
DtxR [81]	Mn, Fe	No
Fur [75]	Mn, Fe, Ni, Zn	Yes
LysR [83,84]	Mo	Yes
MarR [85]	Zn	Yes
NikR [86]	Ni	No

* Oxidative stress sensing indicates if any family member senses cytosolic oxidative stress. ArsR, arsenic-resistance regulatory protein; CopY, copper-responsive repressor protein; CsoR, copper-sensing transcriptional repressor; MerR, mercuric ion resistance regulator; TetR, tetracycline repressor protein; DtxR, diphtheria toxin repressor; Fur, ferric-uptake regulator; LysR, lysine regulator; MarR, multiple antibiotic resistance regulator; NikR, nickel responsive transcription factor.

5.1.4 Antioxidant enzymes in bacteria

Even with a tightly regulated metal homeostasis, bacteria encounter elevated levels of ROS that are produced both endogenously and exogenously. Consequently, bacteria produce a variety of compounds that elicit antioxidant features both *in vitro* and *in vivo*. For example, polyamines scavenge ROS [87]. Mn^{2+} has also been reported to function as ROS scavenger. Indeed, high levels of Mn^{2+} may compensate for the lack of ROS scavenging enzymes in some lactic acid bacteria [88,89]. Some non-enzymatic antioxidant molecules, such as glutathione, not only act as ROS scavengers but also function as substrates in certain enzymes involved in oxidative stress protection [90].

From the enzymatic point of view and regarding the three oxygen radicals, H_2O_2 , $\cdot O_2^-$, and $\cdot OH$, the former two can be enzymatically detoxified. Because $\cdot OH$ has a half-life of 10^{-9} s [91], its detoxification is not enzymatically feasible. Bacteria possess several enzymes that detoxify either H_2O_2 or $\cdot O_2^-$. The H_2O_2 and $\cdot O_2^-$ detoxification also reduces the availability of H_2O_2 and $\cdot O_2^-$ as substrates for the Haber-Weiss reaction and, therefore, the $\cdot OH$ formation in the cells is decreased.

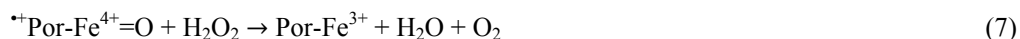
5.1.4.1 Hydrogen peroxide scavengers

Most bacteria utilize catalases and peroxidases as H_2O_2 scavengers. Catalases decompose H_2O_2 into O_2 and H_2O (Eq. 4) and constitute a diverse enzyme family. Peroxidases are enzymes that use a variety of electron donors to reduce H_2O_2 to H_2O (Eq. 5).

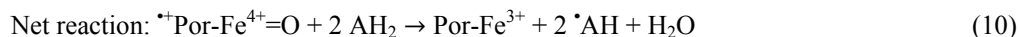
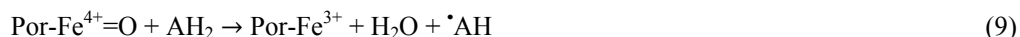


Most of catalases are heme enzymes but some have a di-manganese active site. The heme-containing catalases are divided into two major groups: monofunctional catalases which only have catalase activity, and bifunctional catalases (catalase-peroxidases) which also have peroxidase activity. A third group, the non-heme or di-manganese catalases (also known as pseudocatalases), constitutes a minor group of catalases.

Monofunctional, heme-containing catalases are the most widespread. They perform the H_2O_2 disproportionation by a common 2-step mechanism. In the first step, the heme in the resting stage enzyme is oxidized by a H_2O_2 molecule to an oxyferryl species [$^{++}\text{Por-Fe}^{4+}=\text{O}$] (compound I, oxoiron porphyrin π -cation radical species), and reduced back to the ferric enzyme in the second stage by a second H_2O_2 molecule. Thus, H_2O_2 functions both as an oxidant (Eq. 6) and a reductant (Eq. 7) in the overall reaction [92].



Despite their strong catalatic activity, bifunctional catalases do not share sequence similarity with monofunctional catalases but exhibit similar fold and active-site architecture as class I peroxidases [93]. Despite the structural differences, the overall catalatic reaction takes place *via* the same two steps (Eq. 6 and 7). Because of the peroxidatic activity, they can also use organic electron donors for the reduction of compound I. This proceeds *via* two one-electron transfers (Eq. 8, 9, and 10) [94]:



Alternatively, they can reduce compound I directly in a two-electron reaction back to the ferric enzyme by oxidizing short-chain aliphatic alcohols, such as ethanol (Eq. 11) [94]:



Non-heme catalases, which have a di-manganese as a catalytic group, are not as widespread as heme-containing catalases. The catalytic mechanism has two steps, like in heme-containing catalases, but the mechanism is essentially different. The di-manganese cluster is equally stable as 2,2 ($\text{Mn}^{2+}\text{-Mn}^{2+}$) or 3,3 ($\text{Mn}^{3+}\text{-Mn}^{3+}$) states and either the oxidation or the reduction stage of the reaction can occur first, depending on which form encounters

H₂O₂. If the 2,2 form encounters H₂O₂ the reaction proceeds *via* Eq. 12, while in the case of the 3,3 form the reaction proceeds *via* Eq. 13 [92].



In Eq. 12, H₂O₂ is an oxidant and the reaction involves removal of two electrons from the manganese cluster. A derivatized reactive intermediate is not produced. In Eq. 13, the H₂O₂ is a reductant and the reaction is simply a transfer of electrons to the manganese cluster with a formation of oxygen [92].

Peroxidases are enzymes that use H₂O₂ to oxidize another substrate. Peroxidases can be classified as heme peroxidases (which also include catalase-peroxidases) and non-heme peroxidases. Non-heme peroxidases include glutathione peroxidases, alkyl hydroperoxide reductases (Ahp), and NADH peroxidases.

An important scavenger of H₂O₂ in many bacteria is the two-component alkyl hydroperoxide reductase, AhpCF [95,96]. AhpC and AhpF are separate enzymes, which undergo electron transfers reactions to catalyze the NADH- (or to lesser extent NADPH-) dependent reduction of hydroperoxide substrates. A reactive, peroxidatic cysteine of AhpC is oxidized to sulfenic acid by H₂O₂, which subsequently condenses with another cysteine to form a disulfide bond. Exchange reactions with other cysteinyl residues rereduce the disulfide bond creating a second disulfide. AhpF, a separate disulfide reductase protein, reduces the second bond and regenerates AhpC in every catalytic cycle *via* electron transfer from NADH to AhpC through a flavin and two disulfide centers [97,98].

A controlled interplay in H₂O₂ scavenging exists in bacteria between catalases and peroxidases. At low concentrations, H₂O₂ is efficiently scavenged by AhpCF in *E. coli*. At very high H₂O₂ concentrations, AhpCF is inactivated probably to prevent the enzyme from exhausting the cellular NADH pool. Concomitantly, catalase becomes the major H₂O₂ scavenging enzyme [95].

5.1.4.2 Superoxide scavengers

The dedicated scavengers of superoxide in bacteria are superoxide dismutases (SOD). Bacteria synthesize various SODs that dismute $\cdot\text{O}_2^-$ to H₂O₂ and O₂. The general reaction is called a “ping-pong” mechanism because it involves the consecutive reduction and oxidation of the metal center with the associated oxidation and reduction of superoxide radicals (Eq. 14-16) [99].





Bacteria synthesize cytosolic SODs co-factored with manganese [100] and iron [101]. In addition, Gram-negative bacteria produce periplasmic copper/zinc co-factored SOD [102]. A nickel co-factored SOD has more recently been characterized even though the mechanism of the dismutation in this particular enzyme remains to be characterized [103]. Although SODs are extremely efficient enzymes (their rate constants approach catalytic perfection), bacteria synthesize them in abundance: they are four orders of magnitude more abundant than their substrate [104]. Some anaerobic bacteria lack SOD, but produce superoxide reductases instead. Superoxide reductases catalyze the reduction rather than the dismutation of superoxide (Eq. 17) [105]:



5.1.4.3 Other mechanisms

In addition to small molecule antioxidants and oxidative stress resistance proteins, bacteria can also employ other means to combat ROS. These means include various DNA and protein repair enzymes, such as those involved in base-excision repair pathways and in disulfide bond reduction. Another crucial aspect of oxidative stress protection is the complexation of Fe^{2+} in a safe form. A major portion of cellular iron in many organisms is complexed in a safe and bioavailable form in ferritins. Ferritins form their own subfamily within a large ferritin-like superfamily. The members of this subfamily have evolved efficient iron detoxification strategies. Details are given in the following sections.

5.2 Overview of the ferritin-like superfamily

The ferritin-like superfamily is widely spread across all kingdoms of life and consists of at least 13 protein families (Table 3). All the members of the superfamily share the same four-helical bundle, or at least part of the structural motif (Figure 3). Three superfamily members (COQ7, Coat F, and DUF2202) are not structurally characterized and their status in the superfamily remains uncertain. Ferritins are part of the superfamily and consist of three sub-families: the classical ferritins (Ftn), bacterioferritins (Bfr), and DNA-binding protein from starved cells (Dps).

Table 3. Members of the ferritin-like superfamily. The data were acquired from the PFM (http://pfam.sanger.ac.uk/) and Interpro (http://www.ebi.ac.uk/interpro/) databases.

Protein family	Main function	Found in
Ferritin	Iron storage / detoxification	Eukarya, Bacteria, Archaea
Ubiquinone biosynthesis protein COQ7	Ubiquinone biosynthesis	Eukarya, Bacteria
Fatty acid desaturase 2	Catalysis of the insertion of a double bond in fatty acids	Eukarya, Bacteria
Coat F	Part of the Bacillales endospore coat	Bacteria
tRNA-(ms[2]io[6]a)-hydroxylase (MiaE)	Hydroxylation of 2-methylthio- <i>N</i> -6-isopentenyl adenosine in tRNAs	Bacteria
Mn-catalase	Disproportionation of H ₂ O ₂	Eukarya, Bacteria, Archaea
Methane/Phenol/Toluene Hydroxylase	Catabolism of phenol and its methylated derivatives	Eukarya, Bacteria, Archaea
Ribonucleotide reductase, small chain	Synthesis of deoxyribonucleotides from ribonucleotides	Eukarya, Bacteria, Archaea
Rubryerythrin	Reduction of H ₂ O ₂	Eukarya, Bacteria, Archaea
Ferritin-like	Not known	Bacteria*
DUF2383	Not known	Eukarya, Bacteria
DUF892	Not known	Eukarya, Bacteria, Archaea
DUF2202	Not known	Bacteria, Archaea

* Taxonomic coverage not available.

5.2.1 Classical ferritins

Ftns are the main iron storage proteins in living organisms. The iron is stored inside a spherical cavity created by the assembly of 24 protein subunits [106,107]. The high iron storage capacity of Ftns (up to 4500 iron atoms per protein shell) makes them ideal for the storage of iron in a safe and bioavailable form. The spherical assembly of the subunits follows a 432-symmetry and has inner and outer diameter of 80 Å and 120 Å, respectively. Each subunit consists of five α -helices designated A, B, C, D, and E. Helices A-D form the four-helix bundle structural motif characteristic to the ferritin superfamily. The E-helix is located at one end of the cylindrical bundle.

Ftns are considered as the archetypical members of the ferritin subfamily. Mammalian Ftns are usually heteropolymers consisting of two types of subunits, H (heavy, \approx 21 kDa)-chain and L (light, \approx 19 kDa)-chain, which assemble in different ratios following tissue-specific distribution [108]. The two subunits are similar in sequence and fold but have functional differences. The H-chain contains an intrasubunit ferroxidase center (FOC) required for the oxidation of Fe²⁺ to Fe³⁺, whereas the L-chain is necessary for the nucleation of the iron core [109,110]. Owing to the differences in the subunit function, the subunit composition of Ftn isoforms influences the properties of the assembled Ftn: H-rich isoforms accumulate and release iron faster than L-rich isoforms and L-rich isoforms contain more iron than H-rich isoforms [111-113]. Hence, Ftn isoforms display a tissue specific

distribution: L-rich isoforms are typical for tissues storing iron (spleen, liver) and H-rich isoforms are more typical for tissues exhibiting high ferroxidase activity (heart, brain) [114,115]. In contrast to mammalian Ftns, the bacterial and plant Ftns are commonly homopolymers, with subunits bearing greater homology to mammalian H-chain than L-chain. Accordingly, the single subunit of bacterial Ftns contains the FOC similar to mammalian H-chain Ftn [116]. The plant Ftn subunits, however, are H/L-hybrids, containing both the H-chain characteristic FOC and L-chain site for iron nucleation [117]. Despite low sequence similarity between bacterial and mammalian Ftns, the protein folds are very similar.

So far, two Ftns from archaea have been structurally characterized. *Pyrococcus furiosus* Ftn is similar to bacterial Ftns [118]. However, Ftn from *Archaeoglobus fulgidis* displays some curious characteristics. Although the subunit is similar to typical Ftns, its quaternary structure has 32-tetrahedral symmetry, instead of the typical 432-octahedral symmetry. This results in a more loosely packed sphere with larger overall dimensions than those of typical Ftns. Another interesting characteristic of the structure is the presence of four large openings of approximately 45 Å in diameter in the protein shell that may allow the diffusion of large molecules inside the protein [119].

5.2.2 Bacterioferritins

Bfrs resemble Ftns although they are found only in bacteria and archaea. They have similar tertiary and quaternary structure as Ftns. Their FOC is located within the four-helix bundle subunit similarly to Ftns. Furthermore, many of the residues that contribute to iron binding are conserved between Bfr and Ftn. The most striking difference between Ftn and Bfr is the presence of 12 iron-protoporphyrin IX (heme) groups in Bfr [120-122] (although *Desulfovibrio desulfuricans* bacterioferritin contains iron-coproporphyrin III) [123]. Each heme moiety is located at the interface of two adjacent subunits and ligated by two Met residues related by a two-fold symmetry. However, not all Bfr subunits have the heme-binding capability. The function of the heme group is, therefore, largely unknown, although heme was recently found to facilitate iron release from the cavity of *E. coli* Bfr [124]. Bfrs have similar function as Ftns in iron storage oxidative stress resistance. Curiously, bacteria utilize either Ftn or Bfr as their main iron storage protein. Accordingly, in *E. coli*, FtnA plays a major role in iron storage, accounting for half of the cellular iron [125] while in *Salmonella typhimurium*, Bfr is the major iron storage protein with FtnA playing a minor role in iron storage [126].

Bfrs are most often homopolymers, but some bacteria (most notably cyanobacteria) encode two Bfr subunits, which seem to assemble in a heteropolymer fashion [127,128]. In this case, one subunit contains the conserved FOC while the other subunit contains heme. Because FOC is required for efficient iron mineralization and heme facilitates iron release, bacteria could efficiently regulate the iron homeostasis by adjusting the subunit composition of oligomeric Bfr.

5.2.3 Other members of the superfamily

Besides the ferritin subfamily, the ferritin-like superfamily contains several other members. They have diverse functions but are not iron storage proteins as ferritins (Table 3). There are also other iron core-forming proteins, such as frataxins [129]. However, they do not share the same four-helical bundle structural motif as the members of ferritin superfamily and are, therefore, not classified as members of this family.

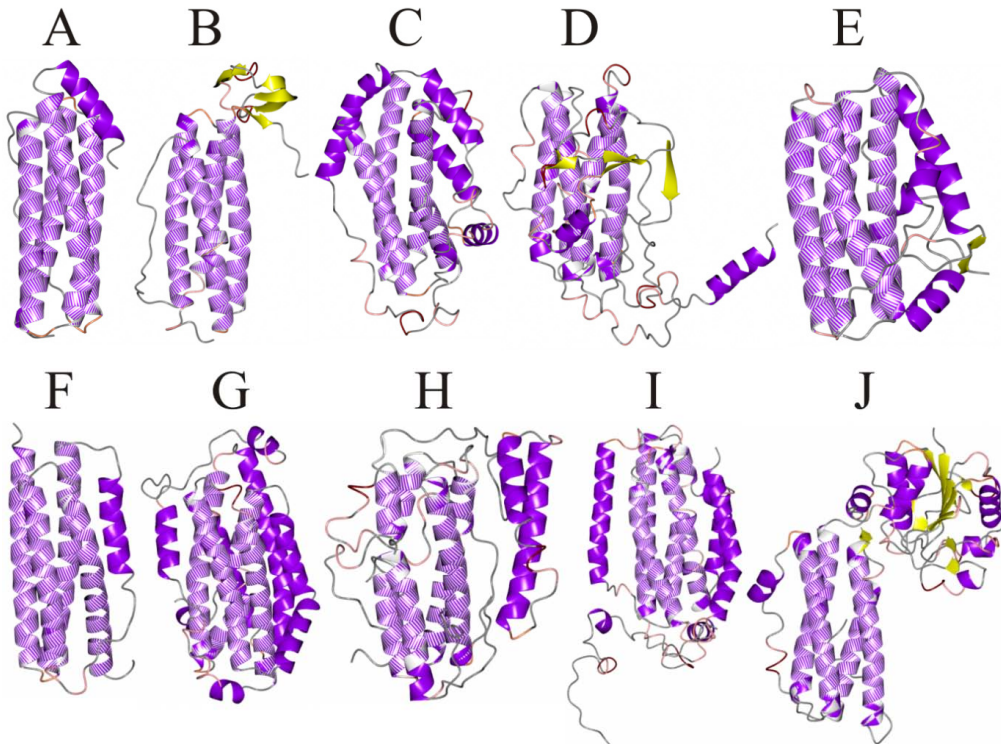


Figure 3. Monomer folds of the representatives of the members of the ferritin-like superfamily with a known structure. The helices belonging to the four-helix bundle fold are shown in light purple. PDB accession codes are shown in parentheses. A) *Escherichia coli* ferritin (1eum) [116], Ferritin; B) *Desulfovibrio vulgaris* rubrerythrin (1lko) [130], Rubrerythrin; C) *Mycobacterium tuberculosis* H37Rv acyl-ACP desaturase (1za0) [131], Fatty acid desaturase 2; D) *Thermus thermophilus* di-manganese catalase (2v8t) [132], Mn-catalase; E) *Pseudomonas Putida* KT2440 tRNA-(ms[2]io[6]a)-hydroxylase (2itb) [Joint Center for Structural Genomics, unpublished], MiaE; F) *Escherichia coli* YciF (2gs4) [133], DUF892; G) *Corynebacterium ammoniagenes* ribonucleotide reductase R2 (3dhz) [134], Ribonucleotide reductase, small chain; H) *Caulobacter crescentus* CB15 ferritin like protein (3h1l) [Joint Center for Structural Genomics, unpublished], Ferritin-like; I) *Pseudomonas mendocina* KR1 toluene 4-monooxygenase hydroxylase (3ge8) [135], Methane/Phenol/Toluene Hydroxylase; J) *Anabaena variabilis* ATCC 29413 two-domain protein containing dj-1/thij/pfpi-like and ferritin-like domains (3fse) [Joint Center for Structural Genomics, unpublished], DUF2383.

5.3 Dps proteins

Dps proteins are prokaryotic proteins found almost in every bacteria and archaea studied so far. As members of the ferritin subfamily, they are related to Ftn and Bfr both structurally and functionally. Because some bacteria encode all three proteins (Ftn, Bfr, and Dps), a question may be asked: Why do some bacteria possess three similar iron storage proteins? A simple answer is that although Dps proteins are well capable of storing iron inside the protein shell, the primary role of the protein is not iron storage but protection against oxidative stress. This is achieved by simultaneous oxidation of Fe^{2+} and reduction of H_2O_2 . In addition, Dps proteins protect the cell in a manner not shared by either Ftn or Bfr. Indeed, Dps is able to physically shield DNA, blocking ROS and other harmful agents from damaging it. Owing to their widespread presence in prokaryotes and abundance in the cell during oxidative stress, Dps proteins can be considered to be in the frontline of defence against ROS in many prokaryotes. However, the functions of Dps proteins are not limited to protection against ROS. Several different, and sometimes surprising, functions have been linked to the protein. Consequently, Dps proteins appear to stand out from the other proteins of the ferritin subfamily by having functions not only in iron detoxification but also in stress response, bacterial survival, and virulence.

5.3.1 Structural characteristics

The first Dps crystal structure was determined in 1998 from *Escherichia coli* [136] and thereafter the structural information of Dps proteins has steadily increased. Now, several Dps crystal structures have been determined, two of them from archaea. All of the Dps proteins have a common tertiary structure (described in the following section) but, unlike Ftn and Bfr proteins, they form 12-mers instead of 24-mers. In addition, the structures of Dps paralogs from the same organism have been determined for a few bacteria. Despite the conservation of the tertiary and quaternary structure, some structural diversity exists among Dps proteins. These differences, although often small, result in key differences in the protein function.

5.3.1.1 Monomer architecture

Dps monomers are relatively small (≈ 20 kDa) all-alpha-helical proteins with approximate diameters of $55 \text{ \AA} \times 39 \text{ \AA} \times 27 \text{ \AA}$ [137]. They fold into a compact four-helix bundle, similarly to the Ftn and Bfr monomers. About 70 % of the residues are situated in five helices: A, B, BC, C, and D, corresponding to residues 22-53, 58-87, 94-102, 113-139, and 141-165, respectively, in *E. coli* Dps (*EcDps*) [136]. Helices A and B are connected by a short loop, as are helices C and D. Together these four helices constitute the classical four-helix bundle of ferritins. A long loop that runs along the length of the bundle connects helices B and C. In the middle of the loop, a short BC helix characteristic to Dps proteins but not to Ftms or Bfrs, is found. Dps misses the fifth, C-terminal E helix present in Ftms and Bfrs. Overall, the core structure of the bundle fold is highly conserved, but variations exist in the N- and C-termini (Fig. 4). Some Dps proteins, for example, have long N- or C-terminal extensions that are

often flexible, lacking a regular secondary structure and are only partially visible in crystal structures. However, in some cases, the termini are stabilized by crystal packing [137] or, in other cases, they form a short helix [138-140].

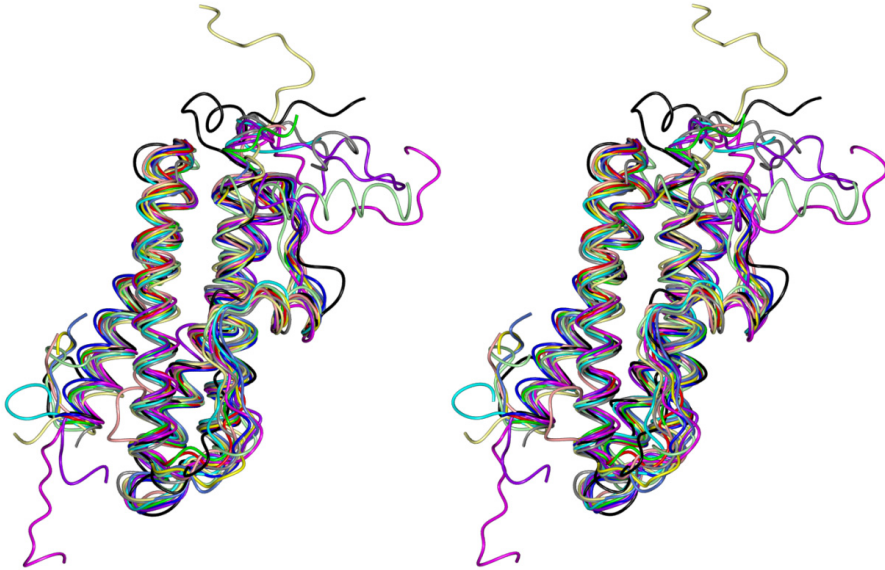


Figure 4. Conservation of the four-helix bundle fold in Dps proteins. Comparison of the monomers of several Dps crystal structures as stereo presentation. PDB accession codes are shown in parentheses. *Escherichia coli* Dps (1dps) [136], grey; *Helicobacter pylori* Nap (1ji4) [141], blue; *Bacillus anthracis* Dps1 (1ji5) [142], red; *Bacillus brevis* Dps (1n1q) [143], green; *Listeria innocua* Dps (1qgh) [144], yellow; *Halobacterium salinarum* DpsA (1tjo) [145], magenta; *Streptococcus suis* Dpr (1umn) [137], light blue; *Mycobacterium smegmatis* Dps1 (1uvh) [146], light green; *Mycobacterium smegmatis* Dps2 (2z90) [147], lemon; *Deinococcus radiodurans* Dps1 (2c2u) [148], purple; *Sulfolobus solfataricus* Dps (2clb) [139], black; *Borrelia burgdorferi* NapA (2pyb) [149], pink.

5.3.1.2 Packing of the dodecamer

Three distinct interfaces can be distinguished in Dps dodecamer: a dimer interface, a trimer interface near the N-termini of the monomers, and another trimer interface near the C-termini of the monomers. Six 2-fold axes can be found in the dodecamer and, as a result, the 12 monomers form six dimers. The monomers are arranged as dimers with their long axes anti-parallel to each other (Fig. 5A). In this way, the BC-helices, the loops around the BC-helices, and helices A and B of both monomers participate in the monomer-monomer interactions.

Near the N-termini of the monomers, a 3-fold axis creates a trimeric interface resembling that of ferritins (Fig. 5B). This interface is built by identical residues from each of the monomers from the C-terminal part of C-helix, the N-terminal part of D-helix, and the loop between them. This axis forms a channel connecting the surface of the dodecamer with the protein interior and is termed as a “ferritin-like” channel (or pore).

The second trimeric interface forms at the other side of the dodecamer, near the C-termini of the monomers (Fig. 5C). This interface is built by identical residues from each of the monomers from the C-terminal part of A-helix, the N-terminal part of B-helix, and the loop between them. Another channel, referred to as a “Dps-like” channel, connecting the protein exterior with the interior forms here. This channel is not found in ferritins and is, therefore, unique to Dps. Moreover, it is generally hydrophobic and more variable in terms of length and diameter than the ferritin-like channel [150].

Upon dodecamer formation, the protein interior encompasses helices B, D, and the C-terminal part of the A-helix, while helices BC, C, and the N-terminal part of the A-helix line the outer surface of the protein. The assembled Dps dodecamer has a 23-symmetry and can be described as a distorted icosahedron. The Dps dodecamer measures ≈ 90 Å in diameter with a central cavity of ≈ 45 Å. The Dps cavity, similarly to that of Ftns, is negatively charged owing to several carboxylate residues that surround it. This feature renders the Dps cavity an ideal environment for sequestration of positively charged metal cations. Despite the fact that dodecamers are the predominant oligomeric states of Dps proteins, a few Dps proteins have also been found to exist as dimers. The dimerization depends on the ionic strength or the pH of the solution [146,151]. However, the physiological relevance of such lower order oligomeric species is not known.

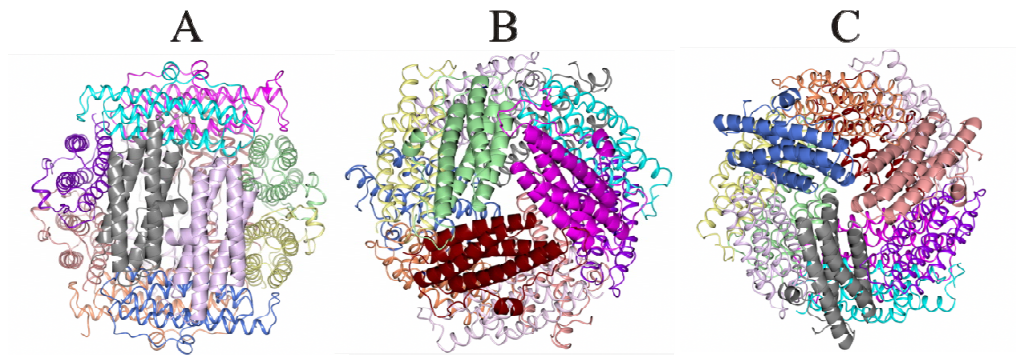


Figure 5. *EcDps* dodecamer (PDB accession code 1dps) [136]. Monomers are coloured in different colours and the monomers forming the presented axis are bolded. A) View down the two-fold axis. B) View down the N-terminal three-fold axis. C) View down the C-terminal three-fold axis.

5.3.1.3 Ferroxidase center

The FOC in Dps proteins is found in a shallow groove formed at the dimer interface. There are 12 FOCs in each Dps dodecamer, two in between each dimer. This arrangement results in two neighbouring centers at 22–24 Å apart from each other [143,144,148]. FOCs are highly conserved and constitute the most distinctive structural feature in Dps proteins; in other ferroxidases, the FOC is located within the four-helix bundle [144]. However, upon closer inspection, the helices A and B from both monomers can be visualized to form a special four-helix bundle accommodating two FOCs (Fig. 6). A conventional FOC is not present in every

Dps protein. *Lactococcus lactis* DpsA and DpsB do not possess a FOC at all [138] and archaeal Dps from *Sulfolobus solfataricus* has a bacterioferritin-like intrasubunit FOC [139].

A typical FOC contains two iron atoms connected by an oxo-bridge. In Ftms, iron is bound to the high-affinity iron-binding site A by a histidine and carboxylate residues. In the lower affinity site B, iron is only coordinated by carboxylates [109,116,152]. In Dps proteins, one subunit from the dimer interface provides metal coordinating histidines and the other subunit metal coordinating carboxylates. The only exception so far is *Thermosynechococcus elongatus* DpsA where a histidine replaces a canonical aspartic acid as a metal ligand in the A site [153].

Despite the structural conservation of the FOC, the metal-binding signature varies among Dps proteins. The FOC was first characterized in *Listeria innocua* Dps (*LiDps*), where one iron atom was found in site A. The iron was coordinated by two carboxylates from one subunit and one histidine from the adjacent subunit across the dimer interface [144]. Thereafter, monometallic FOCs were characterized from several Dps proteins, including *Helicobacter pylori* neutrophil-activating protein (*HpNap*), *Bacillus anthracis* Dps1 and Dps2, *Deinococcus radiodurans* Dps1 and *Streptococcus suis* Dps-like peroxide resistance protein (Dpr), while some Dps, like that of *E. coli*, contain two water molecules in the FOC [141,142,148,154,155]. A di-iron FOC has been observed in *Bacillus brevis* Dps (*BbDps*), *Borrelia burgdorferi* neutrophil-activating protein A (*BbNapA*), and in *Halobacterium salinarum* DpsA (*HsDpsA*) [143,145,149]. In addition, a di-zinc FOC has been found in *T. elongatus* DpsA [153] while the di-metallic character of the Dps FOC has been detected in titration measurements [156,157]. In di-metallic FOCs, another histidine also functions as a metal ligand. In *BbDps*, the ligands for iron in site A are His31, Asp58, and Glu62, while site B iron is liganded to His43, Glu62, and Glu47 via a water molecule (Fig. 6). A μ -oxo bridge was found between the iron atoms and the distance between the iron atoms was 3.3 Å, which is a typical value for di-iron sites in ferritins [116]. The μ -oxo bridge between two iron atoms represents a $\text{Fe}^{3+}\text{-O-Fe}^{3+}$ reaction intermediate during the oxidation of Fe^{2+} and it has also been observed in UV-visible difference spectrophotometric measurements of Dps and Bfr proteins [156,158-160], UV-visible difference spectrophotometric and Mössbauer studies of Ftms [161,162], as well as in Ftn crystal structures [116].

In *HsDpsA* low-iron state structure, a conserved water molecule in the B-site of mono-iron FOC was replaced by an iron atom in high-iron state structure [145]. This observation lent further proof for the role of the B-site as a more transient site in the iron oxidation. Altogether, the differences observed in the metal-binding properties despite the structural conservation of the FOC imply that metal ligands in the second coordination shell are important for the iron binding and oxidation properties of Dps.

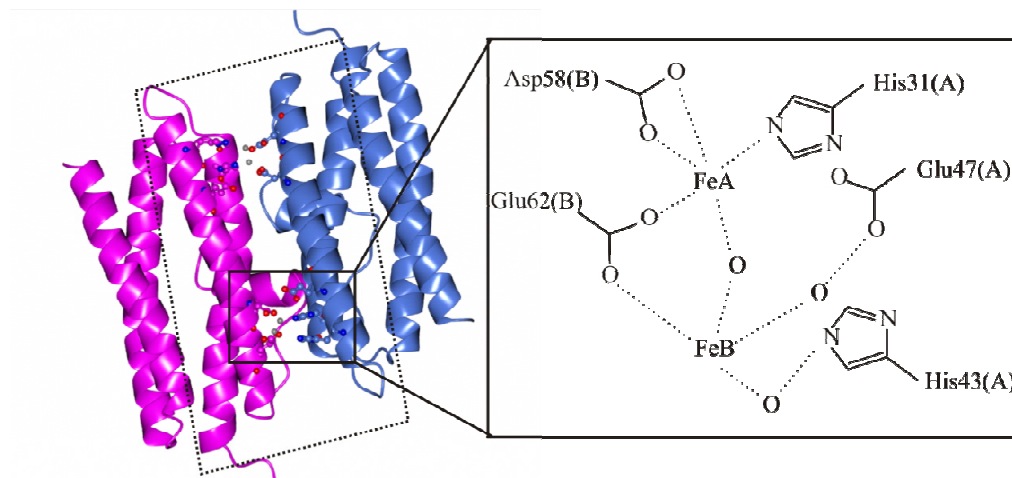


Figure 6. Di-iron ferroxidase center of Dps proteins. Overview of the dimer interface of *BbDps* (PDB accession code 1n1q) [143] and a schematic presentation of the di-iron FOC as an inset. The box with the dashed lines depicts the special four-helix bundle with two FOCs.

5.3.2 Detoxification of iron

Iron must be able to access the interior of the protein for oxidation at FOC and subsequent storage. The route of free, cytosolic Fe^{2+} to its final form as mineralized ferrihydrite (Fe^{3+}OOH) is a 5-step process: 1) Entry of Fe^{2+} inside the protein *via* entry channels, 2) Binding of Fe^{2+} to the ferroxidase centers, 3) Oxidation of Fe^{2+} to Fe^{3+} , 4) Nucleation of Fe^{3+} , and 5) Mineralization inside the cavity as Fe^{3+}OOH .

5.3.2.1 Entry to the protein shell

Dps proteins have eight 3-fold symmetry generated channels/pores that lead from the surface of the dodecamer to the interior (Section 5.3.1.2). Four of these channels are located near the N-termini of the monomers and the other four near the C-termini of the monomers. Iron enters the dodecamer *via* the N-terminal ferritin-like pores, which also correspond to the iron route of the mammalian Ftns [163-167]. The hydrophilic character of the channels is thought to guide Fe^{2+} inside the protein (Fig. 7A). The negative charge of the ferritin-like pores is contributed from a row of conserved carboxylate residues, which also function as metal ligands in the channels [140,148,153,168]. These pores are ≈ 10 Å in length and wide enough (7-11 Å at the inner opening) to allow for the passage of iron [169]. Although in some Dps proteins the pore narrows down significantly before opening to the cavity, iron passage is possible with minor structural rearrangements. Iron uptake is significantly reduced when the narrowest part of the channel (a conserved Asp) is blocked (Asp substituted by Phe) [170] or when the electrostatic potential of the narrowest part is changed (Asp substituted by Asn) [171], supporting the idea that the pores are used in iron transport. The only other openings to

the cavity are the Dps-like pores. However, these are significantly narrower than the ferritin-like pores and highly hydrophobic, rendering them unsuitable for efficient iron transport (Fig. 7B).

Archaeal DpsA from *H. salinarum* has an alternative iron translocation pathway. The ferritin-like pores of *HsDpsA* are blocked and cannot be used for iron transport without structural rearrangements. Instead, the protein uses 12 non-symmetric translocation pores, which form an alternative passage for iron inside the protein. This pathway is not conserved in bacterial Dps and might represent an adaptation of the protein to hypersaline environment. Because of the extreme salt concentration of the *H. salinarum* cytosol (5 M KCl), the electrostatic guidance of iron *via* ferritin-like pores as in bacterial Dps can not be achieved because long-range electrostatic interactions are shielded in high salt cytosol. In addition, *HsDpsA* uses histidines instead of carboxylates as iron ligands in the iron translocation pathway. The interference of potassium ions for iron binding in carboxylates might hamper iron transport in the protein whereas potassium does not compete with iron binding to histidines [145].

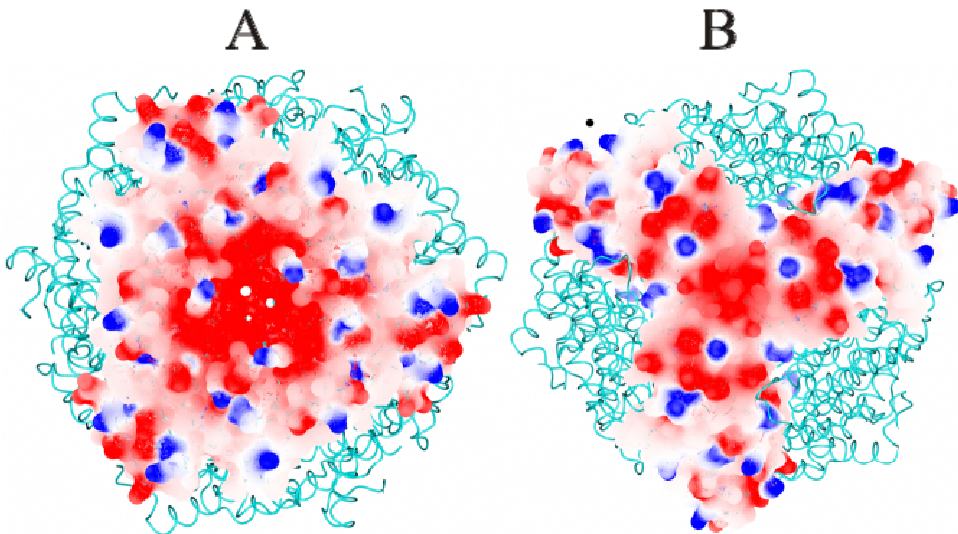


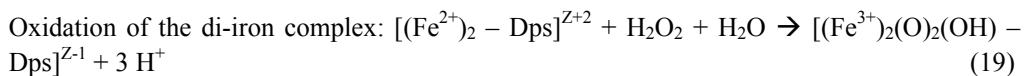
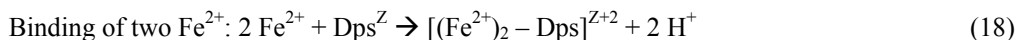
Figure 7. Electrostatic potential of the pores formed at the three-fold axes of *EcDps* (PDB accession code 1dps) [136]. The surfaces of the trimers contributing to the pores are shown according to their electrostatic potential. A) Pore formed at the N-terminal interface. B) Pore formed at the C-terminal interface.

5.3.2.2 Ferroxidase reaction

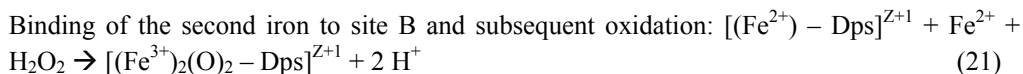
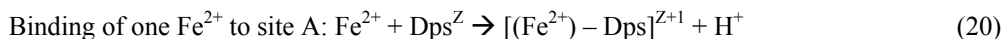
Once inside the protein, Fe^{2+} binds to the FOCs at the dimer interfaces (Fig. 6). In each FOC, two Fe^{2+} are oxidized per one H_2O_2 molecule reduced, efficiently limiting the formation of hydroxyl radicals [156,158]. Consequently, the iron oxidation reaction protects DNA by minimizing the dangerous combination of Fe^{2+} and H_2O_2 . At the same time, it also attenuates

the deleterious properties of H₂O₂. The FOC is required for the inhibition of the Fenton reaction but not for iron oxidation in the absence of H₂O₂ [157], indicating the primary role of Dps in oxidative stress resistance but not in iron storage.

The iron binding affinity of *LiDps* is ≈ 300 times higher than that of the human H-chain ferritin and ≈ 10 times higher than that of *E. coli* FtnA [158,166,172]. The overall reactions for iron binding and oxidation determined for *EcDps* and *LiDps* are similar. However, while *EcDps* binds two Fe²⁺ to FOC prior to oxidation, in *LiDps* the second Fe²⁺ binds and becomes oxidized only after the addition of oxidant (H₂O₂) [156,158]. Thus, the reaction mechanism for iron binding and oxidation for *EcDps* is:



In *LiDps* the reaction proceeds as follows:



O₂ can also be utilized as an oxidant but the reaction proceeds at a much lower rate than with H₂O₂ [156,158]. However, a few Dps proteins have been found to utilize O₂ as iron oxidant nearly as efficiently as H₂O₂ [153,159]. More surprisingly, Dps1 from *B. anthracis* does not have any ferroxidase activity in the presence of H₂O₂ but is able to use O₂ as iron oxidant [159].

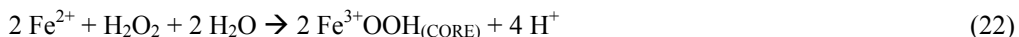
In iron limiting situations where bacteria encounter H₂O₂-mediated oxidative stress, the cytoplasmic Fe²⁺ concentration may not be enough to saturate the FOC with two Fe²⁺. Thus, the iron oxidation cannot proceed with the mechanisms presented above, leading to the production of odd electrons and, consequently, intraprotein radicals. These radicals do not diffuse out of the protein shell but are trapped by Trp and Tyr residues near the FOC. This adds yet another role for the protein cage as a trap of free electrons preventing them from damaging DNA [173].

5.3.2.3 Nucleation of iron and the structure of the iron core

After iron has been oxidized in the FOCs, it starts to nucleate. This is the initial stage of the formation of the mineral core. Mammalian Ftns contain distinct nucleation sites formed as clusters of glutamic acid residues within the L-subunits [113,174,175]. In bacterial Dps proteins, distinct nucleation sites have not been identified although residues similar to L-chain ferritin in *LiDps* have been suggested to be involved in iron nucleation [144]. However, these residues are not strictly conserved among Dps proteins and other negatively charged residues around the cavity might be utilized in iron core nucleation. It is also possible that no

distinct nucleation site exists in bacterial Dps but the nucleation is initiated by a negatively charged environment near the FOC. However, in archaeal Dps, alternative nucleation sites have been identified [145]. Again, the residues in these sites are not conserved among Dps and the sites probably represent novel nucleation sites in *HsDpsA*.

After nucleation, the iron accumulates in the negatively charged cavity as a microcrystalline core. The maximum iron capacity of Dps proteins is ≈ 500 iron atoms [156,159,176], significantly smaller than that of ferritins. The direct core formation inside the protein cavity proceeds similarly in both *EcDps* and *LiDps* [156,158]:



The mineralization reaction is faster than the ferroxidation reaction, a property different from Ftns where the mineralization reaction is slower than the ferroxidation reaction [156,160,162].

The structures of Ftn iron cores have been more widely studied than Dps iron cores. However, Dps cores have recently received attention as well, largely because of their potential in various applications in nanotechnology. Dps iron cores exhibit the same characteristics as Ftn iron cores. Iron forms a microcrystalline oxyhydroxide core that can be mobilized upon reduction and was initially found to display a tetrahedral coordination [155]. X-ray absorption near edge structure (XANES) from *Trichodesmium erythraeum* Dps, in turn, suggested that iron inside the fully loaded core is octahedrally coordinated [177]. Later, in extended X-ray absorption fine structure (EXAFS) analysis, the iron core of *S. suis* Dps was suggested to be a mixture of tetrahedrally and octahedrally coordinated species according to the ferrihydrite model proposed by Eggleton and Fitzpatrick [154,178].

Because the main function of Dps is not iron storage, the bioavailability of the deposited iron is not studied in detail. Iron can be reduced and released from the Dps cavity by sodium dithionite in anaerobic conditions and, in more physiologically relevant aerobic conditions, by NADH/FMN. The reduced iron has been found to exit the dodecamer *via* the same route as it enters, e.g., the ferritin-like pores [171]. Some studies, however, have suggested that the C-terminal Dps-like pore might be utilized for iron exit [148,168]. Nevertheless, it is not known whether iron release is actually physiologically relevant and if iron release from Dps proteins contributes to the cytosolic free iron pool during iron limitation.

5.3.3 DNA shielding

DNA damaging agents such as ROS and UV irradiation pose greater danger to bacteria during starvation than to actively growing cells. This is due to the scarcity of genetic material in nutrient deplete cells. Whereas log-phase cells contain several copies of chromosome, only one copy is usually found in stationary-phase cells [179]. This leads to several difficulties in managing DNA damage, as lesions cannot be repaired through homologous recombination pathways. Moreover, DNA repair requires rapid protein synthesis and energy, and is not

feasible in starved cells [180]. Accordingly, instead of achieving DNA protection via chemical processes, physical protection becomes an alternative means for bacteria.

5.3.3.1 DNA-binding signatures

The most distinct function of Dps proteins compared to the other members of the ferritin subfamily is their DNA-binding capability. Dps was first characterized as a DNA-binding protein and was not at that time known to exhibit any ferroxidase activity [181]. Although not all Dps proteins have DNA-binding ability, such property is an important factor in protecting DNA against ROS. Dps proteins do not have any classical DNA-binding motifs but they have been found to bind preferentially to duplex DNA that possesses two complete turns in the major groove [182].

The mobile N-terminus and its positively charged lysine residues have been found to contribute to the DNA-binding ability of *EcDps* [136,183]. The N-terminus has been linked to the DNA-binding ability of other Dps, as well [138,182]. In *Mycobacterium smegmatis* Dps1, which does not contain a protruded, flexible N-terminus, a long positively charged C-terminal tail is required for DNA-binding [146,184]. The absence of long, positively charged N-terminal tails has been found to correlate well with the absence of DNA-binding activity [142,176,185]. Furthermore, the lack of flexibility in the positively charged N-terminus seems to abolish DNA-binding ability, as seen in *Agrobacterium tumefaciens* Dps crystal structure where the positively charged tail interacts with the rest of the protein and becomes immobilized on the dodecamer's surface [186].

HpNap binds DNA despite the absence of N- or C-terminal tails and, therefore, bears unique DNA-binding properties among Dps proteins. The DNA-binding ability of *HpNap* is linked to the electrostatics of the dodecamer surface. Unlike other characterized Dps proteins, the *HpNap* dodecamer surface is positively charged at near neutral pH values, which enables it to bind the negatively charged DNA polymer [187].

Furthermore, *D. radiodurans* Dps1 has an unusual DNA-binding signature. In low salt solution it exists as a dimer and is capable of binding and protecting DNA against $\cdot\text{OH}$ and DNase I-mediated cleavage. While the dodecameric form is also able to bind DNA, it does not provide efficient protection to DNA [151].

In addition to pH, which controls the electrostatics of the N- and C-terminal tails and the dodecamer, Mg^{2+} has also been linked to the DNA-binding ability of Dps proteins [188]. MgCl_2 is able to abolish DNA condensation by Dps at appropriate concentrations but the specific role of Mg^{2+} in DNA binding is still not understood [183].

5.3.3.2 Biocrystallization

In stationary growth phase, Dps becomes the most abundant nucleoid component in *E. coli* and causes the compaction of DNA [189,190]. The binding of Dps to DNA results in large

and highly ordered complexes that represent a honeycomb arrangement when viewed with electron microscope both *in vivo* and *in vitro* [181,188,191]. These complexes form crystalline assemblies and can be essentially called biocrystals. The biocrystals protect DNA from ROS and other damaging agents [181,192,193]. The condensation of DNA is fully reversible and normal chromatin structure is restored when signals responsible for the Dps-dependent nucleoid condensation are removed [188].

Since Dps does not contain any classical DNA-binding motifs, the DNA-binding mode of the protein is not thoroughly understood. However, prolonged incubation of Dps was found to result in self-aggregation of the protein in solution [183,191]. Electron microscopic studies showed that these aggregates are two-dimensional crystals packed hexagonally with a spacing of $78 \pm 1 \text{ \AA}$ [191]. The self-aggregation behaviour of Dps is tightly linked to Dps-DNA co-crystallization [183]. When DNA is added to Dps, similar crystals are formed, indicating that incorporation of DNA does not disturb the hexagonal packing or the intraplanar spacing of the dodecamers. This, combined with similar packing of Dps observed in crystal structures, suggests that DNA is packed between layers of hexagonally arranged Dps dodecamers within the crystals [143,191,194].

5.3.4 Regulation in response to stress signals

The regulation of Dps expression displays significant variations between bacterial species. Generally, the production of Dps is induced at the onset of stationary phase when nutrients become scarce [181,195,196] and in response to oxidative stress [197-200] although some Dps proteins are not responsive to oxidative stress [201,202] or nutrient availability [200,201].

EcDps has functioned as a model protein in many studies concerning the regulation of Dps. *E. coli dps* transcription is induced at the onset of stationary phase by stationary phase-specific transcription factor, σ^S (also termed σ^{38}) [181], and the histone-like integration host factor (IHF) is required for the induction [197]. OxyR induces *dps* transcription when cells are treated with H_2O_2 in exponential growth phase [197]. OxyR also upregulates Dps expression in other bacteria [203-205]. When exponentially growing cells do not encounter oxidative stress, the *E. coli dps* transcription is repressed by the factor for inversion stimulation (Fis) and histone-like nucleoid structuring protein (H-NS) that bind to *dps* promoter [206].

EcDps is also under proteolytic regulation. During the exponential growth phase, Dps is degraded by ClpXP protease. However, the degradation ceases upon carbon starvation, suggesting that the degradation is efficiently controlled. During the stationary phase of the growth, however, proteolysis does not seem to play any significant role in controlling the Dps levels. Another protease, ClpAP, controls the Dps levels in an opposite way by indirectly maintaining the *dps* mRNA synthesis in stationary phase [207]. Recently, *EcDps* was found degraded by the N-end rule degradation pathway. The N-end rule degradation pathway is based on the fact that proteins have different half-lives depending on their N-terminal

residues [208]. After the cleavage of a few N-terminal residues from Dps (the mechanism is still unknown), ClpS interacts with the new N-terminal residue (Leu) and targets Dps for ClpAP degradation [209].

Several bacteria contain two or more Dps paralogs that are differentially regulated and can perform different functions. For example, nitrogen-fixing cyanobacteria possess multiple Dps proteins. These organisms have nitrogenase, a very sensitive enzyme to oxidative environment. Therefore, the presence of multiple Dps can be linked to the enhanced ROS scavenging requirements posed by the oxidizing environment [147].

Bacillus subtilis contains two genes encoding Dps paralogs that are differentially regulated, MrgA (metal-regulated gene A) and Dps. *mrgA* functions as a specific stress-regulated gene and is induced in response to oxidative stress, but not in response to other types of stress [200]. *mrgA* is also induced at the end of the logarithmic growth phase in the absence of iron and the induction is prevented by the excess of manganese, iron, cobalt, or copper, with manganese being the most potent effector. Additionally, the limitation of both iron and manganese is sufficient to start *mrgA* induction in exponentially growing cells [210]. PerR functions as a peroxide-sensing and metal sensing repressor of *mrgA* [211] and PerR has been found to be a transcriptional repressor of genes encoding Dps proteins also in other bacteria [212-214]. *B. subtilis* Dps expression is regulated by the general stress and starvation sigma factor, σ^B . Its expression is induced after heat, salt and ethanol stress, and in glucose starvation. However, *B. subtilis* Dps is not induced in response to oxidative stress [200].

Although the best-studied regulators of Dps expression are OxyR and PerR, Fur has also been found to play a role in the regulation of Dps [215-218]. Despite the fact that the expression of Dps proteins is generally linked to oxidative stress and starvation, the Dps proteins are also expressed in response to other stress signals. *Listeria monocytogenes* Dps is induced in response to cold or heat shock [219] and *Streptococcus thermophilus* Dps is expressed during cold shock [196,220]. *Campylobacter jejuni* Dps is constitutively expressed in logarithmic and stationary phase and no induction of Dps occurs in response to either H₂O₂ stress or during iron limitation or iron excess [185].

5.3.5 Other biological functions

The function of Dps proteins is not limited to the protection only against ROS. Indeed, Dps proteins confer protection against a multitude of stresses. In addition to stress protection, they exhibit an array of other biological functions, some of which have just recently been discovered and are still poorly characterized (Table 4).

EcDps offer resistance against copper stress whilst its DNA-binding activity is not necessary for the protection [221]. Because *EcDps* does not store copper inside the cavity and cells lacking Dps exhibit higher copper concentrations, an interesting question arises: Does Dps have a role in copper efflux? Dps also confers resistance to zinc stress [222,223]. Because the concentrations of both zinc and copper are increased in the sites of inflammation

[224], pathogenic bacteria may use Dps to cope with elevated metal concentrations during infection.

Pathogenic bacteria encounter extreme acidic conditions in the stomach of hosts and in the phagolysosome after their uptake by phagocytic cells. The acidic environment is extremely toxic to macromolecules, particularly DNA, resulting in depurination and depyrimidination. Acidification of cytosol is also harmful to the activity of several enzymes, which do not perform well outside near physiological pH values. Dps has been shown to protect DNA from acid stress as well as alkaline stress [222,223,225]. The DNA strand breakage induced by acid stress is prevented by the DNA-co-crystallization of *EcDps* [193]. However, because *Streptococcus pyogenes* Dpr also protects cells from acid stress and does not bind DNA, another mechanism, such as Dpr-mediated induction of genes that mitigate acid damage, may be involved.

Dps proteins confer resistance against heat stress, high-pressure stress, and gamma and UV irradiation [222,226]. The underlying protective mechanisms against these stresses are not well characterized. They may, for example, involve the prevention of single- and double-strand breaks in DNA by DNA condensation, or by recruitment of DNA repair enzymes. Moreover, ferroxidase activity might be employed as a defence mechanism since high pressure has been shown to increase oxidative stress [227].

Dps is also important for the virulence of several bacteria. Bacterial cells lacking Dps have been found to be less virulent. In agreement with that, *dps* deletion decreases the survival of bacteria in host cells as well as the lethality of the infected host [203,228]. Some of these properties can be attributed to the enhanced ROS resistance conferred by the protein e.g., against respiratory burst during phagocytosis.

The role of Dps in virulence is best studied in *HpNap*, a Dps homolog which was first discovered owing to its ability to induce the production of ROS in neutrophils [229]. *HpNap* is a major antigen in the human immune response. Antibodies against *HpNap* have been found in patients with several gastric diseases, including peptic ulcer and gastric cancer [230,231]. Following cells lysis, *H. pylori* releases *HpNap* that can subsequently cross the stomach epithelial layer and endothelium and stimulate the adherence and migration of leukocytes to the infected area [232,233]. *HpNap* also induces the activation of resident mast cells resulting in the release of proinflammatory mediators [232]. *HpNap* functions as a Toll-like receptor 2 agonist, stimulating neutrophils and monocytes to release interleukin (IL)-12 and IL-23 secretion, thus redirecting immune response towards Th1 cytotoxic type [234]. *HpNap* has actually been included in a promising vaccine, which is currently in clinical trial [235].

Dps from other bacteria can also contribute to virulence in various ways. *Campylobacter jejuni* enteritis is the most common antecedent to Guillain-Barré syndrome (GBS) [236]. *C. jejuni* Dps can bind and damage myelinated nerves *in vivo* suggesting that Dps is involved in *C. jejuni*-related GBS [237,238]. Finally, *B. burgdorferi*, the agent of Lyme disease, requires Dps for persistence within ticks [239]. Its Dps protein also possesses specific immune

modulatory properties. More specifically, it is able to induce the production of IL-1 β , IL-6, IL-23, and transforming growth factor β (TGF- β) by the cells of the innate immune system. It also drives synovial fluid T helper 17 (Th17) cell responses that might play a crucial role in the pathogenesis of Lyme arthritis [240].

A much wider array of functions has started to emerge for Dps proteins in recent years. *EcDps* has been discovered to function as a DNA replication gatekeeper during oxidative stress. The protein inhibits DnaA function in initiation by interfering with the strand opening in the replication origin [241]. Interestingly, a novel role for Dps as an *N*-acyl amino acid hydrolase, a catalyst of amide cleavage and amide formation, has been described in insect gut bacteria [242]. Surprising roles for Dps proteins might still emerge. For example, Dps proteins have been found localized to OM, where they have been linked to disinfectant-tolerance, antibiotic sensitivity, and resistance to bacteriophages [243-245].

Table 4. Various functions of Dps proteins in different organisms.

Protein	Ferroxidase activity	DNA binding	Other functions
<i>AtDps</i>	Yes [186]	No [186]	N.d.
<i>BaDps1</i>	Yes [142]	No [142]	N.d.
<i>BaDps2</i>	Yes [142]	No [142]	N.d.
<i>BbDps</i>	Yes [143]	Yes [143]	N.d.
<i>BbNapA</i>	Yes [149]	N.d.	Involved in virulence [149]
<i>CjDps</i>	Yes [185]	No [185]	Involved in virulence [237]
<i>DrDps1</i>	Yes [168]	Yes [182]	N.d.
<i>DrDps2</i>	Yes [140]	N.d.	N.d.
<i>EcDps</i>	Yes [156]	Yes [181]	Copper, acid, alkaline, high pressure, heat and gamma/UV irradiation stress resistance [221,222,226]
<i>HpNap</i>	Yes [246]	Yes [187]	Involved in virulence [246]
<i>HsDpsA</i>	Yes [145]	N.d.	N.d.
<i>LiDps</i>	Yes [176]	No [176]	N.d.
<i>LIDpsA</i>	No [138]	Yes [138]	N.d.
<i>LIDpsB</i>	No [138]	Yes [138]	N.d.
<i>LmDps</i>	Yes [247]	N.d.	Involved in virulence [248]
<i>MaDps</i>	Yes [242]	No [242]	<i>N</i> -acyl amino acid hydrolase [242]
<i>MsDps1</i>	Yes [146]	Yes [146]	N.d.
<i>MsDps2</i>	Yes [147]	Yes [249]	N.d.
<i>PfDps</i>	Yes [250]	N.d.	N.d.
<i>SeDps</i>	Yes [228]	N.d.	Involved in virulence [228]
<i>SmDpr</i>	Yes [251]	No [251]	N.d.
<i>SpDpr</i>	Yes [223]	No [223]	Acid, alkaline, and zinc stress resistance [223]
<i>SsDpr</i>	Yes [154]	No [252]	N.d.
<i>SsDps</i>	Yes [199]	N.d.	N.d.
<i>TeDps</i>	Yes [150]	No [150]	N.d.
<i>TeDpsA</i>	Yes [153]	No [153]	N.d.

N.d., Not determined. Ferroxidase activity has been marked as “yes” for proteins which have been found to bind iron at the FOC or the activity has been measured by other means. *AtDps*, *Agrobacterium tumefaciens* Dps; *BaDps1*, *Bacillus anthracis* Dps1; *BaDps2*, *Bacillus anthracis* Dps2; *BbDps*, *Bacillus brevis* Dps; *BbNapA*, *Borrelia burgdorferi* NapA; *CjDps*, *Campylobacter jejuni* Dps; *DrDps1*, *Deinococcus radiodurans* Dps1; *DrDps2*, *Deinococcus radiodurans* Dps2; *EcDps*, *Escherichia coli* Dps; *HpNap*, *Helicobacter pylori* Nap; *HsDpsA*, *Halobacterium salinarum* DpsA; *LiDps*, *Listeria innocua* Dps; *LIDpsA*, *Lactococcus lactis* DpsA; *LIDpsB*, *Lactococcus lactis* DpsB; *LmDps*, *Listeria monocytogenes* Dps; *MaDps*, *Microbacterium arborescens* Dps; *MsDps1*, *Mycobacterium smegmatis* Dps1; *MsDps2*, *Mycobacterium smegmatis* Dps2; *PfDps*, *Pyrococcus furiosus* Dps; *SeDps*, *Salmonella enterica* serovar Typhimurium Dps; *SmDpr*, *Streptococcus mutans* Dpr; *SpDpr*, *Streptococcus pyogenes* Dpr; *SsDpr*, *Streptococcus suis* Dpr; *SsDps*, *Sulfolobus solfataricus* Dps; *TeDps*, *Thermosynechococcus elongatus* Dps; *TeDpsA*, *Thermosynechococcus elongatus* DpsA.

5.3.6 Applications in nanotechnology

Protein cages have a potential to be used in a variety of applications, such as nanoscale material synthesis [253-255], magnetic resonance imaging [256], and cell-specific targeting [257]. Protein cages are useful in nanomaterial synthesis because they offer size-constrained

reaction templates. Ftns are doubly useful because of their intrinsic biomineralizing capability, allowing the synthesis of various minerals inside the protein.

Compared to 24-meric Ftns and Bfrs, Dps proteins provide an additional benefit in nanoparticle synthesis as the smaller size of the protein cavity allows the synthesis of nanoparticles with reduced dimensions. In addition, many Dps proteins are stable at high temperatures, a fact that further facilitates the usefulness of these proteins in synthetic applications. The characterization of Dps proteins from hyperthermophilic archaea is, therefore, of interest also from a biotechnological standpoint [199,250].

Protein cages are also amenable to genetic manipulation. Mutational redesign of the hydrophilic Dps cavity to a hydrophobic one can open new avenues for the use of the cavity in the synthesis of novel materials [258]. Notably, the re-design of the entire Dps assembly has been successfully conducted by adding the E-helix of Bfr to Dps. The resultant protein formed assemblies of intermediate size between Dps and Bfr despite the fact that they still consisted of 12 monomers [259].

LiDps has been used as a template of nanomaterial synthesis in various studies. Different nanoparticles composed of various metals, such as cobalt and platinum, have been synthesized inside the protein cage [260,261]. Biominerals have also been produced under various conditions in Dps. Under physiological conditions, iron forms amorphous ferric oxyhydroxide, while mineralization at high pH and temperature, and substoichiometric amounts of H₂O₂ result in the formation of maghemite (γ -Fe₂O₃) as evidenced by electron powder diffraction [262].

6 AIMS OF THE STUDY

S. suis and *S. pyogenes* are Gram-positive animal and human pathogens that can cause life-threatening illnesses. Importantly, they are catalase-negative even though they both endogenously produce high levels of H₂O₂ and also encounter elevated levels of H₂O₂ released by phagocytes during infection. Hence, Dpr proteins are especially important for the survival and pathogenesis of both bacteria and present a good target for the study of oxidative resistance mechanisms in these organisms.

This study aimed to:

- Provide further understanding of the structure-function relationship of iron-mediated oxidative stress defence in *S. suis* Dpr and *S. pyogenes* Dpr.
- Structurally characterize the FOC of Dpr proteins by using various metals as substitutes for iron.
- Study the protective mechanisms of Dpr in stress conditions induced by transition metals.
- Utilize site-directed mutagenesis to analyze the iron nucleation and mineralization process.
- Analyze the structure and magnetic properties of the iron core and study the applicability of *S. suis* Dpr in nanotechnological applications.

7 SUMMARY OF MATERIALS AND METHODS

7.1 Protein expression and purification

Truncated (7 residues deleted from the N-terminus) *S. suis* Dpr (*SsDpr*) and the *SsDpr* point mutants (D74A, E64A, E67A, E68A, and E75A) were cloned into the pET-30 Ek/LIC vector for overexpression. The vectors were transformed into BL21(DE3)pLysS competent cells by the heat shock method. The protein expression was carried out in LB medium supplemented with chloramphenicol (30 µg/ml) and kanamycin (30 µg/ml). The cultures were grown at 37 °C until OD₆₀₀ reached 0.5 and subsequently induced with 1 mM IPTG at 30 °C for 6 hours. Protein purification was performed by immobilized metal affinity chromatography followed by a thrombin cleavage of the 6xHis-tag at room temperature overnight. The proteins were further purified with gel filtration by the HiPrep 26/60 Sephacryl S-300 HR (GE Healthcare) column pre-equilibrated with 10 mM Tris-HCl pH 7.5, 150 mM NaCl. Protein concentrations were measured with a NanoDrop 2000c (Thermo Scientific). Purified recombinant *S. pyogenes* Dpr (*SpDpr*) was provided by Prof. J.-J. Wu [223].

7.2 *In vitro* iron loading and end-point iron staining

The maximal iron loading capacity of *SsDpr* was determined by an end-point *in vitro* iron incorporation assay. *SsDpr* (1 mg/ml) was incubated with different concentrations (ranging from 0 to 500 molar excess) of $\text{Fe}(\text{NH}_4)_2(\text{SO}_4)_2 \times 6 \text{H}_2\text{O}$ on ice for 1 hour. The samples were resolved with native PAGE and the adventitiously bound iron was removed by incubating the gel in 50 mM MES pH 6.0, 0.15 M NaCl, 5 mM EDTA, at room temperature for 2×15 min. Subsequently, the gel was incubated in 350 mM HCl, 25 mM potassium ferrocyanide at room temperature for 10 min and washed with distilled water 3×5 min. Finally, the gel was incubated in 50 mM Tris-HCl pH 8.0, 150 mM NaCl, 10 mM 3,3'-diaminobenzidine tetrahydrochloride, 10 mM H₂O₂ in dark for 5 min and thoroughly washed with distilled water. The maximal iron-loading capacity was determined from the stained gels.

Large scale iron loading to *SsDpr* and E64A, E67A, E68A, and E75A was carried out by incubating 1 mg/ml of protein with 500 molar excess of $\text{Fe}(\text{NH}_4)_2(\text{SO}_4)_2 \times 6 \text{H}_2\text{O}$ on ice for 1 hour. The proteins were subsequently dialyzed and filtered with 0.22 µm polyvinylidene fluoride (PVDF) filters to remove any excess of iron. The amount of incorporated iron was verified with inductively coupled plasma mass spectrometry (ICP-MS).

7.3 X-ray crystallography

7.3.1 Crystallizations

7.3.1.1 *S. suis* Dpr

SsDpr, E64A, E67A, E68A, and E75A were crystallized by the hanging drop vapour-diffusion method. Equal amounts of protein (10-15 mg/ml) and precipitant solution (20-35 %

v/v PEG400, 0.2 M CaCl₂, 0.1 M HEPES pH 7.0-7.5) were incubated at 16 °C. Normally the crystals appeared after 1-5 days and grew to a maximal size of 0.2 x 0.2 x 0.2 mm³ within 1-2 weeks afterwards.

Iron-soaked crystals were prepared by soaking apo-crystals in a freshly prepared reservoir solution containing 10 mM (NH₄)₂Fe(SO₄)₂ × 6 H₂O and 1 mM Na₂S₂O₄ for 10 min.

Co-crystallizations were performed by adding 1 mM CoCl₂ × 6H₂O, 1 mM CuCl₂ × 2H₂O, 2 mM MnCl₂ × 4H₂O, 0.75 mM NiCl₂ × 6H₂O, or 2 mM MgCl₂ × 6H₂O to the protein solution prior to crystallization.

7.3.1.2 *S. pyogenes* Dpr

Crystallization conditions for *SpDpr* were screened by the sitting drop vapour-diffusion method. Prior to crystallization, the protein was concentrated to 8 mg/ml in 20 mM Tris-HCl pH 7.5, 100 mM NaCl. Crystals were obtained with Formulation 34 (1 M succinic acid pH 7.0, 0.1 M HEPES pH 7.0, 1 % w/v PEG 2000 MME) of the INDEX Screen (Hampton). The crystal quality was improved by optimizing the crystallization conditions in a hanging drop vapour-diffusion setup. The optimized condition for the crystallizations was 1 M succinic acid pH 7.0, 0.1 M HEPES pH 7.0, 1 % w/v PEG 2000 MME, 5 % 2-propanol. Equal volumes of the precipitant and protein solutions were used and crystallization plates were equilibrated at 16 °C. Crystals appeared after a few days and grew to a full size of approximately 0.05 × 0.05 × 0.05 mm³ in a few weeks (Fig. 8). Prior to data collection the crystals were soaked for a few seconds in precipitant solution supplemented with 20 % v/v glycerol for cryo-protection.

Iron-loaded crystals were prepared by soaking the apo-crystals in precipitant solution supplemented with 20 % v/v glycerol, 20 mM Fe(NH₄)₂(SO₄)₂ × 6H₂O, 2 mM Na₂S₂O₄ for 30 min. Zinc soakings were prepared by soaking the apo-crystals in precipitant solution supplemented with 20 % v/v glycerol and 10 mM ZnCl₂ for 10 min.

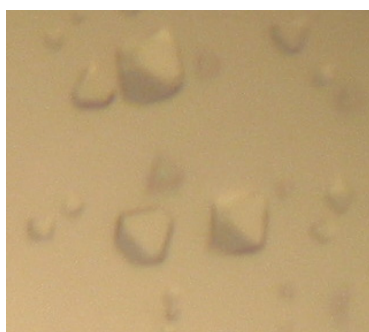


Figure 8. *SpDpr* crystals.

7.3.2 Data collection and processing

All X-ray diffraction data sets were collected on X12, X13, and BW7A beamlines at EMBL Hamburg (c/o DESY) at 100 K. The data were processed with the XDS package [263] or with MOSFLM [264] followed by SCALA [265]. All the SsDpr crystals belonged to the orthorhombic $P2_12_12_1$ space group and contained 12 monomers in the asymmetric unit. The SpDpr crystals were cubic ($F4_132$ space group) and contained one monomer in the asymmetric unit. The data processing statistics are displayed in Tables 5 (SsDpr-metal cation complexes), 6 (SsDpr mutants), and 7 (SpDpr).

Table 5. Data processing and refinement statistics for SsDpr-metal cation complexes.

	SsDpr-Ni ²⁺	SsDpr-Co ²⁺	SsDpr-Cu ²⁺	SsDpr-Mn ²⁺	SsDpr-Mg ²⁺
<i>Data processing</i>					
Beamline	EMBL-DESY X12	EMBL-DESY X12	EMBL-DESY X12	EMBL-DESY BW7A	EMBL-DESY BW7A
Wavelength (Å)	1.48746	1.60846	1.38047	0.90000	0.90000
Space group	$P2_12_12_1$	$P2_12_12_1$	$P2_12_12_1$	$P2_12_12_1$	$P2_12_12_1$
Unit cell parameters					
<i>a</i> , <i>b</i> , <i>c</i> (Å)	104.9, 137.5, 141.7	104.9, 137.4, 141.9	105.2, 138.1, 142.6	106.2, 139.5, 143.8	106.2, 139.7, 144.5
Resolution range (Å)	20.0–2.10 (2.21–2.10)*	25.0–2.30 (2.36–2.30)	25.0–2.10 (2.15–2.10)	50.0–2.40 (2.53–2.40)	40.0–2.20 (2.32–2.20)
Completeness (%)	99.0 (95.5)	96.6 (77.2)	98.4 (86.4)	99.9 (99.9)	99.9 (100.0)
$\langle I/\sigma(I) \rangle$	23.3 (9.7)	23.3 (9.7)	17.4 (3.7)	14.1 (2.8)	19.7 (4.4)
R_{merge}	6.7 (36.9)	5.4 (12.0)	6.9 (38.4)	10.0 (49.4)	8.1 (45.4)
Wilson B-factor (Å ²)	43.1	43.3	35.4	46.6	35.2
<i>Refinement</i>					
$R_{\text{cryst}}/R_{\text{free}}$ (%)	17.6/22.2	17.4/23.2	16.3/21.4	18.3/24.5	-
RMSD from ideal geometry					
Bond lengths (Å)	0.015	0.014	0.014	0.015	-
Bond angles (°)	1.4	1.3	1.3	1.3	-
PDB ID	2xjo	2xjm	2xjn	2xqb	-

* Statistics for the highest resolution shell are shown in parentheses.

Table 6. Data processing statistics for SsDpr mutants.

	E64A	E67A	E68A	E75A
<i>Data processing</i>				
Beamline	EMBL-DESY X12	EMBL-DESY X12	EMBL-DESY X12	EMBL-DESY X12
Wavelength (Å)	1.72003	1.72003	1.72005	1.72196
Space group	$P2_12_12_1$	$P2_12_12_1$	$P2_12_12_1$	$P2_12_12_1$
Unit cell parameters				
a, b, c (Å)	104.9, 137.3, 141.4	105.5, 137.7, 142.2	104.5, 137.5, 141.6	104.5, 137.8, 142.0
Resolution range (Å)	50.0-2.70 (2.85-2.70)*	20.0-2.85 (2.92-2.85)	25.0-2.20 (2.32-2.20)	40.0-2.40 (2.53-2.40)
Completeness (%)	100.0 (100.0)	99.5 (99.6)	99.9 (100.0)	92.3 (61.9)
$\langle I/\sigma(I) \rangle$	20.2 (5.2)	22.3 (3.6)	17.7 (6.5)	25.4 (5.8)
R_{merge}	9.2 (53.0)	10.6 (73.0)	10.2 (36.4)	6.6 (34.6)
Wilson B-factor (Å ²)	65.5	46.8	31.1	48.8

* Statistics for the highest resolution shell are shown in parentheses.

Table 7. Data processing and refinement statistics for SpDpr data sets.

	SpDpr	SpDpr-Fe ²⁺	SpDpr-Zn ²⁺
<i>Data processing</i>			
Beamline	EMBL-DESY X13	EMBL-DESY X13	EMBL-DESY X12
Wavelength (Å)	0.81	0.81	1.0
Space group	$F4_132$	$F4_132$	$F4_132$
Unit cell parameters			
$a = b = c$ (Å)	189.3	188.3	187.1
Resolution range (Å)	33.00-2.00 (2.11-2.00)*	43.20-1.93 (2.03-1.93)	60.0-2.1 (2.21-2.10)
Completeness (%)	99.9 (100.0)	92.7 (79.1)	100 (100)
$\langle I/\sigma(I) \rangle$	10.8 (3.5)	16.0 (4.9)	17.3 (5.8)
R_{merge}	15.4 (48.8)	9.3 (32.7)	16.4 (43.6)
Wilson B-factor (Å ²)	13.4	15.3	16.6
<i>Refinement</i>			
$R_{\text{cryst}}/R_{\text{free}}$ (%)	15.3/18.2	14.6/16.3	14.4/17.2
RMSD from ideal geometry			
Bond lengths (Å)	0.011	0.010	0.014
Bond angles (°)	1.0	1.0	1.2
PDB ID	2wla	2wlu	2xgw

* Statistics for the highest resolution shell are shown in parentheses.

7.3.3 Structure determination, refinement, and validation

7.3.3.1 *S. suis* Dpr

For all the *SsDpr* crystal structures, the phases were directly obtained from the apo-crystal structure (PDB accession code 1umn) [137]. Dpr crystal structures complexed with copper, manganese, cobalt, and nickel were refined with REFMAC5 [266] and the Translation/Libration/Screw refinement parameters were applied in the refinement. Manual building of the structures was performed with COOT [267] and the stereochemistry of the structures was validated with PROCHECK [265]. The data refinement statistics are displayed in Table 5.

E64A, E67A, E68A, and E75A mutants were refined with PHENIX.REFINE [268]. The manual building of the structures was performed with COOT and the stereochemistry of the structures was validated with MOLPROBITY [269]. The structures were not fully refined, because no structural differences were observed when compared with *SsDpr* crystal structure (PDB accession code 1umn) [137]. The R_{free} values for the partially refined structures are 23.2, 22.0, 22.7, and 23.7 % for E64A, E67A, E68A, and E75A, respectively.

7.3.3.2 *S. pyogenes* Dpr

The *SpDpr* structure was solved with molecular replacement. A polyalanine model of the monomer of *S. suis* Dpr (PDB accession code 1umn, sequence identity 48.2 %) [137] was used as a search model in PHASER [270]. The initial model was built with ARP/wARP [271] and further refined with REFMAC5. The phases for the iron and zinc loaded structures were derived directly from the *SpDpr* crystal structure and refined with REFMAC5. Manual building was performed in COOT and the stereochemistry of the structures was analyzed with PROCHECK. The data refinement statistics are displayed in Table 7.

7.4 X-ray absorption spectroscopy

7.4.1 Data collection

The iron-loaded samples of E64A, E67A, E68A, and E75A were supplemented with 20 % v/v glycerol and concentrated to 50 mg/ml. The samples were transferred into plastic sample holders with polyimide windows, frozen in liquid nitrogen and kept at 4 K during data collection. X-ray absorption spectra were collected at the Fe K-edge in fluorescence mode at Wiggler station 7-3 (Stanford Synchrotron Radiation Lightsource, Menlo Park, CA, USA), equipped with a Si(220) double-crystal monochromatic, a focusing mirror and a 30-element germanium solid-state fluorescence detector (Canberra). Dead-time correction was applied to the fluorescence signals and saturation effects were excluded because the dead time was always below 20 %. The energy axis of each scan was calibrated using a reference sample (Fe foil; absorption edge calibrated to 7112 eV). Scan averaging, normalization, and data reduction were performed with the KEMP2 [272] program using $E_0(\text{Fe}) = 7120$ eV.

7.4.2 Data analysis

The pre-edge peak areas were analyzed with WinXAS [273]. The K-edge EXAFS data were converted to photoelectron wave vector k -space and weighted by k^3 . The EXAFS data were refined with the DL_EXCURV package [274]. To avoid the overinterpretation of the data, the Debye-Waller factors were grouped according to distances for the iron shells. The number of oxygen ligands was fixed according to the pre-edge results. The R factors were used as a measure of the goodness of the fits.

7.5 Isothermal titration calorimetry

The interactions of SsDpr and D74A with the metal cations were studied with isothermal titration calorimetry (ITC) on a MCS-ITC titration calorimeter. Both the proteins and the metal cations were in 10 mM Tris-HCl (pH 7.5), 150 mM NaCl, except in the measurements with CuCl₂ where 10 mM Pipes (pH 7.5) were used instead of Tris-HCl, due to the high affinity of Tris for Cu²⁺. For MgCl₂, NiCl₂, CuCl₂, ZnCl₂, and CoCl₂ titrations, 5 μM of Dpr was titrated with a 4 mM solution of the metal chloride. Due to the low-enthalpy output of the reaction in the MnCl₂ titration, 15 μM of Dpr was titrated with 8 mM MnCl₂ solution. All the experiments were performed at 25 °C under aerobic conditions and repeated for at least three times. Origin® 5.0 (<http://www.originlab.com>) was used to fit the ITC data to a one-set-of-sites binding model and to a two-set-of-sites binding model.

7.6 Mössbauer spectroscopy

For the Mössbauer measurements, the iron-loaded SsDpr, E64A, E67A, E68A, and E75A were concentrated to 25 mg/ml and freeze-dried. The measurements were performed using a 25 mCi ⁵⁷Co:Rh source (Cyclotron Co.) at fixed temperatures of 77 and 300 K in transmission geometry with a maximum Doppler velocity of 2.05 mm/s and with a few additional measurements of 10.0 mm/s. The spectra were fitted using three spectral components defined by the following hyperfine parameters: the chemical isomer shift relative to α-Fe, the relative component intensities, the quadrupole coupling constants, and the resonance line width which was constrained to be equal for all three components.

7.7 Magnetic measurements

The samples were prepared the same way as those for the Mössbauer measurements. Direct current (DC) magnetization measurements were performed in a superconducting quantum interference device (SQUID) magnetometer at temperatures of 5-80 K and in magnetic fields up to 6 T. The samples were zero-field-cooled (ZFC), the magnetic field was increased to 10 mT and the temperature dependence of magnetization was measured. After it had reached 80 K, the temperature was decreased and the field-cooled (FC) curve was recorded. The magnetization loops were measured at 5, 20, 40, and 80 K and the maximum magnetic field

was 6 T. The alternating current (AC) magnetization measurements were performed in a Quantum Design physical property measurement system with the ACMS option at 1.9–20 K. The DC magnetic field was zero, the AC-field amplitude was 1 mT, and the magnetic field frequencies used were 100, 316, 1000, 3162, and 10000 Hz.

7.8 Inductively coupled plasma mass spectrometry

The concentrations of iron and phosphorus were determined with ICP-MS measurements. PerkinElmer Elan 6100 DRC+ was used in the analysis with masses 56 (Fe) and 31 (P). For mass 56, the dynamic reaction chamber was used to eliminate the ArO interference effect. The measurements were repeated 5 times.

8 RESULTS AND DISCUSSION

All lactic acid bacteria (*Streptococcus*, *Enterococcus*, and *Lactococcus*) lack the biosynthetic pathway of heme production. Therefore, they cannot synthesize cytochrome oxidases required for oxidative energy-linked metabolism or catalase required for H₂O₂ decomposition [275]. Some streptococci, such as *S. suis* and *S. pyogenes* also lack NADH peroxidase which catalyzes the breakdown of H₂O₂ to H₂O [276,277]. However, streptococci themselves produce H₂O₂ that is subsequently utilized as a virulence factor [278-282]. H₂O₂ is also encountered by the bacteria inside the host's phagocytes as part of the host defences during infection [283,284]. In addition, many Gram-positive bacteria cannot synthesize glutathione, an important molecule in the oxidative stress resistance, although some bacteria can acquire it from the growth medium. Consequently, several streptococci lack the high levels of intracellular glutathione found in many Gram-negative bacteria [285,286]. Taken together, one would think that without these widespread mechanisms for handling oxidative stress, aerobic conditions could pose severe restrictions for streptococcal growth. However, most streptococci are facultative anaerobes and many of them display a somewhat surprising level of aerotolerance [287].

Since lactic acid bacteria do not contain Ftn or Bfr [251], it seems they have very little use of iron storage proteins. Curiously, *S. suis* does not require iron for growth if manganese is available [8]. However, there is still an influx of iron cations into the cytosol if iron is present in the extracellular media. The role of Dpr in streptococci seems to be tightly linked to the detoxification of iron and H₂O₂. In addition, Dpr participates in the interplay of various stress resistances in streptococci [223].

8.1 Crystal structures of *S. pyogenes* Dpr (STUDIES I AND II)

Although crystal structures of several Dps proteins have been determined from a variety of bacteria, Dpr structures from only one streptococcus bacterium were available at the beginning of this thesis [137]. The lack of streptococcal Dpr structures is rather surprising since streptococci comprise a large group of bacteria that contain many human pathogens. Because of their lack of many other defence mechanisms against oxidative stress, streptococci are ideal organisms to study the role of Dpr in oxidative stress resistance.

The crystal structures of *Sp*Dpr without and with iron (*Sp*Dpr-Fe) and the structure of *Sp*Dpr complexed with zinc (*Sp*Dpr-Zn) were solved and refined to 2.0-, 1.93-, and 2.1-Å resolution, respectively. The quality of the structures is good based on the crystallographic residuals. The final R_{crist} and R_{free} for *Sp*Dpr are 15.3 % and 18.2 %, for *Sp*Dpr-Fe 14.6 % and 16.3 %, and for *Sp*Dpr-Zn 14.4 % and 17.2 %. A loop running between the first and the second α -helix in all the structures was only partially visible, and was not modelled in its entirety owing to the lack of electron density. There were no major changes in the overall structure between the complexes and the apo-structure, as indicated by the small root-mean-

square deviation between C α atoms (0.14 Å between *SpDpr* and *SpDpr*-Fe and 0.23 Å between *SpDpr* and *SpDpr*-Zn).

8.1.1 Description of the structures

SpDpr was crystallized as a monomer. The biologically active dodecamer with 23 point-group symmetry was created by applying the crystal symmetry operators. The *SpDpr* monomer follows the common four-helix bundle fold as other Dps proteins (Fig. 9A). In addition to the conserved bundle, *SpDpr* contains an N-terminal helix (N α), which is connected to helix A by a flexible loop that is only partially visible in the crystal structures. Helix N α is positioned almost perpendicularly to the four-helix bundle and is situated on the top of helices A and C. The overall structure of the dodecamer is similar to other Dps proteins forming a hollow sphere with inner and outer diameter of ≈ 45 Å and ≈ 90 Å, respectively (Fig. 9B). The two pores leading to the dodecamer cavity follow the general trend in Dps proteins. The N-terminal ferritin-like pore is hydrophilic and wide enough for cation transport. In contrast, the C-terminal Dps-like pore is hydrophobic and more constricted. In addition, three symmetry-related Tyr residues that restrict any cation passage block the Dps-like pore. This excludes the possibility that the Dps-like pore might be used as an auxiliary route for iron entry to the cavity or as an iron exit, as suggested for some Dps proteins [148,168]. The ferritin-like pores have conserved Asp residues that provide negative charges and bind iron and other metals in some Dps proteins. No metal ions were observed in the ferritin-like pore of *SpDpr* structures. However, a spherical electron density was found in the ferritin-like pore of *SpDpr*-Fe and it was assigned to a bound sodium ion based also on the nature of the surrounding residues. In a recently published structure of *Microbacterium arborescens* Dps, an iron cation was situated in the ferritin-like pore in a similar position as the sodium ion in *SpDpr*-Fe [288]. This suggests that the spherical electron density might actually arise from a low occupancy iron cation instead of a sodium ion.

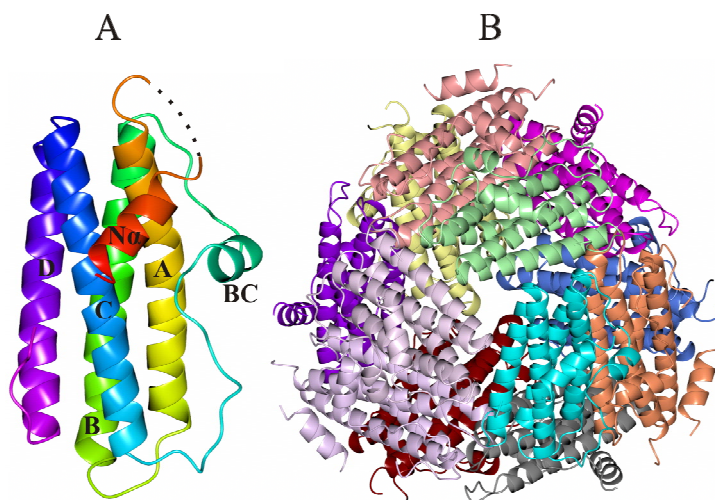


(Figure legend on the following page).

Figure 9. The tertiary and quaternary structure of *SpDpr*. A) *SpDpr* monomer. The helices are labelled and the flexible loop connecting the N-terminal helix and helix A is shown as a dotted line. B) *SpDpr* dodecamer. The view is down the 3-fold axis with the N-terminal pore towards the viewer. Monomers are coloured in different colours.

8.1.2 Novel N-terminal helix

A striking difference between *SpDpr* and most of the other Dps proteins is the presence of the N-terminal helix (N α). N-terminal helices have been found in three other Dps proteins, namely, in DpsA and DpsB from *L. lactis* MG1363 [138] and in *S. solfataricus* Dps [139]. However, in *SpDpr* three symmetry-related N α helices fold around the N-terminal pore creating a funnel around the channel contrary to the other three Dps proteins. Moreover, the N α in *SpDpr* does not participate in dodecamer stabilization as it does not interact with adjacent subunits. Helix N α contains no lysines and accordingly *SpDpr* does not interact with DNA as also confirmed by a gel mobility shift assay [223]. Conversely, the N-terminal helices of *L. lactis* and *S. solfataricus* Dps proteins have been implicated in DNA binding and contain lysines in their respective helices. Furthermore, the N α helix contains no metal binding sites, in contrast to the N-terminal helices of *L. lactis* DpsA and DpsB. Consequently, the biological role of the N α helix in *SpDpr* is still unanswered. Nevertheless, owing to its location around the N-terminal pore, it might help guiding the iron cations inside the protein for oxidation.

8.1.3 Variant ferroxidase centers

8.1.3.1 Binding of iron and changes in the ferroxidase center

SpDpr has the canonical FOC situated at the interface of two symmetry-related subunits. No metal cations were found in the crystal structure of *SpDpr*. Following the soaking with iron, the formation of a mono-iron FOC was observed. Mono-metal FOCs have previously been characterized from several other Dps crystal structures. Although the di-iron FOC is thought to be the functional form of the FOC, its characterization crystallographically is difficult owing to the transient role of the second iron-binding site in the oxidation process.

The iron in the *SpDpr*-Fe complex is coordinated to His50 from one subunit and Asp77 and Glu81 from a second subunit at the dimer interface. In addition, a water molecule was found ligated to iron. A glycerol molecule was located close to FOC and involved in an interaction with the iron. The coordination of the iron *SpDpr*-Fe FOC is very similar to other mono-iron FOCs in Dps proteins, except for the presence of the glycerol molecule. The binding of only one iron in the FOC might actually be explained by the presence of the glycerol molecule, which occupies the position of iron in the B-site. A glycerol molecule has also been found in the FOC of *D. radiodurans* Dps1, where it is also ligated to iron [148]. In the second ligation sphere three residues bind iron *via* the water and the glycerol molecules. Asp66 binds to iron *via* the water molecule and His62 and Lys160 *via* the glycerol molecule.

The binding of iron leads to conformational changes in the carboxylic residues around the FOC, indicating that the FOC is not preformed.

8.1.3.2 The di-zinc ferroxidase center

Zinc is a useful redox-stable replacement of iron in binding studies. The soaking of *SpDpr* crystals with zinc led to the binding of two zinc cations (ZN1 and ZN2) to the FOC (Fig. 10). ZN1 was also found to exist in two alternative conformations, A and B. The distance between ZN1A–ZN2 (3.51 Å) is typical for di-iron and di-zinc sites in proteins, whereas the ZN1B–ZN2 distance (2.71 Å) is shorter than normally found [116]. This led to the conclusion that ZN1B could represent an intermediate position of iron during the oxidation process. ZN1B is coordinated in a similar manner as the iron in the *SpDpr*-Fe complex, except that Asp66 also contributes to the binding. ZN1A occupies the position of the conserved water molecule (W2065) in the *SpDpr*-Fe FOC and is coordinated by His50 from one subunit and Asp66 and Asp77 from the second subunit. ZN2 is coordinated by one residue from each subunit, namely, His62 and Glu81. Instead of the glycerol molecule found in the *SpDpr*-Fe FOC, a succinic acid molecule was found bound near the FOC and involved in a direct interaction with ZN2.

The co-crystallization of *SsDpr* with zinc has been shown to result in a mono-zinc FOC [289]. The zinc superimposes well with ZN1B in *SpDpr*-Zn and is coordinated in a similar fashion by surrounding residues. A conserved water molecule in *SsDpr* FOC was proposed to be a zinc cation based on a low-resolution crystal structure. The presence of ZN2 at this site in *SpDpr*-Zn supports this hypothesis.

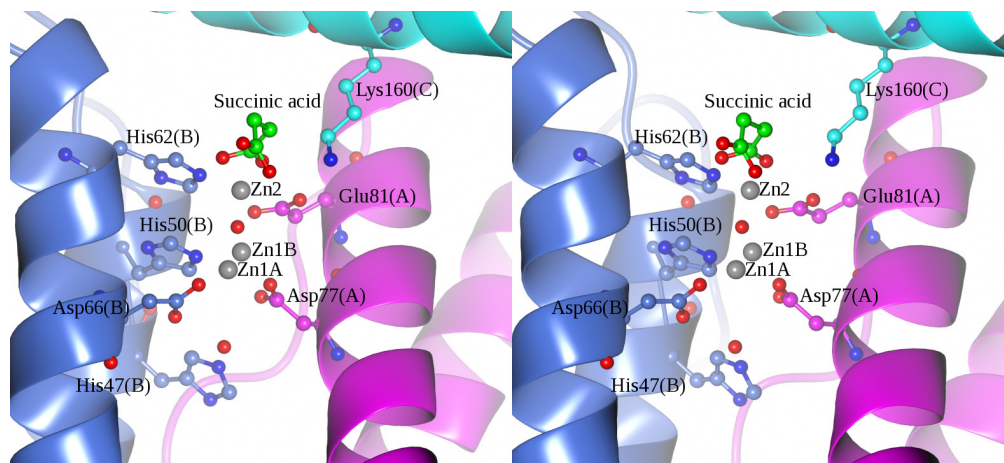


Figure 10. Stereo presentation of the di-zinc ferroxidase center of *SpDpr*.

8.1.3.3 Comparison of di-metal ferroxidase centers of Dps proteins

Di-iron FOCs from *BbDps* [143], *BbNapA* [149], and in archaeal *HsDpsA* [145] have been structurally characterized. The coordination of the two iron cations (in sites A and B) in the three proteins is very similar. Moreover, the conformations of the residues in the FOCs show high similarity, especially between the bacterial proteins *BbDps* and *BbNapA*.

Interestingly, in *SpDpr-Zn*, the two zinc cations do not superimpose well with the iron cations in the di-iron FOCs with the exception of ZN1B that superimposes with the FE1 of *BbDps* and *BbNapA*. In addition, all of the structures contain a bridging water molecule (or an oxo ion) between the metal cations.

The conformation of the residues involved in the metal binding, however, is similar with *SpDpr-Zn*, *BbDps*, and *BbNapA*. The only major difference between the *SpDpr-Zn* FOC and *BbDps* and *BbNapA* FOCs is the role of a single structurally aligned residue in the metal binding (Asp66 in *SpDpr-Zn*, Glu47 in *BbDps*, and Gln54 in *BbNapA*). Whereas Asp66 binds directly to ZN1, Glu47 binds FE2 *via* a water molecule and Gln54 does not participate in any interactions in the FOC. Because of the differences between the di-iron FOCs and the di-zinc FOC in *SpDpr-Zn*, the *SpDpr-Zn* FOC might represent a catalytically stable intermediate in the ferroxidase reaction.

A di-zinc FOC has also been identified in DpsA from *T. elongatus*. In *T. elongatus* DpsA, however, the conserved carboxylate residue in the FOC is replaced by a non-conserved histidine [153]. This feature alters the binding of the zinc cations considerably compared to other di-metal FOCs of Dps proteins. The ability of *T. elongatus* DpsA to bind two zinc cations was attributed to the presence of the histidine residue. Nevertheless, as shown with *SpDpr-Zn*, and also suggested for *SsDpr*, the binding of two zinc cations does not absolutely require a variant FOC. Taken together, the structural features of the *T. elongatus* DpsA FOC are not shared with *SpDpr*, and the two proteins might utilize different mechanisms for ferroxidase reaction.

The ferroxidase reaction mechanisms of Dps proteins in general might not be as similar as they could be thought based on the similarities of the FOC. Subtle but structurally significant changes on the first and the second ligation sphere of the metal cation might have an impact in the ferroxidase reaction mechanism and the reaction rate. The effect of the second ligation sphere residues has already been demonstrated for ferritins [290]. In Dps proteins, the ferroxidase reaction has been found to proceed slightly different in *EcDps* and *LiDps* despite the conservation of the FOC [156,158] (Section 5.3.2.2). In addition, the conformation of the residues in the FOCs of *B. anthracis* Dps1 and Dps2 are very similar but, unlike Dps2, Dps1 cannot utilize H₂O₂ as an oxidant in the ferroxidase reaction. Notably, the ferroxidase reaction also proceeds at different rates in the two proteins.

8.1.3.4 The effect of point-mutations to iron and zinc binding

In vitro iron and zinc loading followed by gel staining was used to study the effect of point mutations around the FOC in the iron and zinc incorporation of *SpDpr*. His50Ala, His62Ala, Asp66Ala, Asp77Ala, and Glu81Ala *SpDpr* mutants displayed a significant reduction in iron and zinc content. All of the above residues bind either directly or indirectly to the metal cations in *SpDpr*-Fe and *SpDpr*-Zn. Asp66 is a conserved FOC residue in Dps proteins and usually either Asp or Glu is found in its place. Surprisingly, a homologous mutation in *SsDpr* (Asp63Ala) did not affect the iron incorporation [170]. Both residues bind iron *via* a conserved water molecule in their respective FOCs except that this interaction seems to have greater importance in *SpDpr*. This lends further proof that subtle differences between the FOCs of Dps proteins can change the mechanism and the rate of iron binding and ferroxidase reaction.

8.1.4 Surface zinc-binding site and potential implications

An additional zinc-binding site was identified on the surface of *SpDpr*-Zn near the dimer interface and it was also capable of binding copper (T.H. and A.C.P., unpublished results). The zinc is coordinated by His100, two water molecules, and a chloride ion (Fig. 11A). Lys99 binds the zinc *via* one of the water molecules. Glu96 and Lys107 bind the zinc cation *via* the second water molecule. The residues are located in the small BC helix. His100 and Glu96 originate from the same monomer whereas Lys107 is located in the two-fold symmetry-related monomer. The only residue directly involved in the zinc binding, His100, is not conserved among Dps proteins. However, other streptococcal Dpr proteins have asparagine in the same place, offering a potential zinc ligand.

Usually zinc sites present in proteins have either structural, catalytic, or co-catalytic functions [291]. The coordination sphere of the zinc did not provide any clues of its possible function. Nevertheless, the concentrations of both zinc and copper are elevated in the site of inflammation and *SpDpr* has been found to protect the bacterium against zinc stress [223]. This novel zinc/copper site might, therefore, play a role in zinc and/or copper scavenging and explain the protective mechanism of Dpr against zinc stress.

Surface zinc sites have also been identified in *L. lactis* DpsA and DpsB, and *D. radiodurans* Dps1 [138,148]. In these proteins, the sites are located at the N-terminal extension (Fig. 11C-D). Although their function is unknown, the location of the sites suggests that they might be involved in DNA binding. In *D. radiodurans* Dps1, the zinc ion was coordinated by four residues (two histidines, one aspartic acid, and one glutamic acid) and thus it might function as a structural zinc site [291]. The site was also suggested to function as metal sensor or as a zinc finger involved in DNA interactions [148].

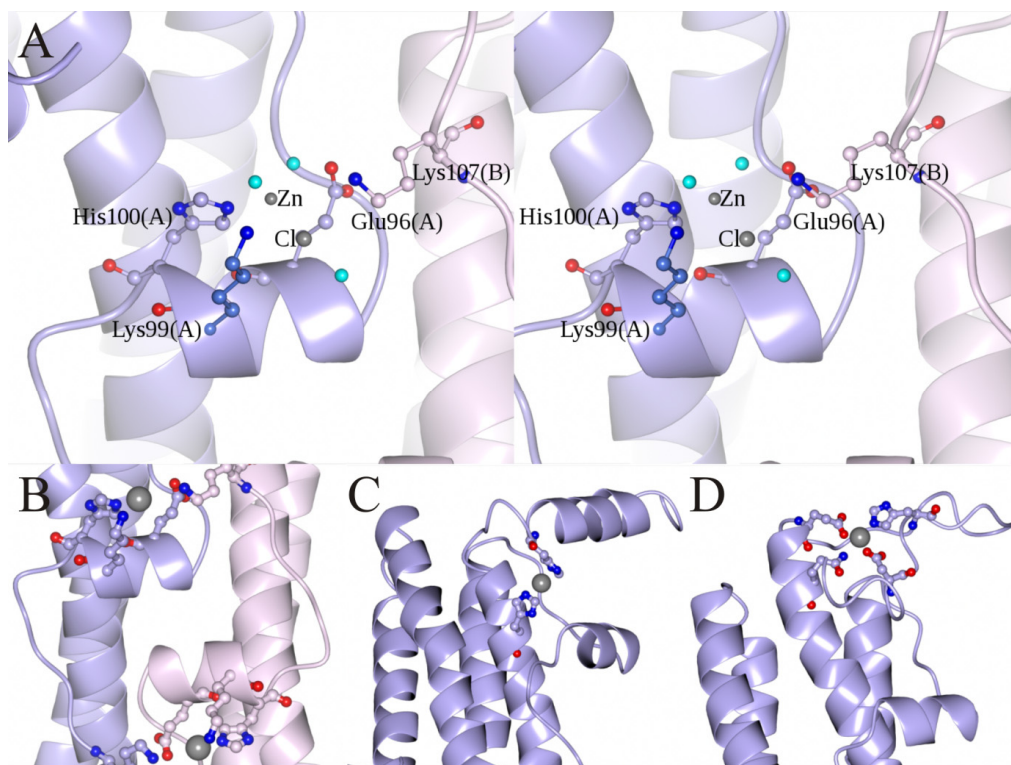


Figure 11. Surface zinc sites of three Dps proteins. A) Close-up stereo view of the surface zinc site in *SpDpr-Zn*. Water molecules are coloured in cyan. B) Surface zinc site in *SpDpr-Zn* near the dimer interface. C) Surface zinc site in *L. lactis* DpsA at the N-terminus (PDB accession code 1zu1) [138]. D) Surface zinc site in *D. radiodurans* Dps1 at the N-terminus (PDB accession code 2c2u) [148].

8.2 Metal cation binding to *S. suis* Dpr (STUDY III)

The binding of iron to Dps proteins has been of major interest in several studies. However, the binding of other transition metal cations has not been studied in detail. Binding sites for other metal cations have usually been discovered as a byproduct of *de novo* structure determination [136,168]. Still, these studies have indicated that Dps proteins are capable of binding various metal cations and possess sites other than the FOC for metal binding. The binding of six metal cations to *SsDpr* was studied in order to characterize different metal binding sites in the protein, to identify new metal binding sites, and to analyze the potential of this protein as a cage for the synthesis of nanosized materials.

8.2.1 Metal binding to the ferroxidase center

The mono-metal FOC of *SsDpr* has been crystallographically characterized before and iron, zinc, and terbium were found coordinated by His47, Asp74, and Asp78 in the FOC

[154,289]. His59 and Asp63 bind these metals indirectly *via* two conserved water molecules. In order to analyze further the metal binding specificity of the *SsDpr* FOC, the binding of four transition metal cations (Cu^{2+} , Co^{2+} , Ni^{2+} , and Mn^{2+}) and that of an alkaline earth metal (Mg^{2+}) were studied by X-ray crystallography. Mg^{2+} did not bind to the FOC, whereas all the other metal cations were found bound to the FOC. The coordination of the transition metal cations was similar to that of iron, zinc, and terbium (Fig. 12).

The binding of Mn^{2+} showed some variation when compared to the rest of the complexes. Glu78 was found tilted away from the binding site and, thus, Glu78OE1 was unable to interact with Mn^{2+} . Furthermore, one of the two conserved water molecules is missing in the structure thus abolishing the indirect interaction of His59 with Mn^{2+} . In the structure complexed with copper, Cu^{2+} was observed to bind with a partial occupancy indicating looser coordination of the complex. Surprisingly, none of the metal cations were found bound to the secondary zinc site observed in the *SsDpr* crystal structure complexed with zinc [289]. This site, therefore, appears to be specific for zinc.

Various metal binding sites have been observed in several Dps proteins. Usually, metal binding sites have been observed at the N- and C-terminal pores. In *SsDpr*, however, no additional metal binding sites besides FOC could be identified. This can be partly due to the low concentration of metal cations used in the co-crystallization as higher concentrations led to protein precipitation or inhibition of crystal growth.

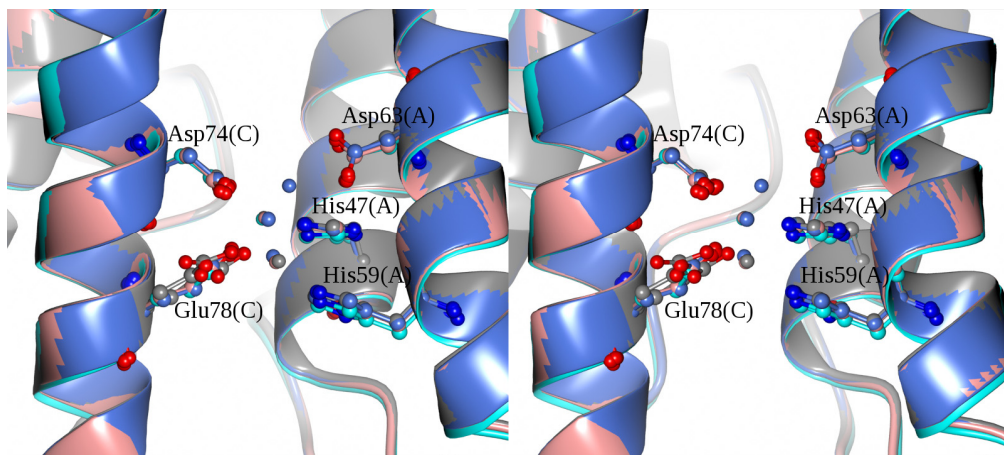


Figure 12. Comparison of the mono-metal ferroxidase centers as stereo presentation. The same colour is used for the protein, the conserved water molecules, and the respective transition metal for each structure. *SsDpr*- Co^{2+} is in pink, *SsDpr*- Cu^{2+} in grey, *SsDpr*- Ni^{2+} in light blue, and *SsDpr*- Mn^{2+} in cyan.

8.2.2 Thermodynamic properties of the metal binding

The binding of metal cations was further studied with ITC. In addition to *SsDpr*, a FOC mutant (D74A) with no ferroxidase activity was used in the titration measurements as a control.

From the metal cations analyzed, Zn^{2+} , Co^{2+} , Ni^{2+} , and Mn^{2+} bind to the protein, whereas Cu^{2+} and Mg^{2+} do not. With Mg^{2+} , the ITC results are consistent with the co-crystallization experiments. However, Cu^{2+} was found in the FOC of the crystal structure but its binding was not detected by ITC. It is possible that a low-enthalpy change of the Cu^{2+} binding prevented its detection with ITC.

Zn^{2+} , Co^{2+} , Ni^{2+} , and Mn^{2+} bind to *SsDpr* in an exothermic process with moderate affinities (binding constants from 0.18×10^{-5} to 0.98×10^{-5} M) indicating small free-energy changes upon complexation. ITC data demonstrated that all the metals bind in 24 sites in the protein suggesting a di-metal FOC (2 sites in each of the 12 monomers). The binding of the metals was driven both by enthalpy and entropy. In the case of Mn^{2+} and Co^{2+} , the two binding sites were thermodynamically equivalent whereas with Ni^{2+} and Zn^{2+} , fitting the data considering that the two sites are not equivalent, resulted in $n = 12$ for each site with differing binding constants. In both cases the binding constants were higher for site 1 than for site 2.

In the *SsDpr*-zinc crystal structure, zinc binds to the secondary zinc site in addition to the FOC [289]. Because only 2 zinc sites were found per monomer in ITC measurements, two scenarios arise from the Zn^{2+} titration data: 1) Zn^{2+} binds to FOC as a single cation, while the second zinc cation binds to the secondary zinc site, or 2) two Zn^{2+} cations bind to the FOC and the binding of the third cation to the secondary zinc site bears no measurable contribution to the ITC results, possibly due to low enthalpy.

Because the *SsDpr* ITC data suggested that two metal cations bind to the FOC even though only one could be seen in the crystal structures, the ITC measurements were repeated with the D74A mutant. Since Asp74 is a residue that ligates metal in the site A in the di-metal FOC of Dps proteins, it was assumed that the mutation of this residue to Ala would abolish the binding of metal cations completely or at least the binding of metal cation to one of the sites.

The binding of Mn^{2+} to D74A was thermodynamically analogous to its binding to *SsDpr*. Therefore, the mutation either does not alter the di-metallic character of the FOC or the other Mn^{2+} cation binds elsewhere in the protein monomer. Furthermore, the binding constant remains essentially unaltered. However, Co^{2+} binds to the D74A with only 12 sites. Despite the similar thermodynamic profile of the binding, the mutation clearly abolishes the second binding site for Co^{2+} . This implies that Co^{2+} cations bind to the FOC as di-metal species. Moreover, the binding of Ni^{2+} to D74A has the stoichiometry of $n = 12$, demonstrating that the mutation leads to the disruption of one of the binding sites. Unlike with Co^{2+} , the mutation also changes the thermodynamic profile of the binding. Although the binding constant does not change much, the mutation leads to an increase in enthalpy and decrease in entropy of the reaction. It, therefore, appears that the binding of Ni^{2+} to site 1 affects the binding of the second Ni^{2+} to site 2.

The binding of Zn^{2+} to D74A shows a substantially different thermodynamic behaviour, compared to other metal cations. The data supports a model in which 24 cations bind to the protein in an exothermic process and 36 cations in an endothermic process. It is unclear if the endothermic process, unique for the zinc binding, stems from the interaction of the FOC with the zinc cations or from the interaction of the zinc cations with the secondary site. It is, thus, not clear if the mutation abolishes the di-metallic character of the FOC although the thermodynamic parameters are severely changed. All in all, based on the ITC results, the SsDpr FOC seems to be di-metallic. However, the mutation of the Asp74 to Ala seems to have different effect on the binding of each metal cation. This can be due to the differences in the stability of the di-metal complexes when bound to FOC.

The binding of Fe^{2+} to SsDpr was not analyzed with ITC. Still, the interaction of *LiDps* with iron ($K_d = 0.023 \mu M$) suggests that Dps proteins have significantly higher affinity for Fe^{2+} than for other divalent transition metals. This indicates that other metals cannot easily compete with iron binding and they can inhibit iron binding only at relatively high concentrations. Nonetheless, at elevated concentrations, other transition metals are able to bind SsDpr and the binding appears to occur solely at the FOC with the exception of zinc. Because no other metal cations were able to bind to the secondary zinc site, a high specificity and a specific functional role of this site in SsDpr could be assumed.

More evidence has accumulated in recent years implicating Dps proteins in the protection of bacteria against metal stress. This form of protection would be especially important for bacterial pathogenesis. However, the specific mechanism of how this protection is achieved is not well studied and remains still elusive. The binding of various transition metal cations to SsDpr FOC indicates that the protective mechanism might be similar to that of iron, i.e., metal sequestration by FOC and deposition inside the cavity.

8.3 Structural and magnetic properties of *S. suis* Dpr iron core (STUDY IV)

The structure of the iron core of Dps proteins is of biological relevance. Indeed, the coordination of iron atoms has direct effects on the mobilization and chemical reactivity of the core. The iron core of Dps proteins consists of microcrystalline iron oxyhydroxide. Based on its microcrystalline nature and the fact that the core does not follow the symmetry of the protein crystal, the iron core can not be studied with X-ray crystallography. Other techniques, such as X-ray absorption spectroscopy (XAS) or high-resolution transmission electron microscopy, have to be utilized to provide structural insights.

Mössbauer spectroscopy together with magnetic measurements provides a powerful approach to study the magnetic properties of the iron core. Mössbauer spectroscopy is used to analyze the internal magnetism of the iron core and to detect local magnetic moments at the iron sites. No external magnetic field is required. Magnetic measurements, in turn, deduce the total magnetic moment of the iron core *via* its interaction with an externally applied magnetic field. The detailed determination of the magnetic properties of the iron core is complicated

due to the nanoscale size of the iron particle, its degree of crystallinity, and the possible heterogeneity of the iron oxyhydroxide phase as well as the varied amounts of phosphate incorporated in the core [292].

8.3.1 Structures of the iron cores

To understand the role of the negatively charged residues lining the *SsDpr* cavity, four point-mutants of *SsDpr* were constructed: E64A, E67A, E68A, and E75A. These mutations are expected to decrease the negative charge of the inner cavity and might affect the iron incorporation, nucleation, and mineralization (Fig. 13). Other residues contributing to the negative charge of the cavity were not mutated because they are part of either the FOC or the ferritin-like pore; thus, their replacement might have changed protein functionality in other ways. Of the mutated residues, Glu64, Glu67, and Glu68 lay close to each other and could form a site for iron nucleation. On the other hand, Glu75 is situated $> 10 \text{ \AA}$ from Glu64, Glu67, and Glu68. The ICP-MS analysis of the *in vitro* loaded iron cores of the *SsDpr* and the mutants revealed that the mutant proteins contained less iron than *SsDpr*. The iron contents in the proteins were 290, 240, 240, 250, and 260 Fe / dodecamer for *SsDpr*, E64A, E67A, E68A, and E75A, respectively. This result suggested that the mutations either affect the nucleation efficiency or decrease the maximum iron loading capacity of the protein. However, the lower iron content was not due to any structural changes in the overall structure of the proteins as evidenced by the crystal structures of the mutants. Additionally, none of the mutations had any significant effect on the iron incorporation, suggesting that none of the mutations disrupted the possible iron nucleation site.

The iron cores of the mutant proteins were analyzed with XAS. The pre-edge spectra were compared to the spectra measured previously for *SsDpr* [154]. The pre-edge features at $\approx 7113.5 \text{ eV}$ correspond to the quasi-forbidden $1s \rightarrow 3d$ transition. This transition is related to the electronic structure of the iron, and specifically to the $3d$ manifold. All the spectra were found to superimpose almost perfectly. This indicated no major changes in the structures of the iron cores between the mutants and wild-type *SsDpr*. The EXAFS analysis revealed essentially identical Fe-Fe distances as in the *SsDpr* core. Based on the pre-edge data, the first shell was best described by the presence of 5 to 6 oxygen atoms and the best fits were obtained by refining 5.5 oxygen atoms in the first shell. This number is slightly higher than previously determined for the *SsDpr* (5 oxygens in the first shell). The best fits were obtained by refining iron in three shells. The iron-iron distances of the refined models corresponded well to those observed in the *SsDpr* core. Because phosphorus had also been detected in the ferritin and Dps iron cores [154,293], a refinement taking into account a phosphate contribution to the scattering was also attempted. However, this approach substantially decreased the coordination number of iron and it was later abandoned when the ICP-MS measurements revealed only a minimal amount of phosphate in the cores. According to the XAS analysis, the structure of the iron cores was compatible with that of ferrihydrite.

The structure of the iron core may have potential implications in the mobilization of the deposited iron. Smaller cores have larger surface-to-interior ratio leading to higher amount of

more loosely packed iron. Smaller cores also seem to have larger amount of phosphate [154], rendering their structure less ordered. This leads to the hypothesis that for the cellular needs the mobilization and reutilization of iron is easier from a small core. When the size of the iron core grows, the packing of the iron becomes tighter and its utilization more difficult. This fits well to the suggested scheme that iron is continuously deposited in and released from the cavity according to the cellular needs [177]. Consequently, under extreme iron excess, the reutilization of the iron from the core would slow down or totally seize, preventing further increase of iron concentration in the cytosol.

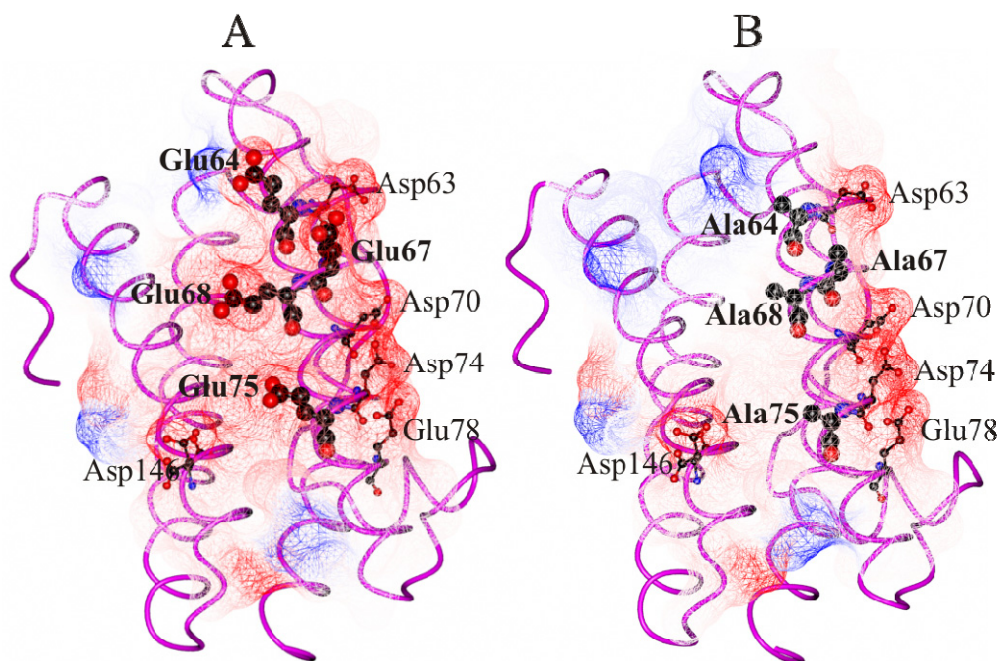


Figure 13. Contribution of the electrostatic potential of the mutated residues to the iron storage cavity of *SsDpr*. Residues contributing to the negative charge of the cavity are labelled and their electrostatic potential is shown. The mutated residues are shown in bold. The CB distances between the mutated residues are: E64-E67, 5.7 Å; E64-E68, 6.7 Å; E64-E75, 17.6 Å; E67-E68, 5.3 Å; E67-E75, 13.1 Å; E68-E75, 10.9 Å). A) *SsDpr* structure showing the distribution of the electrostatic potential of the labelled residues on the cavity surface. B) *SsDpr* structure showing the change in the electrostatic potential when Glu64, Glu67, Glu68, and Glu75 are replaced with Ala. PDB accession code 1um9 [137].

8.3.2 Magnetic properties of the iron nanoparticles

Although they are better studied in Ftms, the magnetic properties of *LiDps* iron core were recently characterized. The iron nanoparticles (about 3 nm in diameter) formed inside the *LiDps* dodecamers have superparamagnetic behaviour above 4.5 K and a large magnetic anisotropy. The lattice parameters of these nanoparticles matched those of maghemite or magnetite instead of ferrihydrite [294]. The iron mineralization was conducted in non-

physiological conditions of elevated temperature and pH and controlled oxidation, where iron mineralizes as maghemite or magnetite [262]. Thus, the magnetite phase does not represent the physiological state of the nanoparticle inside the *LiDps* cavity.

8.3.2.1 Magnetic measurements of the iron cores

The analysis of the magnetic properties of the iron cores of *SsDpr* and the four mutants were carried out with SQUID magnetometry. Similar behaviour was practically observed for all the proteins with superparamagnetism (i.e., random variations in magnetization as a result of thermal fluctuations) exhibited at a blocking temperature below 5 K in DC measurements. Accordingly, the ZFC and FC curves did not deviate from each other. The magnetic moment (i.e., the torque exerted on a magnet within a magnetic field) of each particle was determined independently, and the moments agreed well with the antiferromagnetic ordering of ferrihydrite. Ferrihydrite has a hexagonal crystal structure and contains two sublattices of Fe^{3+} ions whose magnetic moments are oriented in opposite directions. These two directions should compensate for each other and result in a magnetic moment of zero [295,296]. However, largely because of the unpaired surface moments and defects in the interior of the core, such as cation vacancies, a small magnetic moment exists in each *SsDpr* iron core [297] (Fig. 14). The magnetic moment of each of the mutants was higher (about 5–10 μ_{B} moment per particle) than for *SsDpr*. This finding can be explained by the smaller size of the iron cores of the mutants, which leads to a higher surface-to-volume ratio of the core and an increase in the number of unpaired spins in the core surface. The *SsDpr* iron core is hence a two-phase spin system as it has also been noticed for ferritin iron cores [292]. The frequency dependence of the blocking temperature was determined by the AC-magnetization measurements. As expected for superparamagnetic samples, the blocking temperature of the samples varies with frequency, and no differences were observed in the attempt frequency or magnetic anisotropy energy in the samples.

In broad perspective, the possibility of changing the iron mineralization rates of *Dps* proteins with selected mutations could allow the growing of superparamagnetic nanoparticles of controlled dimensions and narrow size distribution. This would give the opportunity to study the magnetism of nanoparticles of varied dimensions and enhance the understanding of magnetism at nanosize levels.

8.3.2.2 Mössbauer analysis of the iron cores

SsDpr and the mutants exhibited identical paramagnetic Mössbauer spectra at 300 K while the cooling of the samples down to 77 K did not cause any magnetic splitting of the resonance lines. The Mössbauer spectra exhibited a clear asymmetry and were modelled using a singlet line close to zero velocity, while the two doublet components were centered around 0.2–0.3 mm/s which is typical for high-spin Fe^{3+} in iron oxides. The nonzero quadrupole coupling constant for these components was compatible with superparamagnetic ferrihydrite particles [298]. The two quadrupole doublets have similar isomer shifts but

different quadrupole splittings. The larger quadrupole splitting probably originates from iron at the surface of the core (Fig. 14, red quadrupole doublet), while the smaller quadrupole splitting (Fig. 14, green quadrupole doublet) arises from the interior of the core. The singlet in the spectra (Fig. 14, blue singlet) covers $\approx 6\%$ of the total intensity of the spectra. This corresponds to ≈ 15 iron atoms, when the two doublets assigned to the iron core correspond to 240 iron atoms. Consequently, the singlet probably originates from the 12 iron atoms coordinated outside the iron core, at the FOC. This is further supported by its differing isomer shift, as the chemical environment of iron at the FOC is different from that of the oxygen-coordinated core iron atoms. An isomer shift close to zero velocity is difficult to be assigned to a specific oxidation state and it could be, for example, a low-spin Fe^{3+} , a zero-spin Fe^{2+} , or even Fe^{4+} . The latter can be excluded based on the iron loading conditions, the known ferroxidase reaction mechanism, and the results from XAS. Considering that iron dissociates from the binding site after oxidation, Fe^{3+} could not be expected at the FOC. Hence, the iron at the FOC is most likely a zero-spin Fe^{2+} .

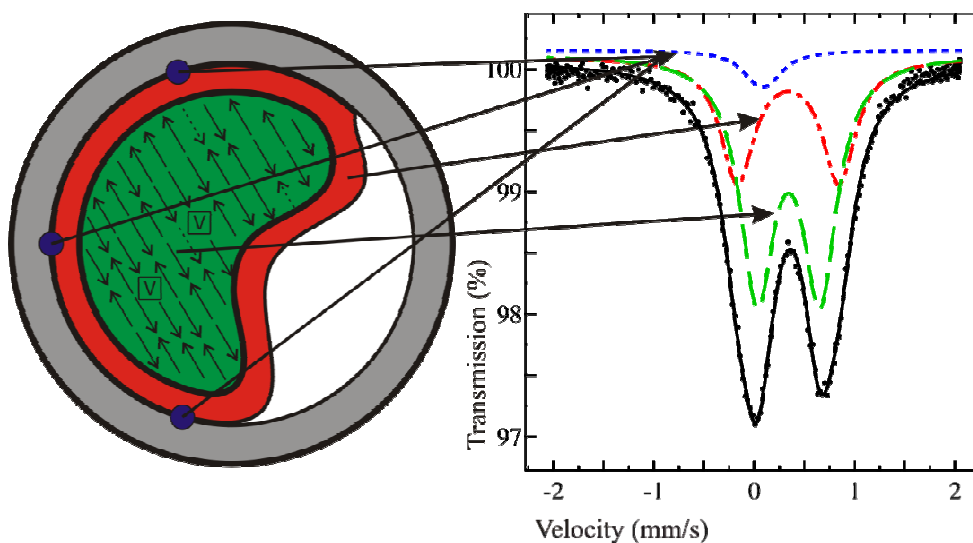


Figure 14. Schematic representation of the iron nanoparticle growth inside the Dps proteins. On the left: A schematic picture of *SsDpr* (gray), FOCs (blue), the interior of the iron core (green), and the surface of the iron core (red). Arrows in the interior of the iron core represent the magnetic organization in ferrihydrite with cation vacancies (V). Uncompensated magnetic moments are depicted with dashed arrows. On the right: The fitted Mössbauer spectrum of E68A recorded at 77 K. The arrows indicate the origin of the spectral components.

8.3.3 Potential nanotechnological applications of Dpr

Different protein cages, such as viruses, heat shock proteins, and ferritins, have been used as size-constrained reaction vessels for the synthesis of nanomaterials (Fig. 15). Compared to

most of the other protein cages, the Dps cavity offers smaller dimensions for the nanomaterial synthesis allowing the production of smaller nanoparticles. In addition, the intrinsic biomineralization ability of the protein renders it a versatile system for nanomaterial synthesis. The mutational redesign of *SsDpr* cavity presented here suggests that the iron incorporation kinetics can be modified *via* selective mutagenesis on the cavity surface. The redesign of the cavity together with varied metal loading conditions could open new possibilities for nanoparticle construction inside Dps proteins. The superparamagnetic character of the nanoparticles makes them potentially useful in a variety of applications. Owing to the inducibility of the magnetic field, the nanoparticles can be heated up or directed to a specific location with an external magnetic field. This behaviour makes them attractive for a number of applications, such as in drug delivery, magnetic hyperthermia (local heating of tumor cells), and magnetofection (transfection of cells) [299].

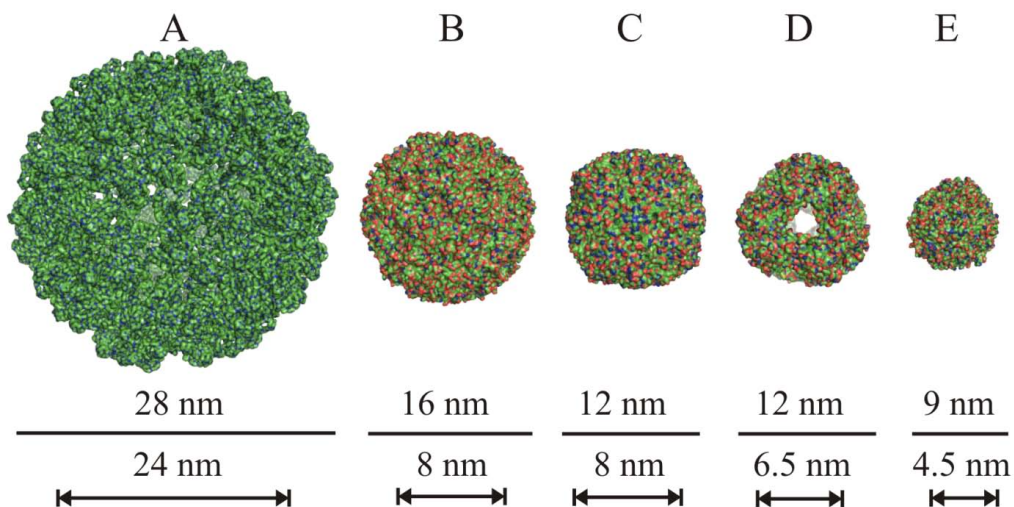


Figure 15. Examples of protein cages used as nanocontainers. The upper line indicates the outer diameter of the protein shell and the lower line shows the diameter of the cavity inside the protein. PDB accession codes are shown in parentheses. A) Cowpea chlorotic mottle virus (1za7) [300], B) *Salmonella typhimurium* LT2 lumazine synthase (3mk3) [301], C) Horse spleen ferritin (3f32) [302], D) *Methanococcus jannaschii* small heat shock protein (1shs) [303], E) *SsDpr* (1umn) [137].

9 CONCLUSIONS AND FUTURE PERSPECTIVES

The main focus of this study was to provide structural and functional details of the FOC, iron nucleation, and core formation of Dpr proteins. Crystal structures of native *SpDpr* as well as those of complexes with iron and zinc were determined. The metal-binding specificity of *SsDpr* was characterized both crystallographically and in solution. Iron nucleation in *SsDpr* was analyzed by site directed mutagenesis and the mineralization process was studied by a combination of X-ray crystallography, XAS, Mössbauer spectroscopy, and magnetic measurements.

The main conclusions of the thesis are:

- *SpDpr* shares the canonical structural features of Dps proteins. It has the conserved FOC which is capable of binding and oxidizing iron. The protein also possesses a novel N-terminal helix which is not involved in DNA binding.
- A di-metal FOC is found in *SpDpr*. The binding of the two zinc cations show variations compared to other di-metal FOCs of Dps proteins.
- A surface zinc/copper site found in *SpDpr* might be linked to zinc/copper resistance.
- *SsDpr* is able to bind Cu^{2+} , Co^{2+} , Ni^{2+} , and Mn^{2+} in the FOC. The binding is similar to that of Fe^{2+} , Zn^{2+} , and Tb^{3+} .
- In solution, the binding of Cu^{2+} , Co^{2+} , Ni^{2+} , Mn^{2+} , and Zn^{2+} leads to two binding sites per monomer. Based on the ITC data, the two cations bind to the FOC resulting in the formation of a di-metal FOC.
- The iron cores in *SsDpr* and in the E64A, E67A, E68A, and E75A mutants are structurally similar. The iron is found as ferrihydrite inside the cavity.
- The mutations decrease the rate of iron mineralization or storage capacity of the *SsDpr* cavity.
- All iron cores exhibit clear superparamagnetic behaviour in magnetic and Mössbauer measurements.
- The iron cores of the mutants have higher magnetic moment than the iron core of the wild type *SsDpr*.

There are still questions that remain to be addressed in future studies. Additionally, new questions invoked by this study remain to be answered. Although it was shown here that Dpr is capable of binding various transition metals, the biological significance of this process is still not fully understood. In particular, the question how Dpr protects against zinc stress is still open: Is the protective mechanism linked, for example, to the surface zinc site identified in *SpDpr* or to the second zinc site in *SsDpr*? Indeed, a more extensive analysis of transition metal binding to Dpr, with necessary and toxic metals, combined with biological data on bacterial growth and survival under metal stress could enlighten the role of Dpr in metal resistance. Due to their involvement in stress protection and virulence, Dps proteins are also potential candidates for drug design.

Further studies are needed to address the ferroxidase mechanism of *SpDpr* as well as the biological role of the $N\alpha$ helix. The exact location of the iron nucleation site in Dps proteins is not known although the evidence (or lack of it) points out that no single nucleation site exists in Dps proteins. A more extensive mutational analysis of the cavity surface could enlighten the critical residues for iron nucleation.

Magnetic analysis of the iron cores of the mutant proteins could assist in understanding magnetism at nanosize levels and enhance our knowledge of magnetism in biological systems. The Dps shell provides an ideal environment to study the fundamental magnetic behaviour of antiferromagnetic nanoparticles because it produces a system with non-interacting single domains. In addition, by loading the Dpr cavity with various metal cations, nanoparticles of novel magnetic properties could be produced.

10 ACKNOWLEDGEMENTS

This study sums up the work I carried out at the Turku Centre for Biotechnology, University of Turku and Åbo Akademi University, during the years 2008-2011.

I thank my supervisor, Docent Tassos Papageorgiou, for introducing me to the world of macromolecular crystallography and giving me the opportunity to develop my skills in this exciting field of science. I am especially thankful for the independence I enjoyed that allowed me to carry out my research and implement my own ideas in the process. I feel that under his supervision I have received a firm ground upon which I can further build my research career.

I express my gratitude to Professor Riitta Lahesmaa, the Director of Turku Centre for Biotechnology, for providing good working conditions and a friendly atmosphere in the labs. I thank Professor Jukka Finne for providing excellent settings for lab work in his group at the Department of Medical Biochemistry and Genetics. I thank Dr. Sauli Haataja for useful discussions and a fruitful collaboration with the Dpr as well as other projects. Other people at the Department are also acknowledged for their valuable assistance. Professor Petriina Paturi and Dr. Johan Lindén are thanked for a smooth collaboration within the Dpr project.

I thank all the international collaborators whom I have been working with: Professor George Nounesis, Professor Jiunn-Jong Wu, Dr. Angelos Thanassoulas, and Dr. Chih-Cheng Tsou. Special acknowledgements go to Dr. Wolfram Meyer-Klaucke for the outstanding crash course he gave me in XAS data processing and analysis.

The entire personnel at Turku Centre for Biotechnology have been very helpful during my studies. I am especially thankful to Petri Vähäköski and Mårten Hedman for the quick IT-service and to Juha Strandén and Pasi Viljakainen for technical assistance. Also, the help of the friendly staff at the administration, Sirkku Grönroos, Eva Hirvensalo, and Aila Jasmavaara, is much appreciated.

I also thank the reviewers of my thesis, Professor Ritva Serimaa and Associate Professor Derek Logan for their thorough work.

I am indebted to a lot of people working in our lab during the past years. I am grateful to Dr. Prathusha Dhavala for her friendship, all the discussions, and advice during the years. I thank Sachin Wakadkar, Bishwa Subedi, and Abdi Muleta for friendly company and good humour in the “office” and in the graphics room.

In the end I express my sincerest thanks to my parents Seppo and Pilvi for all the support. I thank my sister Heli for giving me her down-to-earth view on things, and my brother Tuomas for all the music-related excursions and numerous pow-wows of all kinds. Finally, I

Acknowledgements

express my gratitude to my fiancée Maria for her understanding, encouragement, and never-ending patience.

This work was financially supported by the Academy of Finland.

Turku, November 2011

A handwritten signature in black ink, consisting of a long horizontal line with several loops and a vertical tick mark near the left end.

Teemu Haikarainen

11 REFERENCES

1. Dupont CL, Yang S, Palenik B, Bourne PE: **Modern proteomes contain putative imprints of ancient shifts in trace metal geochemistry.** *Proc Natl Acad Sci U S A* 2006, **103**:17822-17827.
2. Andreini C, Bertini I, Rosato A: **A hint to search for metalloproteins in gene banks.** *Bioinformatics* 2004, **20**:1373-1380.
3. Ercal N, Gurer-Orhan H, Aykin-Burns N: **Toxic metals and oxidative stress part I: mechanisms involved in metal-induced oxidative damage.** *Curr Top Med Chem* 2001, **1**:529-539.
4. Nies DH: **Microbial heavy-metal resistance.** *Appl Microbiol Biotechnol* 1999, **51**:730-750.
5. Silver S, Phung le T: **A bacterial view of the periodic table: genes and proteins for toxic inorganic ions.** *J Ind Microbiol Biotechnol* 2005, **32**:587-605.
6. Valko M, Morris H, Cronin MT: **Metals, toxicity and oxidative stress.** *Curr Med Chem* 2005, **12**:1161-1208.
7. Lippard SJ, Berg JM: *Principles of Bioinorganic Chemistry.* Mill Valley, CA: University Science Books; 1994.
8. Niven DF, Ekins A, al-Samaurai AA: **Effects of iron and manganese availability on growth and production of superoxide dismutase by *Streptococcus suis*.** *Can J Microbiol* 1999, **45**:1027-1032.
9. Posey JE, Gherardini FC: **Lack of a role for iron in the Lyme disease pathogen.** *Science* 2000, **288**:1651-1653.
10. Deemagarn T, Wiseman B, Carpena X, Ivancich A, Fita I, Loewen PC: **Two alternative substrate paths for compound I formation and reduction in catalase-peroxidase KatG from *Burkholderia pseudomallei*.** *Proteins* 2007, **66**:219-228.
11. Ouellet H, Johnston JB, Ortiz de Montellano PR: **The *Mycobacterium tuberculosis* cytochrome P450 system.** *Arch Biochem Biophys* 2010, **493**:82-95.
12. Halliwell B, Gutteridge JM: *Free radicals in biology and medicine* edn 3. New York, U.S.A: Oxford University Press; 1999.
13. Rifkind JM, Ramasamy S, Manoharan PT, Nagababu E, Mohanty JG: **Redox reactions of hemoglobin.** *Antioxid Redox Signal* 2004, **6**:657-666.
14. Field SJ, Roldan MD, Marritt SJ, Butt JN, Richardson DJ, Watmough NJ: **Electron transfer to the active site of the bacterial nitric oxide reductase is controlled by ligand binding to heme b.** *Biochim Biophys Acta* 2011, **1807**:451-457.
15. Vallee BL, Auld DS: **Zinc coordination, function, and structure of zinc enzymes and other proteins.** *Biochemistry* 1990, **29**:5647-5659.
16. Vassilyev DG, Sekine S, Laptenko O, Lee J, Vassilyeva MN, Borukhov S, Yokoyama S: **Crystal structure of a bacterial RNA polymerase holoenzyme at 2.6 Å resolution.** *Nature* 2002, **417**:712-719.
17. Dua R, Edwards S, Levy DL, Campbell JL: **Subunit interactions within the *Saccharomyces cerevisiae* DNA polymerase ε (pol ε) complex. Demonstration of a dimeric pol ε.** *J Biol Chem* 2000, **275**:28816-28825.
18. Natori Y, Nanamiya H, Akanuma G, Kosono S, Kudo T, Ochi K, Kawamura F: **A fail-safe system for the ribosome under zinc-limiting conditions in *Bacillus subtilis*.** *Mol Microbiol* 2007, **63**:294-307.
19. Xaplanteri MA, Papadopoulos G, Leontiadou F, Choli-Papadopoulou T, Kalpaxis DL: **The contribution of the zinc-finger motif to the function of *Thermus thermophilus* ribosomal protein S14.** *J Mol Biol* 2007, **369**:489-497.
20. Härd T, Rak A, Allard P, Kloos L, Garber M: **The solution structure of ribosomal protein L36 from *Thermus thermophilus* reveals a zinc-ribbon-like fold.** *J Mol Biol* 2000, **296**:169-180.
21. Papp-Wallace KM, Maguire ME: **Manganese transport and the role of manganese in virulence.** *Annu Rev Microbiol* 2006, **60**:187-209.
22. Williamson A, Conlan B, Hillier W, Wydrzynski T: **The evolution of Photosystem II: insights into the past and future.** *Photosynth Res* 2011, **107**:71-86.
23. Archambaud C, Gouin E, Pizarro-Cerda J, Cossart P, Dussurget O: **Translation elongation factor EF-Tu is a target for Stp, a serine-threonine phosphatase involved in virulence of *Listeria monocytogenes*.** *Mol Microbiol* 2005, **56**:383-396.
24. Martin JE, Imlay JA: **The alternative aerobic ribonucleotide reductase of *Escherichia coli*, NrdEF, is a manganese-dependent enzyme that enables cell replication during periods of iron starvation.** *Mol Microbiol* 2011, **80**:319-334.
25. Tottey S, Harvie DR, Robinson NJ: **Understanding how cells allocate metals using metal sensors and metallochaperones.** *Acc Chem Res* 2005, **38**:775-783.
26. Fairhead M, Thony-Meyer L: **Bacterial tyrosinases: old enzymes with new relevance to biotechnology.** *N Biotechnol* 2011, In Press.
27. Wilmot CM, Murray JM, Alton G, Parsons MR, Convery MA, Blakeley V, Corner AS, Palcic MM, Knowles PF, McPherson MJ, et al.: **Catalytic mechanism of the quinoenzyme amine oxidase from *Escherichia coli*: exploring the reductive half-reaction.** *Biochemistry* 1997, **36**:1608-1620.
28. Banerjee R, Ragsdale SW: **The many faces of vitamin B12: catalysis by cobalamin-dependent enzymes.** *Annu Rev Biochem* 2003, **72**:209-247.
29. Miyanaga A, Fushinobu S, Ito K, Wakagi T: **Crystal structure of cobalt-containing nitrile hydratase.** *Biochem Biophys Res Commun* 2001, **288**:1169-1174.

30. Hall PR, Zheng R, Antony L, Pusztai-Carey M, Carey PR, Yee VC: **Transcarboxylase 5S structures: assembly and catalytic mechanism of a multienzyme complex subunit.** *EMBO J* 2004, **23**:3621-3631.
31. Ogata H, Kellers P, Lubitz W: **The crystal structure of the [NiFe] hydrogenase from the photosynthetic bacterium *Allochromatium vinosum*: characterization of the oxidized enzyme (Ni-A state).** *J Mol Biol* 2010, **402**:428-444.
32. Ha NC, Oh ST, Sung JY, Cha KA, Lee MH, Oh BH: **Supramolecular assembly and acid resistance of *Helicobacter pylori* urease.** *Nat Struct Biol* 2001, **8**:505-509.
33. Korshunov S, Imlay JA: **Detection and quantification of superoxide formed within the periplasm of *Escherichia coli*.** *J Bacteriol* 2006, **188**:6326-6334.
34. Messner KR, Imlay JA: **The identification of primary sites of superoxide and hydrogen peroxide formation in the aerobic respiratory chain and sulfite reductase complex of *Escherichia coli*.** *J Biol Chem* 1999, **274**:10119-10128.
35. Hassan HM, Fridovich I: **Intracellular production of superoxide radical and of hydrogen peroxide by redox active compounds.** *Arch Biochem Biophys* 1979, **196**:385-395.
36. Seaver LC, Imlay JA: **Hydrogen peroxide fluxes and compartmentalization inside growing *Escherichia coli*.** *J Bacteriol* 2001, **183**:7182-7189.
37. Duane PG, Rubins JB, Weisel HR, Janoff EN: **Identification of hydrogen peroxide as a *Streptococcus pneumoniae* toxin for rat alveolar epithelial cells.** *Infect Immun* 1993, **61**:4392-4397.
38. Taniai H, Iida K, Seki M, Saito M, Shiota S, Nakayama H, Yoshida S: **Concerted action of lactate oxidase and pyruvate oxidase in aerobic growth of *Streptococcus pneumoniae*: role of lactate as an energy source.** *J Bacteriol* 2008, **190**:3572-3579.
39. Seki M, Iida K, Saito M, Nakayama H, Yoshida S: **Hydrogen peroxide production in *Streptococcus pyogenes*: involvement of lactate oxidase and coupling with aerobic utilization of lactate.** *J Bacteriol* 2004, **186**:2046-2051.
40. Spellberg B, Cundell DR, Sandros J, Pearce BJ, Idanpaan-Heikkila I, Rosenow C, Masure HR: **Pyruvate oxidase, as a determinant of virulence in *Streptococcus pneumoniae*.** *Mol Microbiol* 1996, **19**:803-813.
41. Robinson JM: **Phagocytic leukocytes and reactive oxygen species.** *Histochem Cell Biol* 2009, **131**:465-469.
42. Flint DH, Smyk-Randall E, Tuminello JF, Draczynska-Lusiak B, Brown OR: **The inactivation of dihydroxy-acid dehydratase in *Escherichia coli* treated with hyperbaric oxygen occurs because of the destruction of its Fe-S cluster, but the enzyme remains in the cell in a form that can be reactivated.** *J Biol Chem* 1993, **268**:25547-25552.
43. Gardner PR, Fridovich I: **Superoxide sensitivity of the *Escherichia coli* 6-phosphogluconate dehydratase.** *J Biol Chem* 1991, **266**:1478-1483.
44. Jang S, Imlay JA: **Micromolar intracellular hydrogen peroxide disrupts metabolism by damaging iron-sulfur enzymes.** *J Biol Chem* 2007, **282**:929-937.
45. Kehrer JP: **The Haber-Weiss reaction and mechanisms of toxicity.** *Toxicology* 2000, **149**:43-50.
46. Buettner GR: **The pecking order of free radicals and antioxidants: lipid peroxidation, α -tocopherol, and ascorbate.** *Arch Biochem Biophys* 1993, **300**:535-543.
47. Welch KD, Davis TZ, Van Eden ME, Aust SD: **Deleterious iron-mediated oxidation of biomolecules.** *Free Radic Biol Med* 2002, **32**:577-583.
48. Teitzel GM, Geddie A, De Long SK, Kirisits MJ, Whiteley M, Parsek MR: **Survival and growth in the presence of elevated copper: transcriptional profiling of copper-stressed *Pseudomonas aeruginosa*.** *J Bacteriol* 2006, **188**:7242-7256.
49. Jones CM, Niederweis M: **Role of porins in iron uptake by *Mycobacterium smegmatis*.** *J Bacteriol* 2010, **192**:6411-6417.
50. Eitinger T, Rodionov DA, Grote M, Schneider E: **Canonical and ECF-type ATP-binding cassette importers in prokaryotes: diversity in modular organization and cellular functions.** *FEMS Microbiol Rev* 2011, **35**:3-67.
51. Arguello JM, Eren E, Gonzalez-Guerrero M: **The structure and function of heavy metal transport PIB-ATPases.** *Biometals* 2007, **20**:233-248.
52. Montanini B, Blaudez D, Jeandroz S, Sanders D, Chalot M: **Phylogenetic and functional analysis of the Cation Diffusion Facilitator (CDF) family: improved signature and prediction of substrate specificity.** *BMC Genomics* 2007, **8**:107.
53. Nevo Y, Nelson N: **The NRAMP family of metal-ion transporters.** *Biochim Biophys Acta* 2006, **1763**:609-620.
54. Zagorski N, Wilson DB: **Characterization and comparison of metal accumulation in two *Escherichia coli* strains expressing either CopA or MntA, heavy metal-transporting bacterial P-type adenosine triphosphatases.** *Appl Biochem Biotechnol* 2004, **117**:33-48.
55. Kloosterman TG, van der Kooi-Pol MM, Bijlsma JJ, Kuipers OP: **The novel transcriptional regulator SczA mediates protection against Zn^{2+} stress by activation of the Zn^{2+} -resistance gene *czcD* in *Streptococcus pneumoniae*.** *Mol Microbiol* 2007, **65**:1049-1063.
56. Hao Z, Chen S, Wilson DB: **Cloning, expression, and characterization of cadmium and manganese uptake genes from *Lactobacillus plantarum*.** *Appl Environ Microbiol* 1999, **65**:4746-4752.

57. Andrews SC, Robinson AK, Rodriguez-Quinones F: **Bacterial iron homeostasis.** *FEMS Microbiol Rev* 2003, **27**:215-237.
58. Krewulak KD, Vogel HJ: **Structural biology of bacterial iron uptake.** *Biochim Biophys Acta* 2008, **1778**:1781-1804.
59. Noinaj N, Guillier M, Barnard TJ, Buchanan SK: **TonB-dependent transporters: regulation, structure, and function.** *Annu Rev Microbiol* 2010, **64**:43-60.
60. Davidson AL, Dassa E, Orelle C, Chen J: **Structure, function, and evolution of bacterial ATP-binding cassette systems.** *Microbiol Mol Biol Rev* 2008, **72**:317-364.
61. Eitinger T, Suhr J, Moore L, Smith JA: **Secondary transporters for nickel and cobalt ions: theme and variations.** *Biometals* 2005, **18**:399-405.
62. Niegowski D, Eshaghi S: **The CorA family: structure and function revisited.** *Cell Mol Life Sci* 2007, **64**:2564-2574.
63. Kim EH, Nies DH, McEvoy MM, Rensing C: **Switch or funnel: how RND-type transport systems control periplasmic metal homeostasis.** *J Bacteriol* 2011, **193**:2381-2387.
64. Rodrigue A, Effantin G, Mandrand-Berthelot MA: **Identification of *rcnA* (*yohM*), a nickel and cobalt resistance gene in *Escherichia coli*.** *J Bacteriol* 2005, **187**:2912-2916.
65. Giedroc DP, Arunkumar AI: **Metal sensor proteins: nature's metalloregulated allosteric switches.** *Dalton Trans* 2007:3107-3120.
66. Outten CE, O'Halloran TV: **Femtomolar sensitivity of metalloregulatory proteins controlling zinc homeostasis.** *Science* 2001, **292**:2488-2492.
67. Brocklehurst KR, Hobman JL, Lawley B, Blank L, Marshall SJ, Brown NL, Morby AP: **ZntR is a Zn(II)-responsive MerR-like transcriptional regulator of *zntA* in *Escherichia coli*.** *Mol Microbiol* 1999, **31**:893-902.
68. Patzer SI, Hantke K: **The zinc-responsive regulator Zur and its control of the *znu* gene cluster encoding the ZnuABC zinc uptake system in *Escherichia coli*.** *J Biol Chem* 2000, **275**:24321-24332.
69. Changela A, Chen K, Xue Y, Holschen J, Outten CE, O'Halloran TV, Mondragon A: **Molecular basis of metal-ion selectivity and zeptomolar sensitivity by CueR.** *Science* 2003, **301**:1383-1387.
70. Hantke K: **Iron and metal regulation in bacteria.** *Curr Opin Microbiol* 2001, **4**:172-177.
71. Bagg A, Neilands JB: **Ferric uptake regulation protein acts as a repressor, employing iron (II) as a cofactor to bind the operator of an iron transport operon in *Escherichia coli*.** *Biochemistry* 1987, **26**:5471-5477.
72. Keyer K, Imlay JA: **Superoxide accelerates DNA damage by elevating free-iron levels.** *Proc Natl Acad Sci U S A* 1996, **93**:13635-13640.
73. Zheng M, Doan B, Schneider TD, Storz G: **OxyR and SoxRS regulation of *fur*.** *J Bacteriol* 1999, **181**:4639-4643.
74. Diaz-Mireles E, Wexler M, Sawers G, Bellini D, Todd JD, Johnston AW: **The Fur-like protein Mur of *Rhizobium leguminosarum* is a Mn²⁺-responsive transcriptional regulator.** *Microbiology* 2004, **150**:1447-1456.
75. Ahn BE, Cha J, Lee EJ, Han AR, Thompson CJ, Roe JH: **Nur, a nickel-responsive regulator of the Fur family, regulates superoxide dismutases and nickel transport in *Streptomyces coelicolor*.** *Mol Microbiol* 2006, **59**:1848-1858.
76. Hill PJ, Cockayne A, Landers P, Morrissey JA, Sims CM, Williams P: **SirR, a novel iron-dependent repressor in *Staphylococcus epidermidis*.** *Infect Immun* 1998, **66**:4123-4129.
77. Liu T, Chen X, Ma Z, Shokes J, Hemmingsen L, Scott RA, Giedroc DP: **A Cu(I)-sensing ArsR family metal sensor protein with a relaxed metal selectivity profile.** *Biochemistry* 2008, **47**:10564-10575.
78. Ehira S, Teramoto H, Inui M, Yukawa H: **A novel redox-sensing transcriptional regulator CyeR controls expression of an Old Yellow Enzyme family protein in *Corynebacterium glutamicum*.** *Microbiology* 2010, **156**:1335-1341.
79. Strausak D, Solioz M: **CopY is a copper-inducible repressor of the *Enterococcus hirae* copper ATPases.** *J Biol Chem* 1997, **272**:8932-8936.
80. Iwig JS, Leitch S, Herbst RW, Maroney MJ, Chivers PT: **Ni(II) and Co(II) sensing by *Escherichia coli* RcnR.** *J Am Chem Soc* 2008, **130**:7592-7606.
81. Chen PR, He C: **Selective recognition of metal ions by metalloregulatory proteins.** *Curr Opin Chem Biol* 2008, **12**:214-221.
82. Kidd SP, Potter AJ, Apicella MA, Jennings MP, McEwan AG: **NmlR of *Neisseria gonorrhoeae*: a novel redox responsive transcription factor from the MerR family.** *Mol Microbiol* 2005, **57**:1676-1689.
83. Chen H, Xu G, Zhao Y, Tian B, Lu H, Yu X, Xu Z, Ying N, Hu S, Hua Y: **A novel OxyR sensor and regulator of hydrogen peroxide stress with one cysteine residue in *Deinococcus radiodurans*.** *PLoS One* 2008, **3**:e1602.
84. Hall DR, Gourley DG, Leonard GA, Duke EM, Anderson LA, Boxer DH, Hunter WN: **The high-resolution crystal structure of the molybdate-dependent transcriptional regulator (ModE) from *Escherichia coli*: a novel combination of domain folds.** *EMBO J* 1999, **18**:1435-1446.
85. Reyes-Caballero H, Guerra AJ, Jacobsen FE, Kazmierczak KM, Cowart D, Koppolu UM, Scott RA, Winkler ME, Giedroc DP: **The metalloregulatory zinc site in *Streptococcus pneumoniae* AdcR, a zinc-activated MarR family repressor.** *J Mol Biol* 2010, **403**:197-216.
86. Schreiter ER, Sintchak MD, Guo Y, Chivers PT, Sauer RT, Drennan CL: **Crystal structure of the nickel-responsive transcription factor NikR.** *Nat Struct Biol* 2003, **10**:794-799.
87. Chattopadhyay MK, Tabor CW, Tabor H: **Polyamines protect *Escherichia coli* cells from**

- the toxic effect of oxygen. *Proc Natl Acad Sci U S A* 2003, **100**:2261-2265.
88. Stadtman ER, Berlett BS, Chock PB: **Manganese-dependent disproportionation of hydrogen peroxide in bicarbonate buffer.** *Proc Natl Acad Sci U S A* 1990, **87**:384-388.
 89. Archibald FS, Fridovich I: **Manganese and defenses against oxygen toxicity in *Lactobacillus plantarum*.** *J Bacteriol* 1981, **145**:442-451.
 90. Brenot A, King KY, Janowiak B, Griffith O, Caparon MG: **Contribution of glutathione peroxidase to the virulence of *Streptococcus pyogenes*.** *Infect Immunol* 2004, **72**:408-413.
 91. Sies H: **Strategies of antioxidant defense.** *Eur J Biochem* 1993, **215**:213-219.
 92. Chelikani P, Fita I, Loewen PC: **Diversity of structures and properties among catalases.** *Cell Mol Life Sci* 2004, **61**:192-208.
 93. Smulevich G, Jakopitsch C, Droghetti E, Obinger C: **Probing the structure and bifunctionality of catalase-peroxidase (KatG).** *J Inorg Biochem* 2006, **100**:568-585.
 94. Zamocky M, Furtmuller PG, Obinger C: **Evolution of catalases from bacteria to humans.** *Antioxid Redox Signal* 2008, **10**:1527-1548.
 95. Seaver LC, Imlay JA: **Alkyl hydroperoxide reductase is the primary scavenger of endogenous hydrogen peroxide in *Escherichia coli*.** *J Bacteriol* 2001, **183**:7173-7181.
 96. Niimura Y, Poole LB, Massey V: ***Amphibacillus xylanus* NADH oxidase and *Salmonella typhimurium* alkyl-hydroperoxide reductase flavoprotein components show extremely high scavenging activity for both alkyl hydroperoxide and hydrogen peroxide in the presence of *S. typhimurium* alkyl-hydroperoxide reductase 22-kDa protein component.** *J Biol Chem* 1995, **270**:25645-25650.
 97. Jönsson TJ, Ellis HR, Poole LB: **Cysteine reactivity and thiol-disulfide interchange pathways in AhpF and AhpC of the bacterial alkyl hydroperoxide reductase system.** *Biochemistry* 2007, **46**:5709-5721.
 98. Poole LB: **Flavin-dependent alkyl hydroperoxide reductase from *Salmonella typhimurium*. 2. Cystine disulfides involved in catalysis of peroxide reduction.** *Biochemistry* 1996, **35**:65-75.
 99. Abreu IA, Cabelli DE: **Superoxide dismutases-a review of the metal-associated mechanistic variations.** *Biochim Biophys Acta* 2010, **1804**:263-274.
 100. Ludwig ML, Metzger AL, Patridge KA, Stallings WC: **Manganese superoxide dismutase from *Thermus thermophilus*. A structural model refined at 1.8 Å resolution.** *J Mol Biol* 1991, **219**:335-358.
 101. Lah MS, Dixon MM, Patridge KA, Stallings WC, Fee JA, Ludwig ML: **Structure-function in *Escherichia coli* iron superoxide dismutase: comparisons with the manganese enzyme from *Thermus thermophilus*.** *Biochemistry* 1995, **34**:1646-1660.
 102. Pesce A, Capasso C, Battistoni A, Folcarelli S, Rotilio G, Desideri A, Bolognesi M: **Unique structural features of the monomeric Cu,Zn superoxide dismutase from *Escherichia coli*, revealed by X-ray crystallography.** *J Mol Biol* 1997, **274**:408-420.
 103. Wuerges J, Lee JW, Yim YI, Yim HS, Kang SO, Djinovic Carugo K: **Crystal structure of nickel-containing superoxide dismutase reveals another type of active site.** *Proc Natl Acad Sci U S A* 2004, **101**:8569-8574.
 104. Imlay JA: **Cellular defenses against superoxide and hydrogen peroxide.** *Annu Rev Biochem* 2008, **77**:755-776.
 105. Pinto AF, Rodrigues JV, Teixeira M: **Reductive elimination of superoxide: Structure and mechanism of superoxide reductases.** *Biochim Biophys Acta* 2010, **1804**:285-297.
 106. Arosio P, Ingrassia R, Cavadini P: **Ferritins: a family of molecules for iron storage, antioxidant and more.** *Biochim Biophys Acta* 2009, **1790**:589-599.
 107. Bou-Abdallah F: **The iron redox and hydrolysis chemistry of the ferritins.** *Biochim Biophys Acta* 2010, **1800**:719-731.
 108. Arosio P, Adelman TG, Drysdale JW: **On ferritin heterogeneity. Further evidence for heteropolymers.** *J Biol Chem* 1978, **253**:4451-4458.
 109. Toussaint L, Bertrand L, Hue L, Crichton RR, Declercq JP: **High-resolution X-ray structures of human apoferritin H-chain mutants correlated with their activity and metal-binding sites.** *J Mol Biol* 2007, **365**:440-452.
 110. Wang Z, Li C, Ellenburg M, Soistman E, Ruble J, Wright B, Ho JX, Carter DC: **Structure of human ferritin L chain.** *Acta Crystallogr D Biol Crystallogr* 2006, **62**:800-806.
 111. Levi S, Santambrogio P, Cozzi A, Rovida E, Corsi B, Tamborini E, Spada S, Albertini A, Arosio P: **The role of the L-chain in ferritin iron incorporation. Studies of homo and heteropolymers.** *J Mol Biol* 1994, **238**:649-654.
 112. Levi S, Luzzago A, Cesareni G, Cozzi A, Franceschinelli F, Albertini A, Arosio P: **Mechanism of ferritin iron uptake: activity of the H-chain and deletion mapping of the ferroxidase site. A study of iron uptake and ferroxidase activity of human liver, recombinant H-chain ferritins, and of two H-chain deletion mutants.** *J Biol Chem* 1988, **263**:18086-18092.
 113. Levi S, Yewdall SJ, Harrison PM, Santambrogio P, Cozzi A, Rovida E, Albertini A, Arosio P: **Evidence of H- and L-chains have co-operative roles in the iron-uptake mechanism of human ferritin.** *Biochem J* 1992, **288** (Pt 2):591-596.
 114. Theil EC: **Ferritin: structure, gene regulation, and cellular function in animals, plants, and microorganisms.** *Annu Rev Biochem* 1987, **56**:289-315.
 115. Dedman DJ, Treffy A, Candy JM, Taylor GA, Morris CM, Bloxham CA, Perry RH, Edwardson JA, Harrison PM: **Iron and aluminium in**

- relation to brain ferritin in normal individuals and Alzheimer's-disease and chronic renal-dialysis patients. *Biochem J* 1992, **287** (Pt 2):509-514.
116. Stillman TJ, Hempstead PD, Artymyuk PJ, Andrews SC, Hudson AJ, Treffry A, Guest JR, Harrison PM: **The high-resolution X-ray crystallographic structure of the ferritin (EcFtnA) of *Escherichia coli*; comparison with human H ferritin (HuHF) and the structures of the Fe³⁺ and Zn²⁺ derivatives.** *J Mol Biol* 2001, **307**:587-603.
 117. Masuda T, Goto F, Yoshihara T, Mikami B: **Crystal structure of plant ferritin reveals a novel metal binding site that functions as a transit site for metal transfer in ferritin.** *J Biol Chem* 2010, **285**:4049-4059.
 118. Tatur J, Hagen WR, Matias PM: **Crystal structure of the ferritin from the hyperthermophilic archaeal anaerobe *Pyrococcus furiosus*.** *J Biol Inorg Chem* 2007, **12**:615-630.
 119. Johnson E, Cascio D, Sawaya MR, Gingery M, Schroder I: **Crystal structures of a tetrahedral open pore ferritin from the hyperthermophilic archaeon *Archaeoglobus fulgidus*.** *Structure* 2005, **13**:637-648.
 120. Frolow F, Kalb AJ, Yariv J: **Structure of a unique twofold symmetric haem-binding site.** *Nat Struct Biol* 1994, **1**:453-460.
 121. Nam KH, Xu Y, Piao S, Priyadarshi A, Lee EH, Kim HY, Jeon YH, Ha NC, Hwang KY: **Crystal structure of bacterioferritin from *Rhodobacter sphaeroides*.** *Biochem Biophys Res Commun* 2010, **391**:990-994.
 122. Liu HL, Zhou HN, Xing WM, Zhao JF, Li SX, Huang JF, Bi RC: **2.6 Å resolution crystal structure of the bacterioferritin from *Azotobacter vinelandii*.** *FEBS Lett* 2004, **573**:93-98.
 123. Macedo S, Romao CV, Mitchell E, Matias PM, Liu MY, Xavier AV, LeGall J, Teixeira M, Lindley P, Carrondo MA: **The nature of the di-iron site in the bacterioferritin from *Desulfovibrio desulfuricans*.** *Nat Struct Biol* 2003, **10**:285-290.
 124. Yasmin S, Andrews SC, Moore GR, Le Brun NE: **A new role for heme, facilitating release of iron from the bacterioferritin iron biomineral.** *J Biol Chem* 2011, **286**:3473-3483.
 125. Abdul-Tehrani H, Hudson AJ, Chang YS, Timms AR, Hawkins C, Williams JM, Harrison PM, Guest JR, Andrews SC: **Ferritin mutants of *Escherichia coli* are iron deficient and growth impaired, and fur mutants are iron deficient.** *J Bacteriol* 1999, **181**:1415-1428.
 126. Velayudhan J, Castor M, Richardson A, Main-Hester KL, Fang FC: **The role of ferritins in the physiology of *Salmonella enterica* sv. Typhimurium: a unique role for ferritin B in iron-sulphur cluster repair and virulence.** *Mol Microbiol* 2007, **63**:1495-1507.
 127. Moore GR, Kadir FH, al-Massad FK, Le Brun NE, Thomson AJ, Greenwood C, Keen JN, Findlay JB: **Structural heterogeneity of *Pseudomonas aeruginosa* bacterioferritin.** *Biochem J* 1994, **304** (Pt 2):493-497.
 128. Keren N, Aurora R, Pakrasi HB: **Critical roles of bacterioferritins in iron storage and proliferation of cyanobacteria.** *Plant Physiol* 2004, **135**:1666-1673.
 129. Bencze KZ, Kondapalli KC, Cook JD, McMahon S, Millan-Pacheco C, Pastor N, Stemmler TL: **The structure and function of frataxin.** *Crit Rev Biochem Mol Biol* 2006, **41**:269-291.
 130. Jin S, Kurtz DM, Jr., Liu ZJ, Rose J, Wang BC: **X-ray crystal structures of reduced rubrerythrin and its azide adduct: a structure-based mechanism for a non-heme diiron peroxidase.** *J Am Chem Soc* 2002, **124**:9845-9855.
 131. Dyer DH, Lyle KS, Rayment I, Fox BG: **X-ray structure of putative acyl-ACP desaturase DesA2 from *Mycobacterium tuberculosis* H37Rv.** *Protein Sci* 2005, **14**:1508-1517.
 132. Antonyuk SV, Melik-Adamyan WR, Popov AN, Lamsin VS, Hempstead PD, Harrison PM, Artymyuk PJ, Barynin VV: **Three-dimensional structure of the enzyme dimanganese catalase from *Thermus Thermophilus* at 1 Å resolution.** *Crystallogr.Rep.(Transl. Kristallografiya)* 2000, **45**:105-116.
 133. Hindupur A, Liu D, Zhao Y, Bellamy HD, White MA, Fox RO: **The crystal structure of the *E. coli* stress protein YciF.** *Protein Sci* 2006, **15**:2605-2611.
 134. Andersson ME, Högbohm M, Rinaldo-Matthis A, Blodig W, Liang Y, Persson BO, Sjöberg BM, Su XD, Nordlund P: **Structural and mutational studies of the carboxylate cluster in iron-free ribonucleotide reductase R2.** *Biochemistry* 2004, **43**:7966-7972.
 135. Elsen NL, Bailey LJ, Hauser AD, Fox BG: **Role for threonine 201 in the catalytic cycle of the soluble diiron hydroxylase toluene 4-monooxygenase.** *Biochemistry* 2009, **48**:3838-3846.
 136. Grant RA, Filman DJ, Finkel SE, Kolter R, Hogle JM: **The crystal structure of Dps, a ferritin homolog that binds and protects DNA.** *Nat Struct Biol* 1998, **5**:294-303.
 137. Kauko A, Haataja S, Pulliainen AT, Finne J, Papageorgiou AC: **Crystal structure of *Streptococcus suis* Dps-like peroxide resistance protein Dpr: implications for iron incorporation.** *J Mol Biol* 2004, **338**:547-558.
 138. Stillman TJ, Upadhyay M, Norte VA, Sedelnikova SE, Carradus M, Tzokov S, Bullough PA, Shearman CA, Gasson MJ, Williams CH, et al.: **The crystal structures of *Lactococcus lactis* MG1363 Dps proteins reveal the presence of an N-terminal helix that is required for DNA binding.** *Mol Microbiol* 2005, **57**:1101-1112.
 139. Gauss GH, Benas P, Wiedenheft B, Young M, Douglas T, Lawrence CM: **Structure of the DPS-like protein from *Sulfolobus solfataricus* reveals**

- a bacterioferritin-like dimetal binding site within a DPS-like dodecameric assembly. *Biochemistry* 2006, **45**:10815-10827.
140. Cuypers MG, Mitchell EP, Romao CV, McSweeney SM: **The crystal structure of the Dps2 from *Deinococcus radiodurans* reveals an unusual pore profile with a non-specific metal binding site.** *J Mol Biol* 2007, **371**:787-799.
141. Zanotti G, Papinutto E, Dundon W, Battistutta R, Seveso M, Giudice G, Rappuoli R, Montecucco C: **Structure of the neutrophil-activating protein from *Helicobacter pylori*.** *J Mol Biol* 2002, **323**:125-130.
142. Papinutto E, Dundon WG, Pitulis N, Battistutta R, Montecucco C, Zanotti G: **Structure of two iron-binding proteins from *Bacillus anthracis*.** *J Biol Chem* 2002, **277**:15093-15098.
143. Ren B, Tibbelin G, Kajino T, Asami O, Ladenstein R: **The multi-layered structure of Dps with a novel di-nuclear ferroxidase center.** *J Mol Biol* 2003, **329**:467-477.
144. Ilari A, Stefanini S, Chiancone E, Tsernoglou D: **The dodecameric ferritin from *Listeria innocua* contains a novel intersubunit iron-binding site.** *Nat Struct Biol* 2000, **7**:38-43.
145. Zeth K, Offermann S, Essen LO, Oesterhelt D: **Iron-oxo clusters biomimetalizing on protein surfaces: structural analysis of *Halobacterium salinarum* DpsA in its low- and high-iron states.** *Proc Natl Acad Sci U S A* 2004, **101**:13780-13785.
146. Ceci P, Ilari A, Falvo E, Giangiacomo L, Chiancone E: **Reassessment of protein stability, DNA binding, and protection of *Mycobacterium smegmatis* Dps.** *J Biol Chem* 2005, **280**:34776-34785.
147. Roy S, Saraswathi R, Chatterji D, Vijayan M: **Structural studies on the second *Mycobacterium smegmatis* Dps: invariant and variable features of structure, assembly and function.** *J Mol Biol* 2008, **375**:948-959.
148. Romao CV, Mitchell EP, McSweeney S: **The crystal structure of *Deinococcus radiodurans* Dps protein (DR2263) reveals the presence of a novel metal centre in the N terminus.** *J Biol Inorg Chem* 2006, **11**:891-902.
149. Codolo G, Papinutto E, Polenghi A, D'Elis MM, Zanotti G, de Bernard M: **Structure and immunomodulatory property relationship in NapA of *Borrelia burgdorferi*.** *Biochim Biophys Acta* 2010, **1804**:2191-2197.
150. Franceschini S, Ceci P, Alaleona F, Chiancone E, Ilari A: **Antioxidant Dps protein from the thermophilic cyanobacterium *Thermosynechococcus elongatus*.** *FEBS J* 2006, **273**:4913-4928.
151. Grove A, Wilkinson SP: **Differential DNA binding and protection by dimeric and dodecameric forms of the ferritin homolog Dps from *Deinococcus radiodurans*.** *J Mol Biol* 2005, **347**:495-508.
152. Stillman TJ, Connolly PP, Latimer CL, Morland AF, Quail MA, Andrews SC, Treffry A, Guest JR, Artymiuk PJ, Harrison PM: **Insights into the effects on metal binding of the systematic substitution of five key glutamate ligands in the ferritin of *Escherichia coli*.** *J Biol Chem* 2003, **278**:26275-26286.
153. Alaleona F, Franceschini S, Ceci P, Ilari A, Chiancone E: ***Thermosynechococcus elongatus* DpsA binds Zn(II) at a unique three histidine-containing ferroxidase center and utilizes O₂ as iron oxidant with very high efficiency, unlike the typical Dps proteins.** *FEBS J* 2010, **277**:903-917.
154. Kauko A, Pulliainen AT, Haataja S, Meyer-Klaucke W, Finne J, Papageorgiou AC: **Iron incorporation in *Streptococcus suis* Dps-like peroxide resistance protein Dpr requires mobility in the ferroxidase center and leads to the formation of a ferrihydrite-like core.** *J Mol Biol* 2006, **364**:97-109.
155. Ilari A, Ceci P, Ferrari D, Rossi GL, Chiancone E: **Iron incorporation into *Escherichia coli* Dps gives rise to a ferritin-like microcrystalline core.** *J Biol Chem* 2002, **277**:37619-37623.
156. Zhao G, Ceci P, Ilari A, Giangiacomo L, Laue TM, Chiancone E, Chasteen ND: **Iron and hydrogen peroxide detoxification properties of DNA-binding protein from starved cells. A ferritin-like DNA-binding protein of *Escherichia coli*.** *J Biol Chem* 2002, **277**:27689-27696.
157. Ilari A, Latella MC, Ceci P, Ribacchi F, Su M, Giangiacomo L, Stefanini S, Chasteen ND, Chiancone E: **The unusual intersubunit ferroxidase center of *Listeria innocua* Dps is required for hydrogen peroxide detoxification but not for iron uptake. A study with site-specific mutants.** *Biochemistry* 2005, **44**:5579-5587.
158. Su M, Cavallo S, Stefanini S, Chiancone E, Chasteen ND: **The so-called *Listeria innocua* ferritin is a Dps protein. Iron incorporation, detoxification, and DNA protection properties.** *Biochemistry* 2005, **44**:5572-5578.
159. Liu X, Kim K, Leighton T, Theil EC: **Paired *Bacillus anthracis* Dps (mini-ferritin) have different reactivities with peroxide.** *J Biol Chem* 2006, **281**:27827-27835.
160. Yang X, Le Brun NE, Thomson AJ, Moore GR, Chasteen ND: **The iron oxidation and hydrolysis chemistry of *Escherichia coli* bacterioferritin.** *Biochemistry* 2000, **39**:4915-4923.
161. Bauminger ER, Harrison PM, Hechel D, Nowik I, Treffry A: **Mössbauer spectroscopic investigation of structure-function relations in ferritins.** *Biochim Biophys Acta* 1991, **1118**:48-58.
162. Yang X, Chen-Barrett Y, Arosio P, Chasteen ND: **Reaction paths of iron oxidation and hydrolysis in horse spleen and recombinant human ferritins.** *Biochemistry* 1998, **37**:9743-9750.
163. Stefanini S, Desideri A, Vecchini P, Drakenberg T, Chiancone E: **Identification of the iron entry channels in apoferritin. Chemical modification**

- and spectroscopic studies. *Biochemistry* 1989, **28**:378-382.
164. Treffry A, Bauminger ER, Hechel D, Hodson NW, Nowik I, Yewdall SJ, Harrison PM: **Defining the roles of the threefold channels in iron uptake, iron oxidation and iron-core formation in ferritin: a study aided by site-directed mutagenesis.** *Biochem J* 1993, **296** (Pt 3):721-728.
165. Levi S, Santambrogio P, Corsi B, Cozzi A, Arosio P: **Evidence that residues exposed on the threefold channels have active roles in the mechanism of ferritin iron incorporation.** *Biochem J* 1996, **317** (Pt 2):467-473.
166. Bou-Abdallah F, Arosio P, Santambrogio P, Yang X, Janus-Chandler C, Chasteen ND: **Ferrous ion binding to recombinant human H-chain ferritin. An isothermal titration calorimetry study.** *Biochemistry* 2002, **41**:11184-11191.
167. Bou-Abdallah F, Arosio P, Levi S, Janus-Chandler C, Chasteen ND: **Defining metal ion inhibitor interactions with recombinant human H- and L-chain ferritins and site-directed variants: an isothermal titration calorimetry study.** *J Biol Inorg Chem* 2003, **8**:489-497.
168. Kim SG, Bhattacharyya G, Grove A, Lee YH: **Crystal structure of Dps-1, a functionally distinct Dps protein from *Deinococcus radiodurans*.** *J Mol Biol* 2006, **361**:105-114.
169. Haikarainen T, Papageorgiou AC: **Dps-like proteins: structural and functional insights into a versatile protein family.** *Cell Mol Life Sci* 2010, **67**:341-351.
170. Pulliainen AT, Kauko A, Haataja S, Papageorgiou AC, Finne J: **Dps/Dpr ferritin-like protein: insights into the mechanism of iron incorporation and evidence for a central role in cellular iron homeostasis in *Streptococcus suis*.** *Mol Microbiol* 2005, **57**:1086-1100.
171. Bellapadrona G, Stefanini S, Zamparelli C, Theil EC, Chiancone E: **Iron translocation into and out of *Listeria innocua* Dps and size distribution of the protein-enclosed nanomineral are modulated by the electrostatic gradient at the 3-fold "ferritin-like" pores.** *J Biol Chem* 2009, **284**:19101-19109.
172. Bou-Abdallah F, Woodhall MR, Velazquez-Campoy A, Andrews SC, Chasteen ND: **Thermodynamic analysis of ferrous ion binding to *Escherichia coli* ferritin EcFtnA.** *Biochemistry* 2005, **44**:13837-13846.
173. Bellapadrona G, Ardini M, Ceci P, Stefanini S, Chiancone E: **Dps proteins prevent Fenton-mediated oxidative damage by trapping hydroxyl radicals within the protein shell.** *Free Radic Biol Med* 2010, **48**:292-297.
174. Granier T, Langlois d'Estaintot B, Gallois B, Chevalier JM, Precigoux G, Santambrogio P, Arosio P: **Structural description of the active sites of mouse L-chain ferritin at 1.2 Å resolution.** *J Biol Inorg Chem* 2003, **8**:105-111.
175. Santambrogio P, Levi S, Cozzi A, Corsi B, Arosio P: **Evidence that the specificity of iron incorporation into homopolymers of human ferritin L- and H-chains is conferred by the nucleation and ferroxidase centres.** *Biochem J* 1996, **314** (Pt 1):139-144.
176. Bozzi M, Mignogna G, Stefanini S, Barra D, Longhi C, Valenti P, Chiancone E: **A novel non-heme iron-binding ferritin related to the DNA-binding proteins of the Dps family in *Listeria innocua*.** *J Biol Chem* 1997, **272**:3259-3265.
177. Castruita M, Saito M, Schottel PC, Elmegreen LA, Myneni S, Stiefel EI, Morel FM: **Overexpression and characterization of an iron storage and DNA-binding Dps protein from *Trichodesmium erythraeum*.** *Appl Environ Microbiol* 2006, **72**:2918-2924.
178. Eggleton RA, Fitzpatrick RW: **New data and a revised structural model for ferrihydrite.** *Clays and Clay Miner.* 1988, **36**:111-124.
179. Givskov M, Eberl L, Moller S, Poulsen LK, Molin S: **Responses to nutrient starvation in *Pseudomonas putida* KT2442: analysis of general cross-protection, cell shape, and macromolecular content.** *J Bacteriol* 1994, **176**:7-14.
180. Frenkiel-Krispin D, Minsky A: **Nucleoid organization and the maintenance of DNA integrity in *E. coli*, *B. subtilis* and *D. radiodurans*.** *J Struct Biol* 2006, **156**:311-319.
181. Almiron M, Link AJ, Furlong D, Kolter R: **A novel DNA-binding protein with regulatory and protective roles in starved *Escherichia coli*.** *Genes Dev* 1992, **6**:2646-2654.
182. Bhattacharyya G, Grove A: **The N-terminal extensions of *Deinococcus radiodurans* Dps-1 mediate DNA major groove interactions as well as assembly of the dodecamer.** *J Biol Chem* 2007, **282**:11921-11930.
183. Ceci P, Cellai S, Falvo E, Rivetti C, Rossi GL, Chiancone E: **DNA condensation and self-aggregation of *Escherichia coli* Dps are coupled phenomena related to the properties of the N-terminus.** *Nucleic Acids Res* 2004, **32**:5935-5944.
184. Roy S, Saraswathi R, Gupta S, Sekar K, Chatterji D, Vijayan M: **Role of N and C-terminal tails in DNA binding and assembly in Dps: structural studies of *Mycobacterium smegmatis* Dps deletion mutants.** *J Mol Biol* 2007, **370**:752-767.
185. Ishikawa T, Mizunoe Y, Kawabata S, Takade A, Harada M, Wai SN, Yoshida S: **The iron-binding protein Dps confers hydrogen peroxide stress resistance to *Campylobacter jejuni*.** *J Bacteriol* 2003, **185**:1010-1017.
186. Ceci P, Ilari A, Falvo E, Chiancone E: **The Dps protein of *Agrobacterium tumefaciens* does not bind to DNA but protects it toward oxidative cleavage: x-ray crystal structure, iron binding, and hydroxyl-radical scavenging properties.** *J Biol Chem* 2003, **278**:20319-20326.
187. Ceci P, Mangiarotti L, Rivetti C, Chiancone E: **The neutrophil-activating Dps protein of *Helicobacter pylori*, HP-NAP, adopts a mechanism different from *Escherichia coli* Dps**

- to bind and condense DNA. *Nucleic Acids Res* 2007, **35**:2247-2256.
188. Frenkiel-Krispin D, Levin-Zaidman S, Shimoni E, Wolf SG, Wachtel EJ, Arad T, Finkel SE, Kolter R, Minsky A: **Regulated phase transitions of bacterial chromatin: a non-enzymatic pathway for generic DNA protection.** *EMBO J* 2001, **20**:1184-1191.
 189. Kim J, Yoshimura SH, Hizume K, Ohniwa RL, Ishihama A, Takeyasu K: **Fundamental structural units of the *Escherichia coli* nucleoid revealed by atomic force microscopy.** *Nucleic Acids Res* 2004, **32**:1982-1992.
 190. Ali Azam T, Iwata A, Nishimura A, Ueda S, Ishihama A: **Growth phase-dependent variation in protein composition of the *Escherichia coli* nucleoid.** *J Bacteriol* 1999, **181**:6361-6370.
 191. Wolf SG, Frenkiel D, Arad T, Finkel SE, Kolter R, Minsky A: **DNA protection by stress-induced biocrystallization.** *Nature* 1999, **400**:83-85.
 192. Martinez A, Kolter R: **Protection of DNA during oxidative stress by the nonspecific DNA-binding protein Dps.** *J Bacteriol* 1997, **179**:5188-5194.
 193. Jeong KC, Hung KF, Baumler DJ, Byrd JJ, Kaspar CW: **Acid stress damage of DNA is prevented by Dps binding in *Escherichia coli* O157:H7.** *BMC Microbiol* 2008, **8**:181.
 194. Frenkiel-Krispin D, Ben-Avraham I, Englander J, Shimoni E, Wolf SG, Minsky A: **Nucleoid restructuring in stationary-state bacteria.** *Mol Microbiol* 2004, **51**:395-405.
 195. Pena MM, Burkhart W, Bullerjahn GS: **Purification and characterization of a *Synechococcus* sp. strain PCC 7942 polypeptide structurally similar to the stress-induced Dps/PexB protein of *Escherichia coli*.** *Arch Microbiol* 1995, **163**:337-344.
 196. Nicodeme M, Perrin C, Hols P, Bracquart P, Gaillard JL: **Identification of an iron-binding protein of the Dps family expressed by *Streptococcus thermophilus*.** *Curr Microbiol* 2004, **48**:51-56.
 197. Altuvia S, Almiron M, Huisman G, Kolter R, Storz G: **The *dps* promoter is activated by OxyR during growth and by IHF and σ^S in stationary phase.** *Mol Microbiol* 1994, **13**:265-272.
 198. Yamamoto Y, Higuchi M, Poole LB, Kamio Y: **Role of the *dpr* product in oxygen tolerance in *Streptococcus mutans*.** *J Bacteriol* 2000, **182**:3740-3747.
 199. Wiedenheft B, Mosolf J, Willits D, Yeager M, Dryden KA, Young M, Douglas T: **An archaeal antioxidant: characterization of a Dps-like protein from *Sulfolobus solfataricus*.** *Proc Natl Acad Sci U S A* 2005, **102**:10551-10556.
 200. Antelmann H, Engelmann S, Schmid R, Sorokin A, Lapidus A, Hecker M: **Expression of a stress- and starvation-induced *dps/pexB*-homologous gene is controlled by the alternative sigma factor σ^B in *Bacillus subtilis*.** *J Bacteriol* 1997, **179**:7251-7256.
 201. Dundon WG, Polenghi A, Del Guidice G, Rappuoli R, Montecucco C: **Neutrophil-activating protein (HP-NAP) versus ferritin (Pfr): comparison of synthesis in *Helicobacter pylori*.** *FEMS Microbiol Lett* 2001, **199**:143-149.
 202. Sen A, Dwivedi K, Rice KA, Bullerjahn GS: **Growth phase and metal-dependent regulation of the *dpsA* gene in *Synechococcus* sp. strain PCC 7942, USA.** *Arch Microbiol* 2000, **173**:352-357.
 203. Ueshima J, Shoji M, Ratnayake DB, Abe K, Yoshida S, Yamamoto K, Nakayama K: **Purification, gene cloning, gene expression, and mutants of Dps from the obligate anaerobe *Porphyromonas gingivalis*.** *Infect Immun* 2003, **71**:1170-1178.
 204. Rocha ER, Owens G, Jr., Smith CJ: **The redox-sensitive transcriptional activator OxyR regulates the peroxide response regulon in the obligate anaerobe *Bacteroides fragilis*.** *J Bacteriol* 2000, **182**:5059-5069.
 205. Colburn-Clifford JM, Scherf JM, Allen C: ***Ralstonia solanacearum* Dps contributes to oxidative stress tolerance and to colonization of and virulence on tomato plants.** *Appl Environ Microbiol* 2010, **76**:7392-7399.
 206. Grainger DC, Goldberg MD, Lee DJ, Busby SJ: **Selective repression by Fis and H-NS at the *Escherichia coli* *dps* promoter.** *Mol Microbiol* 2008, **68**:1366-1377.
 207. Stephani K, Weichart D, Hengge R: **Dynamic control of Dps protein levels by ClpXP and ClpAP proteases in *Escherichia coli*.** *Mol Microbiol* 2003, **49**:1605-1614.
 208. Mogk A, Schmidt R, Bukau B: **The N-end rule pathway for regulated proteolysis: prokaryotic and eukaryotic strategies.** *Trends Cell Biol* 2007, **17**:165-172.
 209. Schmidt R, Zahn R, Bukau B, Mogk A: **ClpS is the recognition component for *Escherichia coli* substrates of the N-end rule degradation pathway.** *Mol Microbiol* 2009, **72**:506-517.
 210. Chen L, James LP, Helmann JD: **Metalloregulation in *Bacillus subtilis*: isolation and characterization of two genes differentially repressed by metal ions.** *J Bacteriol* 1993, **175**:5428-5437.
 211. Bsat N, Chen L, Helmann JD: **Mutation of the *Bacillus subtilis* alkyl hydroperoxide reductase (*ahpCF*) operon reveals compensatory interactions among hydrogen peroxide stress genes.** *J Bacteriol* 1996, **178**:6579-6586.
 212. Horsburgh MJ, Clements MO, Crossley H, Ingham E, Foster JE: **PerR controls oxidative stress resistance and iron storage proteins and is required for virulence in *Staphylococcus aureus*.** *Infect Immun* 2001, **69**:3744-3754.
 213. Brenot A, King KY, Caparon MG: **The PerR regulon in peroxide resistance and virulence of *Streptococcus pyogenes*.** *Mol Microbiol* 2005, **55**:221-234.
 214. Tsou CC, Chiang-Ni C, Lin YS, Chuang WJ, Lin MT, Liu CC, Wu JJ: **Oxidative stress and metal**

- ions regulate a ferritin-like gene, *dpr*, in *Streptococcus pyogenes*. *Int J Med Microbiol* 2010, **300**:259-264.
215. Cooksley C, Jenks PJ, Green A, Cockayne A, Logan RP, Hardie KR: **NapA protects *Helicobacter pylori* from oxidative stress damage, and its production is influenced by the ferric uptake regulator.** *J Med Microbiol* 2003, **52**:461-469.
 216. Fiorini F, Stefanini S, Valenti P, Chiancone E, De Biase D: **Transcription of the *Listeria monocytogenes* *fri* gene is growth-phase dependent and is repressed directly by Fur, the ferric uptake regulator.** *Gene* 2008, **410**:113-121.
 217. Yoo AY, Kim SW, Yu JE, Kim YH, Cha J, Oh JI, Eo SK, Lee JH, Kang HY: **Requirement of Fur for the full induction of *dps* expression in *Salmonella enterica* serovar typhimurium.** *J Microbiol Biotechnol* 2007, **17**:1452-1459.
 218. Katona LI, Tokarz R, Kuhlow CJ, Benach J, Benach JL: **The Fur homologue in *Borrelia burgdorferi*.** *J Bacteriol* 2004, **186**:6443-6456.
 219. Hebraud M, Guzzo J: **The main cold shock protein of *Listeria monocytogenes* belongs to the family of ferritin-like proteins.** *FEMS Microbiol Lett* 2000, **190**:29-34.
 220. Perrin C, Guimont C, Bracquart P, Gaillard JL: **Expression of a new cold shock protein of 21.5 kDa and of the major cold shock protein by *Streptococcus thermophilus* after cold shock.** *Curr Microbiol* 1999, **39**:342-0347.
 221. Thieme D, Grass G: **The Dps protein of *Escherichia coli* is involved in copper homeostasis.** *Microbiol Res* 2010, **165**:108-115.
 222. Nair S, Finkel SE: **Dps protects cells against multiple stresses during stationary phase.** *J Bacteriol* 2004, **186**:4192-4198.
 223. Tsou CC, Chiang-Ni C, Lin YS, Chuang WJ, Lin MT, Liu CC, Wu JJ: **An iron-binding protein, Dpr, decreases hydrogen peroxide stress and protects *Streptococcus pyogenes* against multiple stresses.** *Infect Immun* 2008, **76**:4038-4045.
 224. Milanino R, Marrella M, Gasperini R, Pasqualicchio M, Velo G: **Copper and zinc body levels in inflammation: an overview of the data obtained from animal and human studies.** *Agents Actions* 1993, **39**:195-209.
 225. Choi SH, Baumler DJ, Kaspar CW: **Contribution of *dps* to acid stress tolerance and oxidative stress tolerance in *Escherichia coli* O157:H7.** *Appl Environ Microbiol* 2000, **66**:3911-3916.
 226. Malone AS, Chung YK, Yousef AE: **Genes of *Escherichia coli* O157:H7 that are involved in high-pressure resistance.** *Appl Environ Microbiol* 2006, **72**:2661-2671.
 227. Aertsen A, De Spiegeleer P, Vanoirbeek K, Lavilla M, Michiels CW: **Induction of oxidative stress by high hydrostatic pressure in *Escherichia coli*.** *Appl Environ Microbiol* 2005, **71**:2226-2231.
 228. Halsey TA, Vazquez-Torres A, Gravidahl DJ, Fang FC, Libby SJ: **The ferritin-like Dps protein is required for *Salmonella enterica* serovar Typhimurium oxidative stress resistance and virulence.** *Infect Immun* 2004, **72**:1155-1158.
 229. Evans DJ, Jr., Evans DG, Takemura T, Nakano H, Lampert HC, Graham DY, Granger DN, Kvietys PR: **Characterization of a *Helicobacter pylori* neutrophil-activating protein.** *Infect Immun* 1995, **63**:2213-2220.
 230. Long M, Luo J, Li Y, Zeng FY, Li M: **Detection and evaluation of antibodies against neutrophil-activating protein of *Helicobacter pylori* in patients with gastric cancer.** *World J Gastroenterol* 2009, **15**:2381-2388.
 231. Satin B, Del Giudice G, Della Bianca V, Dusi S, Laudanna C, Tonello F, Kelleher D, Rappuoli R, Montecucco C, Rossi F: **The neutrophil-activating protein (HP-NAP) of *Helicobacter pylori* is a protective antigen and a major virulence factor.** *J Exp Med* 2000, **191**:1467-1476.
 232. Montemurro P, Nishioka H, Dundon WG, de Bernard M, Del Giudice G, Rappuoli R, Montecucco C: **The neutrophil-activating protein (HP-NAP) of *Helicobacter pylori* is a potent stimulant of mast cells.** *Eur J Immunol* 2002, **32**:671-676.
 233. Polenghi A, Bossi F, Fischetti F, Durigutto P, Cabrelle A, Tamassia N, Cassatella MA, Montecucco C, Tedesco F, de Bernard M: **The neutrophil-activating protein of *Helicobacter pylori* crosses endothelia to promote neutrophil adhesion in vivo.** *J Immunol* 2007, **178**:1312-1320.
 234. Amedei A, Cappon A, Codolo G, Cabrelle A, Polenghi A, Benagiano M, Tasca E, Azzurri A, D'Elia MM, Del Prete G, et al.: **The neutrophil-activating protein of *Helicobacter pylori* promotes Th1 immune responses.** *J Clin Invest* 2006, **116**:1092-1101.
 235. Malfertheiner P, Schultze V, Rosenkranz B, Kaufmann SH, Ulrichs T, Novicki D, Norelli F, Contorni M, Peppoloni S, Berti D, et al.: **Safety and immunogenicity of an intramuscular *Helicobacter pylori* vaccine in noninfected volunteers: a phase I study.** *Gastroenterology* 2008, **135**:787-795.
 236. Yuki N: **Infectious origins of, and molecular mimicry in, Guillain-Barré and Fisher syndromes.** *Lancet Infect Dis* 2001, **1**:29-37.
 237. Piao H, Minohara M, Kawamura N, Li W, Mizunoe Y, Umehara F, Goto Y, Kusunoki S, Matsushita T, Ikenaka K, et al.: **Induction of paranodal myelin detachment and sodium channel loss in vivo by *Campylobacter jejuni* DNA-binding protein from starved cells (C-Dps) in myelinated nerve fibers.** *J Neurol Sci* 2010, **288**:54-62.
 238. Piao H, Minohara M, Kawamura N, Li W, Matsushita T, Yamasaki R, Mizunoe Y, Kira J: **Tissue binding patterns and in vitro effects of *Campylobacter jejuni* DNA-binding protein**

- from starved cells. *Neurochem Res* 2011, **36**:58-66.
239. Li X, Pal U, Ramamoorthi N, Liu X, Desrosiers DC, Eggers CH, Anderson JF, Radolf JD, Fikrig E: **The Lyme disease agent *Borrelia burgdorferi* requires BB0690, a Dps homologue, to persist within ticks.** *Mol Microbiol* 2007, **63**:694-710.
240. Codolo G, Amedei A, Steere AC, Papinutto E, Cappon A, Polenghi A, Benaglio M, Paccani SR, Sambri V, Del Prete G, et al.: ***Borrelia burgdorferi* NapA-driven Th17 cell inflammation in Lyme arthritis.** *Arthritis Rheum* 2008, **58**:3609-3617.
241. Chodavarapu S, Gomez R, Vicente M, Kaguni JM: ***Escherichia coli* Dps interacts with DnaA protein to impede initiation: a model of adaptive mutation.** *Mol Microbiol* 2008, **67**:1331-1346.
242. Ping L, Buchler R, Mithofer A, Svatos A, Spittler D, Dettner K, Grmeiner S, Piel J, Schlott B, Boland W: **A novel Dps-type protein from insect gut bacteria catalyses hydrolysis and synthesis of *N*-acyl amino acids.** *Environ Microbiol* 2007, **9**:1572-1583.
243. Lacqua A, Wanner O, Colangelo T, Martinotti MG, Landini P: **Emergence of biofilm-forming subpopulations upon exposure of *Escherichia coli* to environmental bacteriophages.** *Appl Environ Microbiol* 2006, **72**:956-959.
244. Li H, Wang BC, Xu WJ, Lin XM, Peng XX: **Identification and network of outer membrane proteins regulating streptomycin resistance in *Escherichia coli*.** *J Proteome Res* 2008, **7**:4040-4049.
245. Zhang DF, Li H, Lin XM, Wang SY, Peng XX: **Characterization of outer membrane proteins of *Escherichia coli* in response to phenol stress.** *Curr Microbiol* 2010.
246. Tonello F, Dundon WG, Satin B, Molinari M, Tognon G, Grandi G, Del Giudice G, Rappuoli R, Montecucco C: **The *Helicobacter pylori* neutrophil-activating protein is an iron-binding protein with dodecameric structure.** *Mol Microbiol* 1999, **34**:238-246.
247. Bellapadrona G, Chiaraluce R, Consalvi V, Ilari A, Stefanini S, Chiancone E: **The mutations Lys 114 --> Gln and Asp 126 --> Asn disrupt an intersubunit salt bridge and convert *Listeria innocua* Dps into its natural mutant *Listeria monocytogenes* Dps. Effects on protein stability at low pH.** *Proteins* 2007, **66**:975-983.
248. Olsen KN, Larsen MH, Gahan CG, Kallipolitis B, Wolf XA, Rea R, Hill C, Ingmer H: **The Dps-like protein Fri of *Listeria monocytogenes* promotes stress tolerance and intracellular multiplication in macrophage-like cells.** *Microbiology* 2005, **151**:925-933.
249. Saraswathi R, Pait Chowdhury R, Williams SM, Ghatak P, Chatterji D: **The mycobacterial MsDps2 protein is a nucleoid-forming DNA binding protein regulated by sigma factors σ^A and σ^B .** *PLoS One* 2009, **4**:e8017.
250. Ramsay B, Wiedenheft B, Allen M, Gauss GH, Lawrence CM, Young M, Douglas T: **Dps-like protein from the hyperthermophilic archaeon *Pyrococcus furiosus*.** *J Inorg Biochem* 2006, **100**:1061-1068.
251. Yamamoto Y, Poole LB, Hantgan RR, Kamio Y: **An iron-binding protein, Dpr, from *Streptococcus mutans* prevents iron-dependent hydroxyl radical formation in vitro.** *J Bacteriol* 2002, **184**:2931-2939.
252. Pulliainen AT, Haataja S, Kahkonen S, Finne J: **Molecular basis of H₂O₂ resistance mediated by Streptococcal Dpr. Demonstration of the functional involvement of the putative ferroxidase center by site-directed mutagenesis in *Streptococcus suis*.** *J Biol Chem* 2003, **278**:7996-8005.
253. Okuda M, Iwahori K, Yamashita I, Yoshimura H: **Fabrication of nickel and chromium nanoparticles using the protein cage of apoferritin.** *Biotechnol Bioeng* 2003, **84**:187-194.
254. Klem MT, Mosolf J, Young M, Douglas T: **Photochemical mineralization of europium, titanium, and iron oxyhydroxide nanoparticles in the ferritin protein cage.** *Inorg Chem* 2008, **47**:2237-2239.
255. Douglas T, Stark VT: **Nanophase cobalt oxyhydroxide mineral synthesized within the protein cage of ferritin.** *Inorg Chem* 2000, **39**:1828-1830.
256. Uchida M, Terashima M, Cunningham CH, Suzuki Y, Willits DA, Willis AF, Yang PC, Tsao PS, McConnell MV, Young MJ, et al.: **A human ferritin iron oxide nano-composite magnetic resonance contrast agent.** *Magn Reson Med* 2008, **60**:1073-1081.
257. Uchida M, Flenniken ML, Allen M, Willits DA, Crowley BE, Brumfield S, Willis AF, Jackiw L, Jutila M, Young MJ, et al.: **Targeting of cancer cells with ferromagnetic ferritin cage nanoparticles.** *J Am Chem Soc* 2006, **128**:16626-16633.
258. Swift J, Wehbi WA, Kelly BD, Stowell XF, Saven JG, Dmochowski JJ: **Design of functional ferritin-like proteins with hydrophobic cavities.** *J Am Chem Soc* 2006, **128**:6611-6619.
259. Fan R, Boyle AL, Cheong VV, Ng SL, Orner BP: **A helix swapping study of two protein cages.** *Biochemistry* 2009, **48**:5623-5630.
260. Allen M, Willits D, Young M, Douglas T: **Constrained synthesis of cobalt oxide nanomaterials in the 12-subunit protein cage from *Listeria innocua*.** *Inorg Chem* 2003, **42**:6300-6305.
261. Kang S, Lucon J, Varpness ZB, Liepold L, Uchida M, Willits D, Young M, Douglas T: **Monitoring biomimetic platinum nanocluster formation using mass spectrometry and cluster-dependent H₂ production.** *Angew Chem Int Ed Engl* 2008, **47**:7845-7848.
262. Allen M, Willits D, Mosolf J, Young M, Douglas T: **Protein cage constrained synthesis of**

- ferrimagnetic iron oxide nanoparticles. *Adv. Mater.* 2002, **14**:1562-1565.
263. Kabsch W: **XDS**. *Acta Crystallogr D Biol Crystallogr* 2010, **66**:125-132.
264. Leslie AG: **The integration of macromolecular diffraction data**. *Acta Crystallogr D Biol Crystallogr* 2006, **62**:48-57.
265. Collaborative Computational Project n: **The CCP4 suite: programs for protein crystallography**. *Acta Crystallogr D Biol Crystallogr* 1994, **50**:760-763.
266. Murshudov GN, Vagin AA, Dodson EJ: **Refinement of macromolecular structures by the maximum-likelihood method**. *Acta Crystallogr D Biol Crystallogr* 1997, **53**:240-255.
267. Emsley P, Cowtan K: **Coot: model-building tools for molecular graphics**. *Acta Crystallogr D Biol Crystallogr* 2004, **60**:2126-2132.
268. Adams PD, Afonine PV, Bunkoczi G, Chen VB, Davis IW, Echols N, Headd JJ, Hung LW, Kapral GJ, Grosse-Kunstleve RW, et al.: **PHENIX: a comprehensive Python-based system for macromolecular structure solution**. *Acta Crystallogr D Biol Crystallogr* 2010, **66**:213-221.
269. Chen VB, Arendall WB, 3rd, Headd JJ, Keedy DA, Immormino RM, Kapral GJ, Murray LW, Richardson JS, Richardson DC: **MolProbity: all-atom structure validation for macromolecular crystallography**. *Acta Crystallogr D Biol Crystallogr* 2010, **66**:12-21.
270. McCoy AJ, Grosse-Kunstleve RW, Adams PD, Winn MD, Storoni LC, Read RJ: **Phaser crystallographic software**. *J Appl Crystallogr* 2007, **40**:658-674.
271. Langer G, Cohen SX, Lamzin VS, Perrakis A: **Automated macromolecular model building for X-ray crystallography using ARP/wARP version 7**. *Nat Protoc* 2008, **3**:1171-1179.
272. Wellenreuther G, Meyer-Klaucke W: **Towards a black-box for biological EXAFS data analysis - III. A universal post-processor for fluorescence XAS: KEMP2**. *J Phys.: Conf. Ser.* 2009, **190**:1-4.
273. Ressler T: **WinXAS: a program for X-ray absorption spectroscopy data analysis under MS-Windows**. *J Synchrotron Radiat* 1998, **5**:118-122.
274. Tomic S, Searle BG, Wander A, Harrison NM, Dent AJ, Mosselmans JFW, Inglesfield JE: **New tools for the analysis of EXAFS: the DL EXCURV package**. *CCLRC Technical Report DL-TR-2005-001* 2005:ISSN 1362-0207.
275. Higuchi M, Yamamoto Y, Kamio Y: **Molecular biology of oxygen tolerance in lactic acid bacteria: Functions of NADH oxidases and Dpr in oxidative stress**. *J Biosci Bioeng* 2000, **90**:484-493.
276. Gibson CM, Mallett TC, Claiborne A, Caparon MG: **Contribution of NADH oxidase to aerobic metabolism of *Streptococcus pyogenes***. *J Bacteriol* 2000, **182**:448-455.
277. Zitzelsberger W, Götz F, Schleifer KH: **Distribution of superoxide dismutases, oxidases, and NADH peroxidase in various streptococci**. *FEMS Microbiol Lett* 1984, **21**:243-246.
278. Malke H, Starke R, Jacob HE, Kohler W: **Bacteriocine-like activity of group-A streptococci due to the production of peroxide**. *J Med Microbiol* 1974, **7**:367-374.
279. Saito M, Ohga S, Endoh M, Nakayama H, Mizunoe Y, Hara T, Yoshida S: **H₂O₂-nonproducing *Streptococcus pyogenes* strains: survival in stationary phase and virulence in chronic granulomatous disease**. *Microbiology* 2001, **147**:2469-2477.
280. Hirst RA, Sikand KS, Rutman A, Mitchell TJ, Andrew PW, O'Callaghan C: **Relative roles of pneumolysin and hydrogen peroxide from *Streptococcus pneumoniae* in inhibition of ependymal ciliary beat frequency**. *Infect Immun* 2000, **68**:1557-1562.
281. Jansen WT, Bolm M, Balling R, Chhatwal GS, Schnabel R: **Hydrogen peroxide-mediated killing of *Caenorhabditis elegans* by *Streptococcus pyogenes***. *Infect Immun* 2002, **70**:5202-5207.
282. Bolm M, Jansen WT, Schnabel R, Chhatwal GS: **Hydrogen peroxide-mediated killing of *Caenorhabditis elegans*: a common feature of different streptococcal species**. *Infect Immun* 2004, **72**:1192-1194.
283. Nathan C, Shiloh MU: **Reactive oxygen and nitrogen intermediates in the relationship between mammalian hosts and microbial pathogens**. *Proc Natl Acad Sci U S A* 2000, **97**:8841-8848.
284. Miller RA, Britigan BE: **Role of oxidants in microbial pathophysiology**. *Clin Microbiol Rev* 1997, **10**:1-18.
285. Sherrill C, Fahey RC: **Import and metabolism of glutathione by *Streptococcus mutans***. *J Bacteriol* 1998, **180**:1454-1459.
286. Fahey RC, Brown WC, Adams WB, Worsham MB: **Occurrence of glutathione in bacteria**. *J Bacteriol* 1978, **133**:1126-1129.
287. Kodama T, Fukui K, Shimamoto T, Ohta H, Kokeguchi S, Kato K: **Effects of oxygen on glucose-limited growth of *Streptococcus mutans***. *Infect Immun* 1987, **55**:169-173.
288. Pasek J, Buechler R, Albrecht R, Boland W, Zeth K: **Structure and mechanism of iron translocation by a DPS protein from *Microbacterium arborescens***. *J Biol Chem* 2011, **286**:34872-34882.
289. Havukainen H, Haataja S, Kauko A, Pulliainen AT, Salminen A, Haikarainen T, Finne J, Papageorgiou AC: **Structural basis of the zinc- and terbium-mediated inhibition of ferroxidase activity in Dps ferritin-like proteins**. *Protein Sci* 2008, **17**:1513-1521.
290. Liu X, Theil EC: **Ferritin reactions: direct identification of the site for the diferric peroxide reaction intermediate**. *Proc Natl Acad Sci U S A* 2004, **101**:8557-8562.

291. Auld DS: **Zinc coordination sphere in biochemical zinc sites.** *Biometals* 2001, **14**:271-313.
292. Papaefthymiou GC: **The Mössbauer and magnetic properties of ferritin cores.** *Biochim Biophys Acta* 2010.
293. Rohrer JS, Islam QT, Watt GD, Sayers DE, Theil EC: **Iron environment in ferritin with large amounts of phosphate, from *Azotobacter vinelandii* and horse spleen, analyzed using extended X-ray absorption fine structure (EXAFS).** *Biochemistry* 1990, **29**:259-264.
294. Ceci P, Chiancone E, Kasyutich O, Bellapadrona G, Castelli L, Fittipaldi M, Gatteschi D, Innocenti C, Sangregorio C: **Synthesis of iron oxide nanoparticles in *Listeria innocua* Dps (DNA-binding protein from starved cells): a study with the wild-type protein and a catalytic centre mutant.** *Chemistry* 2010, **16**:709-717.
295. Gossuin Y, Gillis P, Hocq A, Vuong QL, Roch A: **Magnetic resonance relaxation properties of superparamagnetic particles.** *Wiley Interdiscip Rev Nanomed Nanobiotechnol* 2009, **1**:299-310.
296. Michel FM, Ehm L, Antao SM, Lee PL, Chupas PJ, Liu G, Strongin DR, Schoonen MA, Phillips BL, Parise JB: **The structure of ferrihydrite, a nanocrystalline material.** *Science* 2007, **316**:1726-1729.
297. Michel FM, Hosein HA, Hausner DB, Debnath S, Parise JB, Strongin DR: **Reactivity of ferritin and the structure of ferritin-derived ferrihydrite.** *Biochim Biophys Acta* 2010, **1800**:871-885.
298. Kundig W, Bommel H, Constabaris G, Lindquist RH: **Some properties of supported small α -Fe₂O₃ particles determined with the Mössbauer effect.** *Phys Rev* 1966, **142**:327-333.
299. Gupta AK, Gupta M: **Synthesis and surface engineering of iron oxide nanoparticles for biomedical applications.** *Biomaterials* 2005, **26**:3995-4021.
300. Speir JA, Bothner B, Qu C, Willits DA, Young MJ, Johnson JE: **Enhanced local symmetry interactions globally stabilize a mutant virus capsid that maintains infectivity and capsid dynamics.** *J Virol* 2006, **80**:3582-3591.
301. Kumar P, Singh M, Karthikeyan S: **Crystal structure analysis of icosahedral lumazine synthase from *Salmonella typhimurium*, an antibacterial drug target.** *Acta Crystallogr D Biol Crystallogr* 2011, **67**:131-139.
302. Vedula LS, Brannigan G, Economou NJ, Xi J, Hall MA, Liu R, Rossi MJ, Dailey WP, Grasty KC, Klein ML, et al.: **A unitary anesthetic binding site at high resolution.** *J Biol Chem* 2009, **284**:24176-24184.
303. Kim KK, Kim R, Kim SH: **Crystal structure of a small heat-shock protein.** *Nature* 1998, **394**:595-599.